



Efficient visible and near-infrared emitting materials based on bismuth and/or lanthanide doped zeolites

Bai, Zhenhua

(Degree)

博士 (学術)

(Date of Degree)

2012-03-25

(Date of Publication)

2012-04-16

(Resource Type)

doctoral thesis

(Report Number)

甲5463

(URL)

<https://hdl.handle.net/20.500.14094/D1005463>

※ 当コンテンツは神戸大学の学術成果です。無断複製・不正使用等を禁じます。著作権法で認められている範囲内で、適切にご利用ください。



Doctoral Dissertation

Efficient visible and near-infrared
emitting materials based on bismuth
and/or lanthanide doped zeolites

January, 2012

Graduate School of Engineering
Kobe University

Zhenhua Bai

Doctoral Dissertation

Efficient visible and near-infrared
emitting materials based on bismuth
and/or lanthanide doped zeolites

January, 2012

Graduate School of Engineering
Kobe University

Zhenhua Bai

Contents

Chapter 1 Introduction	1
1.1 Zeolites	1
1.1.1 Structure	1
1.1.2 Application	3
1.1.3 Zeolites used as optical host materials	5
1.2 Near-infrared emission from Bi ions	10
1.3 Optical properties of Bi doped zeolites	14
1.4 Chapter Overview and Goal of this thesis	17
1.4.1 Photoluminescence properties of Bi doped zeolites	17
1.4.2 Photoluminescence properties of Bi and lanthanide ions co-doped zeolites	18
1.4.3 Simultaneously doping of different kinds of lanthanide ions in Bi doped zeolites	19
 Part I Photoluminescence properties of Bi doped zeolites	 27
 Chapter 2 Effect of doping concentration on broadband near-infrared emis- sion of Bi doped zeolites	 29
2.1 Introduction	29
2.2 Experimental details	30
2.3 Results and discussion	31
2.4 Conclusion	39
 Chapter 3 Controlling the optical properties by annealing atmosphere - Co-existence of Bi with multiple valence states in zeolites	 43
3.1 Introduction	43
3.2 Experimental details	44
3.3 Results and discussion	45
3.4 Conclusion	52

Part II Photoluminescence properties of Bi and lanthanide ions co-doped zeolites **55****Chapter 4 Efficient near-infrared luminescence and energy transfer in erbium/bismuth co-doped zeolites** **57**

4.1	Introduction	57
4.2	Experimental details	58
4.3	Results and discussion	59
4.4	Conclusion	65

Chapter 5 Efficient near-infrared emission from neodymium by broadband sensitization of bismuth in zeolites **69**

5.1	Introduction	69
5.2	Experimental details	70
5.3	Results and discussion	71
5.4	Conclusion	76

Chapter 6 Bismuth sensitized efficient near-infrared luminescence from ytterbium in zeolites **79**

6.1	Introduction	79
6.2	Experimental details	80
6.3	Results and discussion	81
6.4	Conclusion	87

Chapter 7 Enhanced red luminescence and energy transfer in Eu-Bi co-doped zeolites for white LEDs **91**

7.1	Introduction	91
7.2	Experimental details	92
7.3	Results and discussion	93
7.4	Conclusion	98

Part III Simultaneously doping of different kinds of lanthanide ions in Bi doped zeolites **101****Chapter 8 Efficient ultraviolet-blue to near-infrared downconversion in Bi-Dy-Yb doped zeolites** **103**

8.1	Introduction	103
8.2	Experimental details	105
8.3	Results and discussion	107

8.4 Conclusion	111
Chapter 9 Conclusion	115
Acknowledgment	119
List of Publications	121

Chapter 1

Introduction

1.1 Zeolites

1.1.1 Structure

Zeolites are microporous crystalline aluminosilicates with nanosized pores. Their framework is composed of SiO_4 and AlO_4 tetrahedra units by sharing oxygen between every two consecutive units, and cations located inside channels or cavities to balance negative charges in the framework [1]. The pores of the zeolites have a very regular shape and size and are defined by the crystal structure. A typical feature of zeolites is also the presence

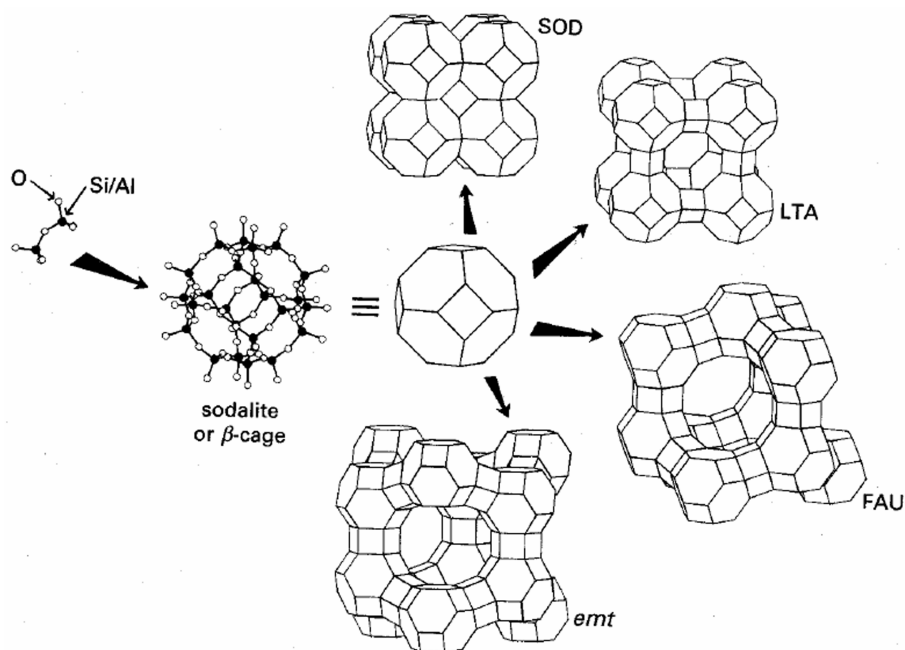


Figure 1.1: The basic building block of zeolite [6].

of large central cavities, the so-called supercages [2]. About 50 types of zeolites occur as minerals in nature, but more than 150 different types of zeolites have been synthesized in the laboratory. Zeolites can be synthesized with a wide range of pores sizes and shapes, and the composition can be modified during synthesis or by post-synthesis treatments, in order to tailor their properties. Zeolites can be prepared with varying silicon to aluminum ratios, but the constraints are that the sum of the number of Si atoms and the number of Al atoms equals 192 and that the total charge of the cations equals the number of Al atoms [3,4]. High silica zeolites are hydrophobic, and on the other hand, high alumina zeolites have large amount of charge balancing ion-exchange sites and have a very high affinity to polar molecules, such as coordinated water [5].

As shown in figure 1.1, the basic building block of this zeolite is the sodalite cage (or β -cage) [6]. The sodalite cage has the shape of a truncated octahedron and thus possesses square and hexagonal faces. Its name derives from the aluminosilicate sodalite whose structure consists of a cubic array of truncated octahedra sharing their square faces. Alternate hexagonal faces, at positions corresponding to the vertices of a tetrahedron, are connected via hexagonal prisms. Each sodalite cage is thus connected to four other sodalite cages via the hexagonal prisms, which form the small pore system of the zeolite. The α -cage or supercage is created by eight β -cages. The faujasite (FAU) type zeolite

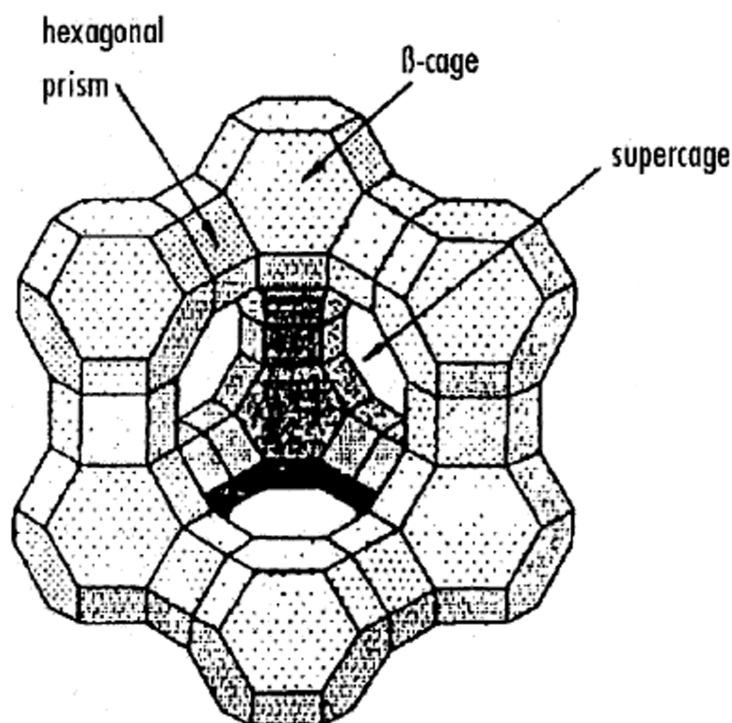


Figure 1.2: Structure of faujasite type zeolites [7].

is one of the most widely used zeolite (figure 1.2). The diameter of the entrance to the supercage is about 7.5 \AA , whereas the diameter of the supercage itself is about 12 \AA . In contrast, the diameter of the sodalite cage is 6.6 \AA and that of the hexagonal prism 1.8 \AA . The water molecules in the zeolite structure can be removed by dehydration and their number is variable [7]. Indeed, a typical feature of zeolites is that they can absorb and lose water without damage to their crystal structures.

1.1.2 Application

Zeolites consist of the combination of many properties, among them the microporous character of the uniform pore dimensions, the ion exchange properties, the ability to develop internal acidity, the high thermal stability and high internal surface area. These make zeolites unique among other inorganic oxides. Almost all of the properties are tunable. Therefore, zeolites have been accepted in a variety of applications namely processes

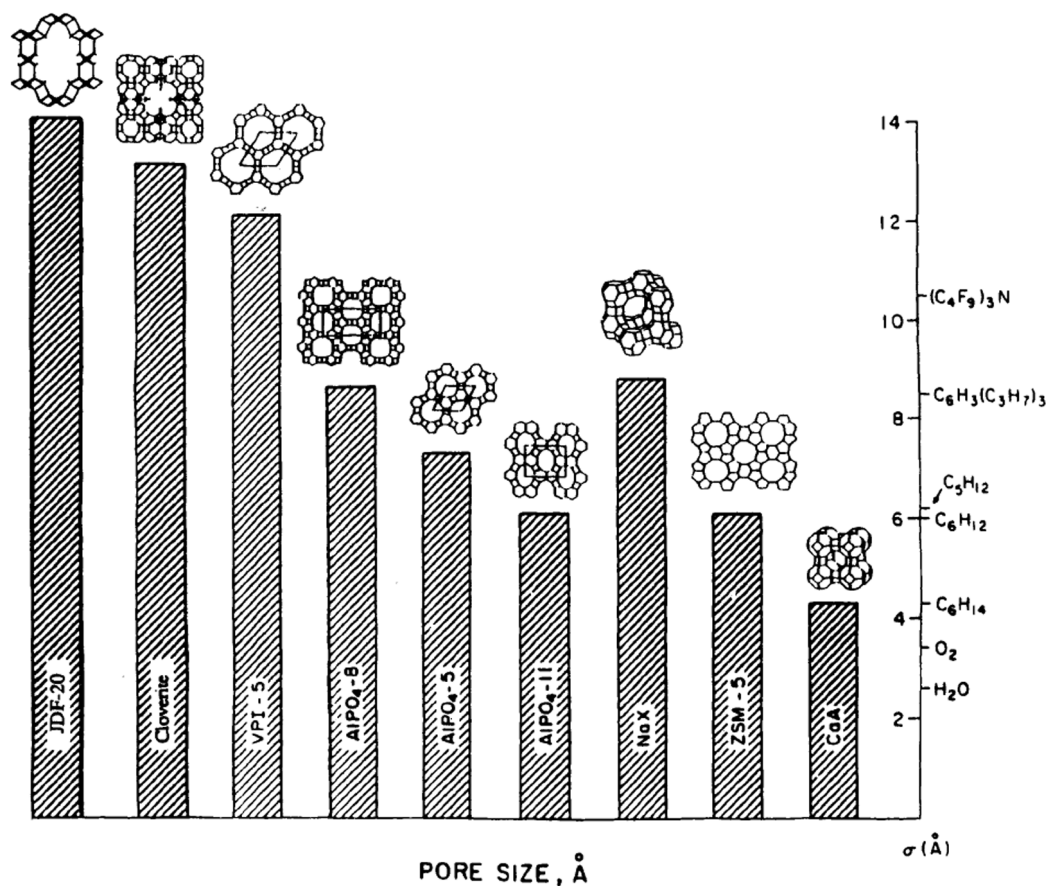


Figure 1.3: Correlation between pore size of molecular sieves and the kinetic diameter of various molecules [6].

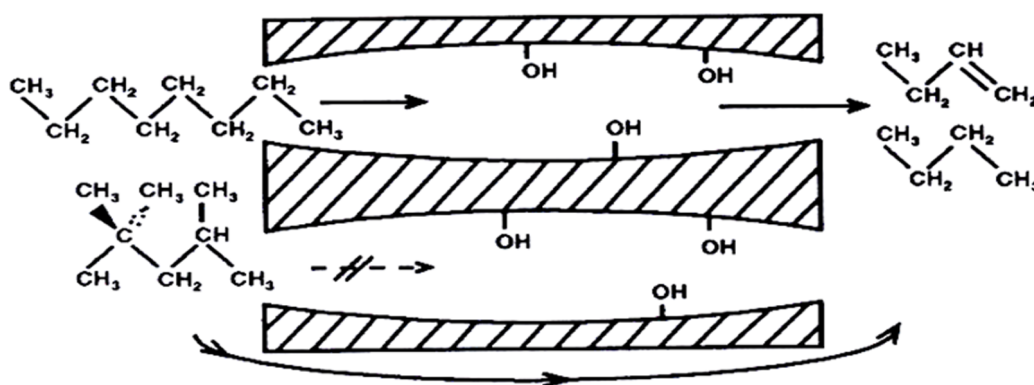


Figure 1.4: Zeolites used as molecular sieves.

involving adsorption, catalysis and ion exchange [8-12].

Zeolites are well known as molecular sieves [8]. Molecular sieve zeolites are a class of stable mineral and synthetic crystalline inorganic compounds characterized by the presence of an open three dimensional oxide framework structure (figure 1.3). This open structure leads to a regular network of uniform pores of specific molecular dimensions. As shown in figure 1.4, the porous structure enables the zeolites to selectively admit some molecules while excluding those that are too large to fit into the pores. This leads to its molecular sieve properties. The dimensions of zeolites' channels and their ability to adsorb gases and water have made zeolite molecular sieves suitable for a number of applications such as in the areas of refinery fuel processing, production of chemicals and environmental pollution control [9,10].

Besides, zeolites are also regarded as shape selective catalysts, which is shown in figure

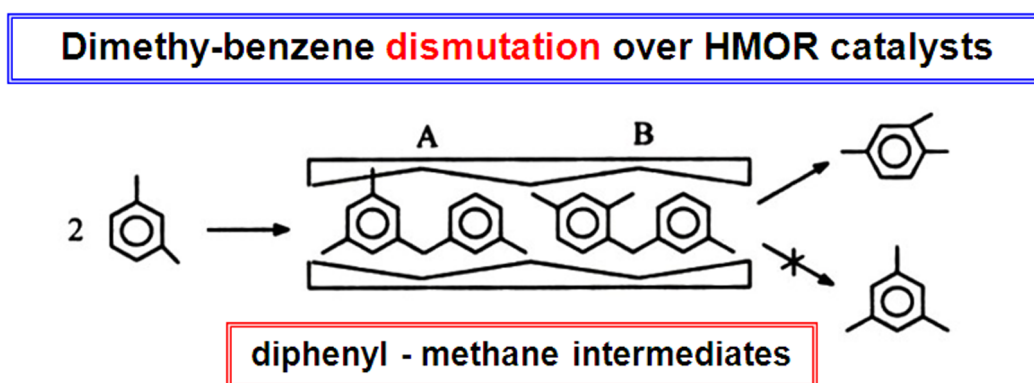


Figure 1.5: Reactants and products can easily diffuse in catalyst structure, but intermediary species formation, in the vicinity of active sites are sterically limited.

1.5. It is based on the formation of active catalyst sites inside the zeolite pore system, which is very uniform in one or more discrete sizes [11]. Molecules with dimensions similar to or slightly larger than the zeolite pores can usually diffuse through the pore structure due to the molecular vibrations or breathing of the zeolite pore and the vibration of the limiting atoms on the diffusing molecule or perturbations of its structure. Bond cleavage, followed by reconstruction of the bond has been suggested for the diffusion of some inorganic materials. In this case, the rate of diffusion controls the rate of reaction rather than by any catalytic phenomenon. Shape selectivity catalysis involves the reactivities of primary, secondary and tertiary carbon atoms, which, can be classified into three major classes. They are reactant selectivity, product selectivity and restricted transition state selectivity [12].

Recently, zeolites acting as a host material of optically active guests have attracted much attention for constructing novel materials designed at nanosized levels, because of their low-frequency vibrational framework, regularly spaced nanochannels and nanopores, and inexpensive price [7].

1.1.3 Zeolites used as optical host materials

Lanthanide ions have frequently been used as luminescent probes to investigate zeolite structures. Luminescence studies are helpful to locate the lanthanide ion within the zeolite framework and to study the local environment of the lanthanide ion [7]. Berry et al.[13] investigated the location of Eu^{3+} cations in an Eu^{3+} -exchanged zeolite-Y, with a framework Si/Al molar ratio of 13.5 ± 2.0 , as a function of heat treatment up to 200 °C. The coordination environment of the Eu^{3+} cation in the sample heated to 100 °C is similar to that in the as-exchanged sample. Heating the Eu^{3+} -exchanged zeolite-Y at 200 °C results in the migration of the Eu^{3+} cations into the sodalite cages. Hazenkamp et al.[14] found that, in a freshly prepared sample containing 5 wt.% Gd^{3+} , one site inside the zeolite is occupied by Gd^{3+} , and other Gd^{3+} ions appear on silica surfaces present in the sample. When measurements on this sample were repeated a few months after preparation, Gd^{3+} ions were found in three sites within the zeolite cages. Hong et al.[15,16] observed that the intrazeolitic migration of Tb^{3+} ions arising from thermal treatments in FAU-type zeolites is strongly dependent on the framework Si/Al ratio. For a low-silica FAU zeolite (Si/Al = 1.37) most of the Tb^{3+} ions exchanged into supercages begin to migrate directly to hexagonal prisms at 423 K without staying at sodalite cages; by contrast, the cations in a high-silica FAU zeolite (Si/Al = 3.40) migrate first to sodalite cages at 373 K and in turn to hexagonal prisms at temperatures higher than 373 K.

Lanthanide-exchanged zeolites have been investigated as cheap inorganic phosphor material as replacements for the conventional inorganic phosphors for lighting applications.

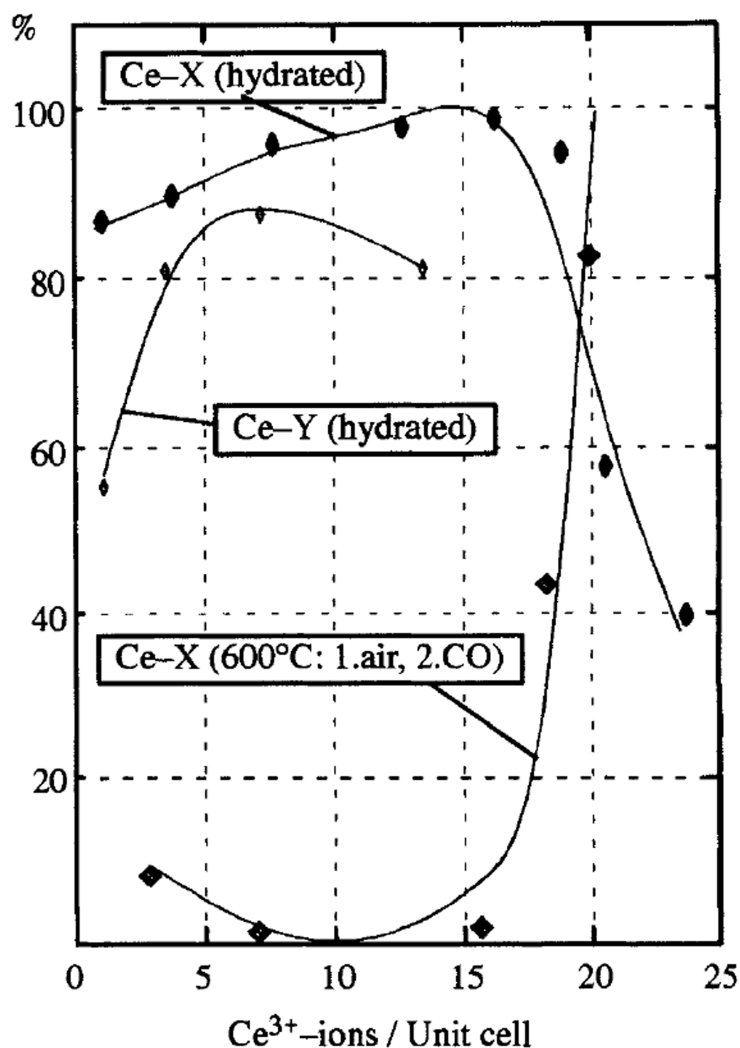


Figure 1.6: Quantum yields of Ce doped zeolites X and Y [17].

Kynast et al.[17] prepared zeolites X and Y with various degrees of Ce-doping by means of ion-exchange and studied their optical properties. The emission spectra are characterized by broad UV-emissions with quantum yields of up to unity within experimental error, and moreover, the allowed nature of the electronic f-d transitions within the cerium ion account for a high absorptivity of $> 90\%$. Figure 1.6 shows the dependence of the quantum yields in zeolites X and Y on the Ce^{3+} doping level. Obviously, in Ce-X the maximum quantum yield is obtained at 16 Ce^{3+} ions per unit cell. The experiments show Ce^{3+} ions can efficiently act as a luminescent center without screening by organic ligands as well. This is due to the provision of sites with large diameter and the non-sensitivity of the Ce^{3+} excited state to high frequency phonons (O-H vibrations), which for Eu^{3+} , inevitably lead to non-radiative decay. Chen et al.[18] studied the photoluminescence and

photostimulated luminescence of Tb^{3+} and Eu^{3+} ions in zeolite-Y. The dehydrated sample treated at 800 °C exhibits strong Tb^{3+} and Eu^{3+} emissions, while the luminescence from the hydrated sample prepared at room temperature is extremely weak. Quenching via high-energy O-H vibrations is responsible for the weak emission in the hydrated zeolite prepared at room temperature. The emission is enhanced largely by heating the sample at 800 °C, which is due to the loss of water and the migration of the ions from the supercages to the sodalite cages.

Because of the weak light absorption by the f-f transitions of Eu^{3+} , the total luminescence output remained low, even after heat treatment, and one had to rely on the antenna effect to increase the luminescence efficiency. Secdor et al.[19] reported that a tremendous gain in luminescence intensity was observed when the Eu^{3+} ions in the cage were complexed with ttfa (1-(2-thenyl)-4, 4, 4-trifluoro-butane-1, 3-dione) (figure 1.7). The Eu^{3+} emission is increased by a factor of 350 after treatment of a $\text{Eu}_8\text{-X}$ sample (i.e., a zeolite-X with eight Eu^{3+} ions per unit cell) with an excess of ttfa, followed by washing and rehydration. The rehydration step was necessary for complex formation, because otherwise the ttfa ligands could not be deprotonated in the zeolite cage and the Eu^{3+} ions could not be released from the walls of the supercage. The luminescence efficiency depended on the Eu/ttfa ratio. A strongly emissive species was found to be $[\text{Eu}(\text{ttfa})_3]\text{-X}$, where the complexes remained attached to the zeolite cage. Increasing the number of Eu^{3+} ions per unit cell resulted in an increase of the luminescence intensity up to eight Eu^{3+} per unit cell. Further addition of Eu^{3+} led to a decrease in the luminescence intensity.

It is not easy to observe near-infrared (NIR) luminescence from lanthanide-exchanged zeolites, due to the strong nonradiative relaxation of the excited states of the NIR emitting lanthanide ions by the water molecules within the pores of the zeolite host. Up until now, an organic and inorganic hybrid synthesis has been the most common method to realize NIR emission of rare earth ions such as Nd^{3+} and Er^{3+} in zeolites [20-31]. Wada et al.[20] succeeded in drastically enhancing the NIR emission of Nd^{3+} by ligating it with bis(perfluoromethylsulfonyl)-aminato (PMS) in cages of a nanocrystalline, large-pore zeolite (FAU type). As displayed in figure 1.8, the resulting Nd-exchanged n-FAU was degassed at 423 K for 1 h and was kept in contact with vapor of PMS at 373 K for 1 h. Furthermore, it was exposed to D_2O vapor for 10 min at 423 K three times to convert O-H with high vibrational frequency to O-D with low vibrational frequency. The success in obtaining the strong emission in this work should be attributed to suppression of the relaxation of the excitation energy of Nd^{3+} through the vibrational excitation by the low-vibrational zeolite cage wall and the energy migration at collisions by locating Nd^{3+} separately in the cages.

Very recently, Monguzzi et al.[28] used the zeolite-L (LTL) which forms highly crystalline microcrystals consisting of parallel arrays of nanometric channels (7 Å pore en-

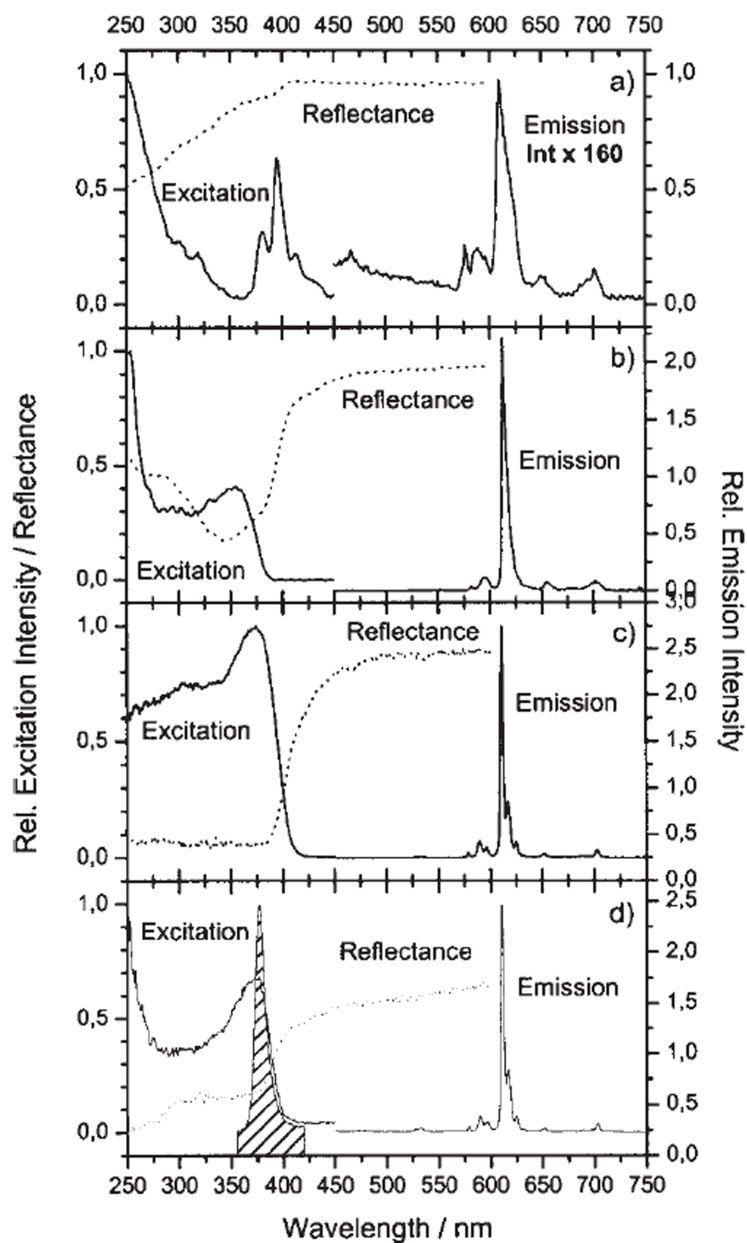


Figure 1.7: Optical spectra of functionalized zeolite X hybrids. Excitation was at 250 nm for $\text{Eu}_8\text{-X}$ and at the respective excitation maxima for Eu-ttfa complexes. Emission intensities scaled relative to $[\text{Eu}(\text{ttfa})_3(\text{H}_2\text{O})_2]$. The hatched curve in (d) represents the emission spectrum of a commercial UV emitting LED (Nichia). (a) $\text{Eu}_8\text{-X}$, (b) $[\text{Eu}(\text{ttfa})_3]$, (c) $[\text{Eu}(\text{ttfa})_3(\text{phen})]$, (d) $[\text{Eu}-(\text{ttfa})_3(\text{phen})\text{-X}$ [19].

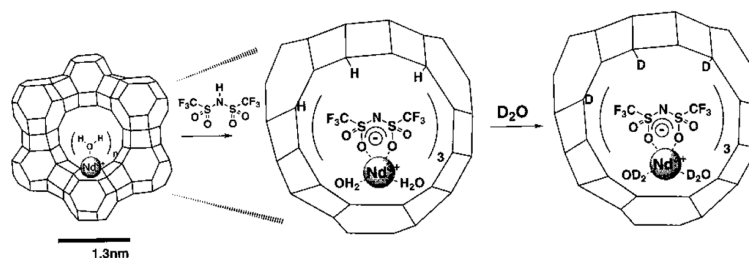


Figure 1.8: The scheme shows the conceptual process of the ship-in-bottle synthesis and the treatment with D_2O [20].

trance, 12 Å inner diameter), which can produce the desired confinement between the sensitizer and the emitting ion. As shown in figure 1.9, they realized the sensitization of Er^{3+} ions by energy transfer between a suitable organic molecule acting as an antenna and the emitting ion arranged in close proximity in zeolites. However, the lifetime at 1535 nm is around $0.9 \mu s$, which is much shorter than the intrinsic radiative lifetime of 10 ms. Though these hybrid composites provide new opportunities to create multifunctional ma-

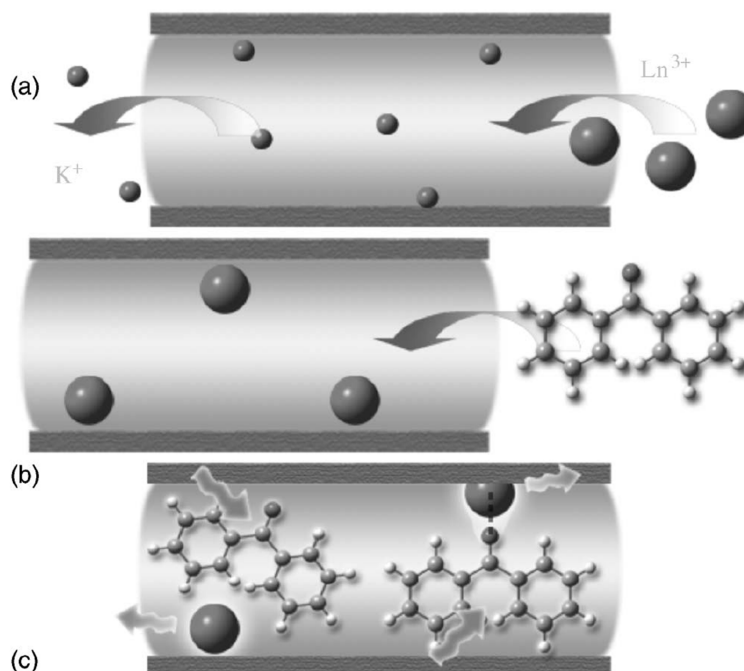


Figure 1.9: (a) Ionic exchange between K^{1+} and Er^{3+} ions in zeolite preparation. (b) Inclusion of benzophenone molecules. (c) Outline of working material. Two possible positions of the benzophenone molecule with respect to the Er^{3+} are sketched (noncoordinated and coordinated to the ion) [28].

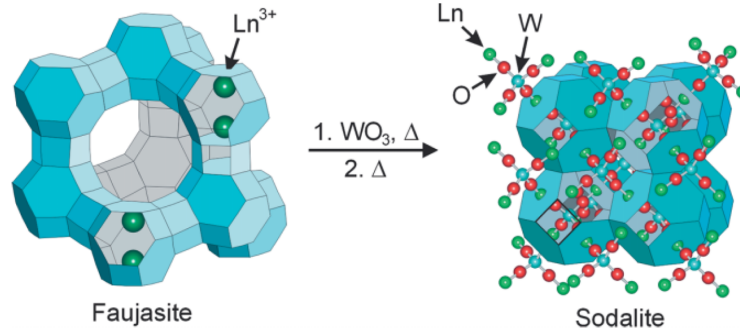


Figure 1.10: Sketch of the nanoporous zeolite structures employed in the work. Oxygen and silicon, and aluminum atoms (not drawn), are positioned at the edges and corners, respectively, of the cuboctahedra. Left: the faujasite structure (zeolites X and Y), right: the sodalite structure (hawyne). Loading with WO_3 (1) was at just above $600\text{ }^\circ\text{C}$, the conversion (2) proceeded at $T > 700\text{ }^\circ\text{C}$ [23].

materials with unique properties by combining the merits of inorganic and organic building blocks, the complicated preparation processes and air instability of these materials limit their practical applications.

In 2006, Lezhnina et al. [23] showed that strong NIR emission of Nd^{3+} can be realized by collapsing the open zeolitic materials into more dense aluminosilicates, such as sodalites, combined with sufficient space filling (figure 1.10). That is, not enough room is left for the admission of water. Essentially, this method is based on phase transition at the expense of the zeolite structure, and additional compounds, such as WO_3 , have to be used to act as auxiliaries to realize it. The similarity of the above strategies is that rare-earth ions were used as active centers, and the full-width at half-maximum (FWHM) of the emission spectra is less than 50 nm.

1.2 Near-infrared emission from Bi ions

As shown in figure 1.11, there are two useful wavelengths for optical communication. One is $1.54\text{ }\mu\text{m}$, which is the maximum transparency wavelength of silica glass fiber. The other useful wavelength is $1.3\text{ }\mu\text{m}$, which is the minimum dispersion region of silica glass fiber; temporal distortion of transferred optical pulses can be minimized at this wavelength. However, one of the main problems faced in optoelectronic integration on silicon is the lack of an efficient silicon-based light source. This is because radiative band-to-band recombination in Si is not efficient due to the indirect band gap [32]. An alternative way to achieve light emission is provided by optical doping. In the past decades, considerable effort has been devoted to develop optical fiber amplifiers to revolutionize the telecom-

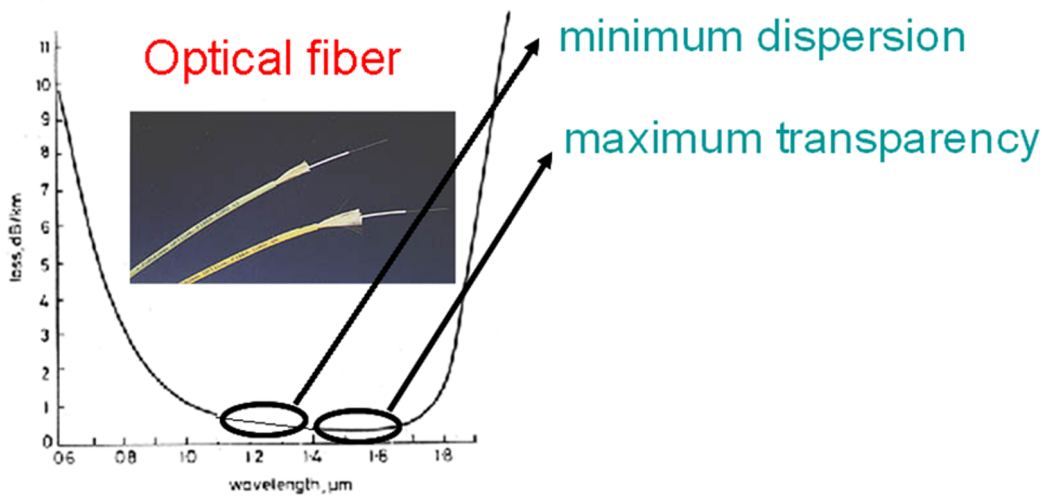


Figure 1.11: Optical loss of silica glass fiber.

munication systems, such as Er-doped fiber amplifiers (EDFA) [33-36], Tm-doped fiber amplifiers (TDFA) [37], and Pr-doped fiber amplifiers (PDFA) [38].

With the rapid development of telecommunication technology, the conventional rare-earth ions doped silica fiber amplifier have difficulty in meeting information transportation requirements with large transmission capacity at fast rates, as their gain bandwidth is as small as 70 nm. An attractive way to meet these requirements is to develop broadband amplifiers and broadly tunable laser sources covering the whole telecommunication windows to achieve an efficient wavelength-division multiplexing (WDM) transmission network [39]. Raman amplifiers (RAs) can realize broadband amplification, but they require multiwavelength pumping schemes and have low gain efficiency [40]. Broadband RAs also have complex structures and require high-power consumption [41]. If broadband amplification is realized with high gain efficiency by the single wavelength pumping, the drastic evolution could be expected to occur in the WDM technology.

Recently, bismuth doped photonic materials have attracted much attention owing to their promising super-wide infrared fluorescence properties (figure 1.12). In 1999, Murata et al.[42] discovered a new fluorescence from bismuth-doped silica glass centered at 1150 nm with a FWHM of 150 nm and a lifetime of 650 μ s. The quantum yield reaches about 66 % when excited at a wavelength of 500 nm. Based on theoretical calculations, it was shown that generation of optical pulses with a duration as short as 13 fs is possible and, hence, the material is of significant interest for use in laser amplification. Furthermore, in 2003, Fujimoto and Nakatsuka experimentally proved the optical amplification at 1.3 μ m from Bi-doped silica glass when pumped with 810 nm [43]. In 2004, Peng et al.[44] extended the group of known NIR emitting Bi-doped glasses to germanates and demonstrated that

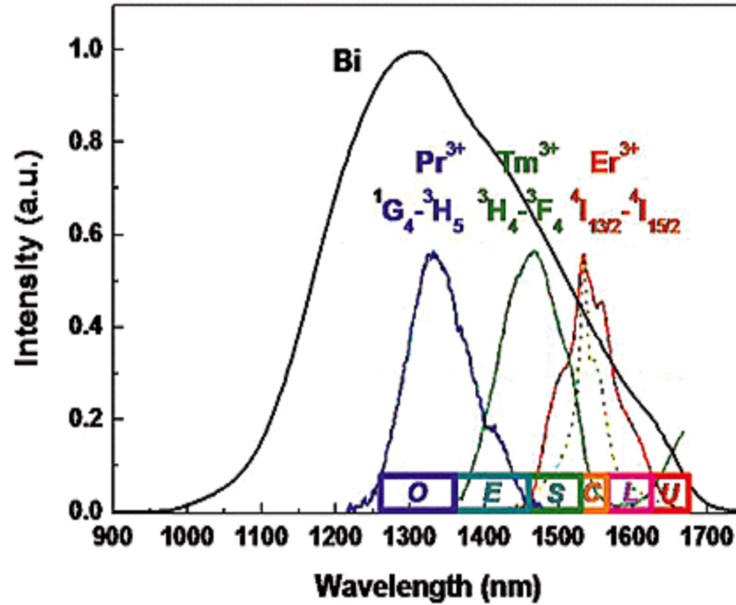


Figure 1.12: NIR emission spectra of Bi-doped silicate glass, Pr^{3+} , Tm^{3+} and Er^{3+} doped tellurate glasses, and Er^{3+} doped silica (dash line).

the FWHM could be as broad as 300 nm. A further breakthrough followed in 2005 with the realization of continuous wave lasing in the spectral region from 1150 to 1300 nm by Dianov et al. [45]. Since then, tremendous research on NIR luminescence from Bi ion has carried out in different host materials, such as glasses, crystals and optical devices [46-69]. Up to now, NIR emission from bismuth based centers has successively been reported for silicate [42,50], germanate [62], aluminoborate [48], aluminophosphate [47,56], chalcogenide [55], germanosilicate [57,61], aluminosilicate [52,58] and borosilicate glasses [49] as well as for polycrystalline SrB_4O_7 [59], single crystals of $RbPb_2Cl_5$ [63], BaF_2 [66], α - BaB_2O_4 [67] and various other materials. Also on the area of device fabrication, a rapid progress has been made in the past years. That is, within only two years, efficient all-fiber optical amplifiers and fiber lasers have emerged from the first demonstration of lasing. Only recently, a quantum efficiency of up to 1.0 ± 0.05 has been reported for a bismuth-doped fiber [70]. For a bismuth-doped chalcogenide glass, NIR luminescence was reported to peak at 1300 nm with an extraordinary FWHM of up to 600 nm at room temperature. The FWHM can be further increased to 850 nm when the temperature is lowered to 5 K. Hence, it covers the entire spectral range of optical telecommunication [71]. Similar spectral properties have not been observed from any rare-earth-doped optical material, or even combinations of materials.

Though broadband luminescence from Bi ions has been observed in a variety of host materials, the origin of Bi-related broadband luminescence is still unknown, because Bi

ions may take the form of multiple valence states in different hosts, such as Bi^{5+} , Bi^{3+} , Bi^{2+} , and Bi^+ . The absorption and emission spectra of Bi-related NIR active centers are much different from the optical properties of Bi^{2+} or Bi^{3+} centers, and the lifetime is almost two orders larger than those of Bi^{2+} or Bi^{3+} [72-77]. Such large differences indicate that the infrared emission might not be originated from Bi^{2+} or Bi^{3+} . Fujimoto et al.[46] ascribed the absorption and emission bands of bismuth-doped silica glasses to the Bi^{5+} transitions between the ground state of $^1\text{S}_0$ and the excited states of $^3\text{D}_{3,2,1}$, and $^1\text{D}_2$. However, Bi^{5+} containing compounds become extremely unstable if the temperature exceeds 300 °C (i.e., well below the typical melting temperature of many Bi-doped glasses), and Bi^{5+} is usually reduced to Bi^{3+} , Bi^{2+} , or Bi metal [69]. Moreover, Meng et al.[48] observed that the photoluminescence intensity decreases monotonically with further addition of BaO, which shows that addition of alkaline earth oxides have a quenching effect on the infrared emission (figure 1.13). Therefore, they suggest tentatively that the infrared emission derives from monovalent bismuth ions based on the energy matching conditions. The simplified energy levels of Bi^+ are presented in figure 1.14. The ground configuration of Bi^+ ($^6\text{S}_2\ ^6\text{P}_2$) is split by spin-orbit coupling interaction into the ground state $^3\text{P}_0$ and the excited states $^1\text{S}_0$, $^1\text{D}_2$ and $^3\text{P}_{2,1}$.

Recently, Peng et al.[78] doped Bi ions into three kinds of alkaline earth pyrophosphate compounds $\text{M}_2\text{P}_2\text{O}_7$ ($\text{M} = \text{Ca}, \text{Sr}, \text{Ba}$) to investigate the size effect of host cations. After preparation in air, all three bismuth-doped samples exhibited typical Bi^{3+} emission. When prepared in CO atmosphere, co-existence of Bi^{3+} and Bi^{2+} was found. NIR emission could

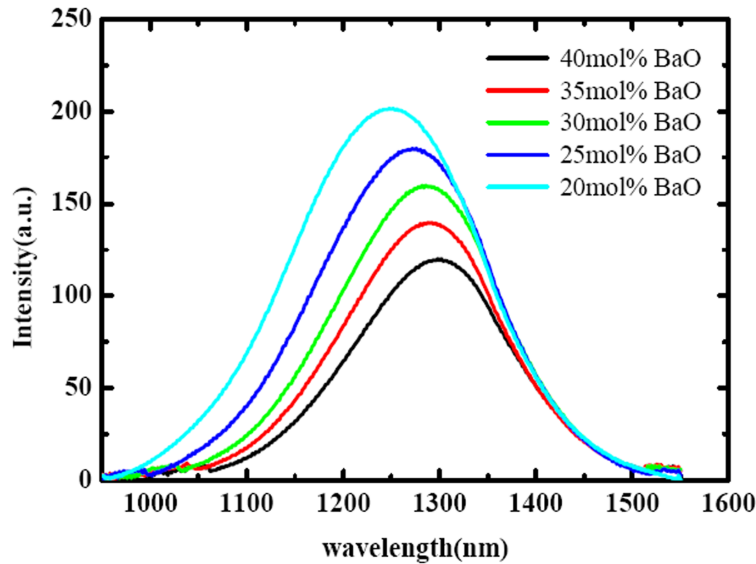


Figure 1.13: Fluorescence spectra of $(95-x)\text{B}_2\text{O}_3-x\text{BaO}-5\text{Al}_2\text{O}_3-2\text{Bi}_2\text{O}_3$ (in mol%, $x = 20, 25, 30, 35, 40$) when excited by 808 nm LD [48].

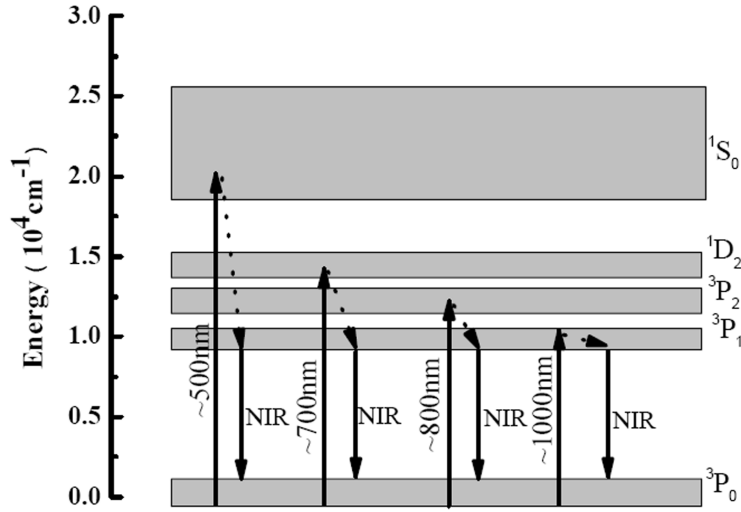


Figure 1.14: Energy level diagram for Bi^{3+} , which is proposed based on energy matching conditions (NIR: near infrared emission) [48].

be detected only from reduced $\text{Ba}_2\text{P}_2\text{O}_7:\text{Bi}$. Based on the radius and charge mismatch between the cation site and each of the species Bi^{3+} , Bi^{2+} , Bi^+ and Bi^0 as well as bismuth dimer ions, it was deduced that Bi^{3+} , Bi^{2+} and Bi^+ can readily substitute either for Ca^{2+} , Sr^{2+} or Ba^{2+} whereas Bi^0 can be incorporated only on Ba^{2+} sites and dimers fit into neither. If Bi^+ was the NIR emission center, NIR emission should have been present from all three compounds. This doesn't agree with the observations. Therefore, they suggests that two types of Bi^0 -species, each located on one of the two available Ba^{2+} lattice sites, are responsible for NIR photoemission.

1.3 Optical properties of Bi doped zeolites

Recently, our group developed a facile and novel strategy to realize strong, air-stable, long-lived, broadband (with a FWHM larger than 160 nm) and tunable NIR photoluminescence (PL) from bismuth compound-embedded FAU-type zeolites and their derived amorphous nanoparticles [79-82]. This method consists of a simple ion-exchange process and subsequent high-temperature annealing under Ar atmospheric conditions. The annealing temperature is gradually increased from 800 °C to 1000 °C. The zeolite structure can be well maintained after thermal treatment at 950 °C, and further increase leads to the destruction of zeolite structure. As shown in figure 1.15 (a), all samples show strong broadband emission from 930 to 1630 nm with the peak wavelength at 1145 nm, and with increasing temperature, the PL intensity monotonously increases. We also find that the PL shows spectral tunability: the peak wavelength and shape of PL closely depend on

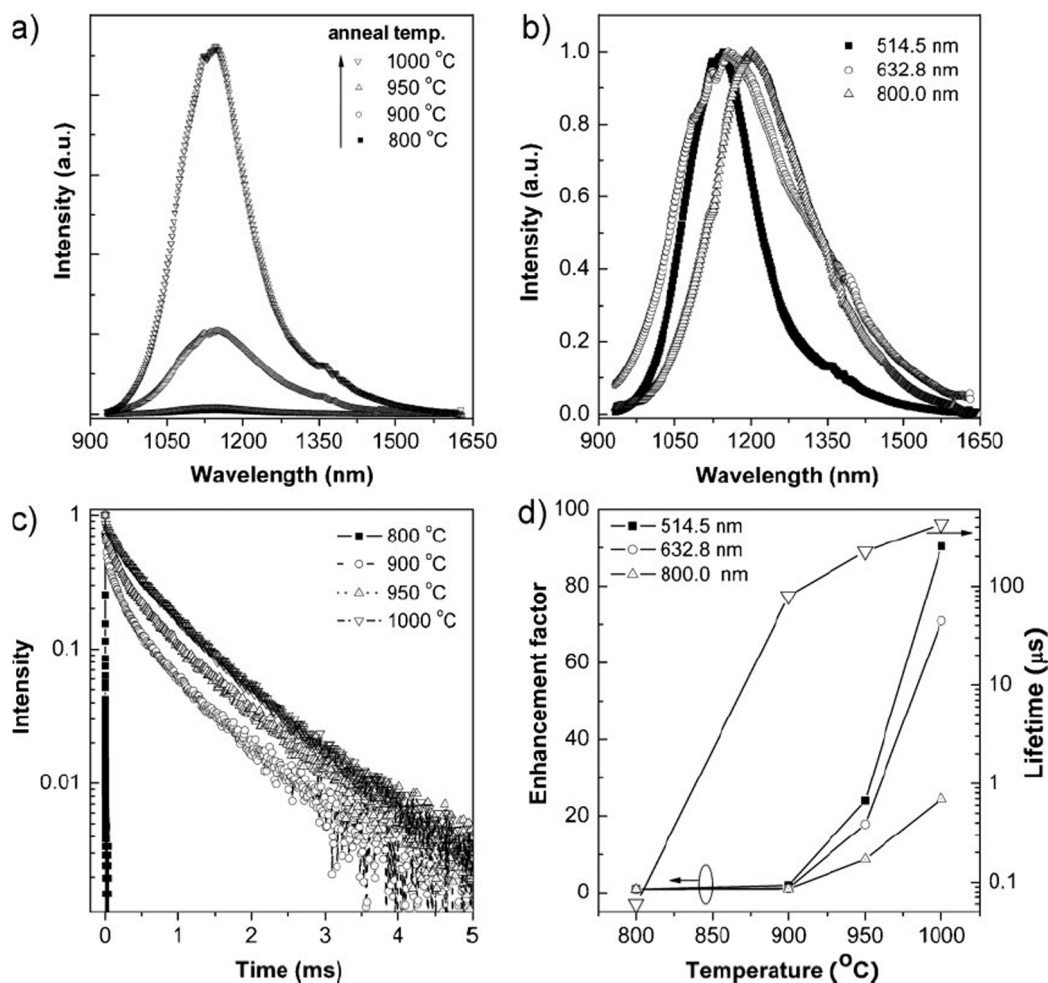


Figure 1.15: (a) Ultra-broadband NIR PL spectra of zeolites annealed at the indicated temperatures in an Ar atmosphere, which were excited by the 514.5 nm line of an Ar laser at a power of 0.014 mW. (b) Normalized NIR PL of the sample annealed at 1000 °C under 514.5, 632.8, and 800 nm excitation. (c) Fluorescence-decay curves of the annealed samples at 300 K. The detected wavelength is 1145 nm. (d) Left axis: annealing temperature dependence of enhancement factor of PL when excited at 514.5, 632.8, and 800 nm. Enhancement factors at different excitation wavelengths were calculated by dividing integrated PL intensities at different temperatures by that at 800 °C. Right axis: temperature dependence of $1/e$ lifetime at 1145 nm [79].

the excitation wavelength. The FWHMs of the PL spectra shown in figure 1.15 (b) are 268 and 221 nm under 632.8 and 800 nm excitation, respectively. In the mother zeolites, we did not detect any NIR PL under the same excitation conditions. Thus, we conclude that the PL is from bismuth-related infrared-active (BiIRA) centers instead of intrinsic structure defects of zeolites. Figure 1.15 (c) demonstrates the fluorescence-decay curves

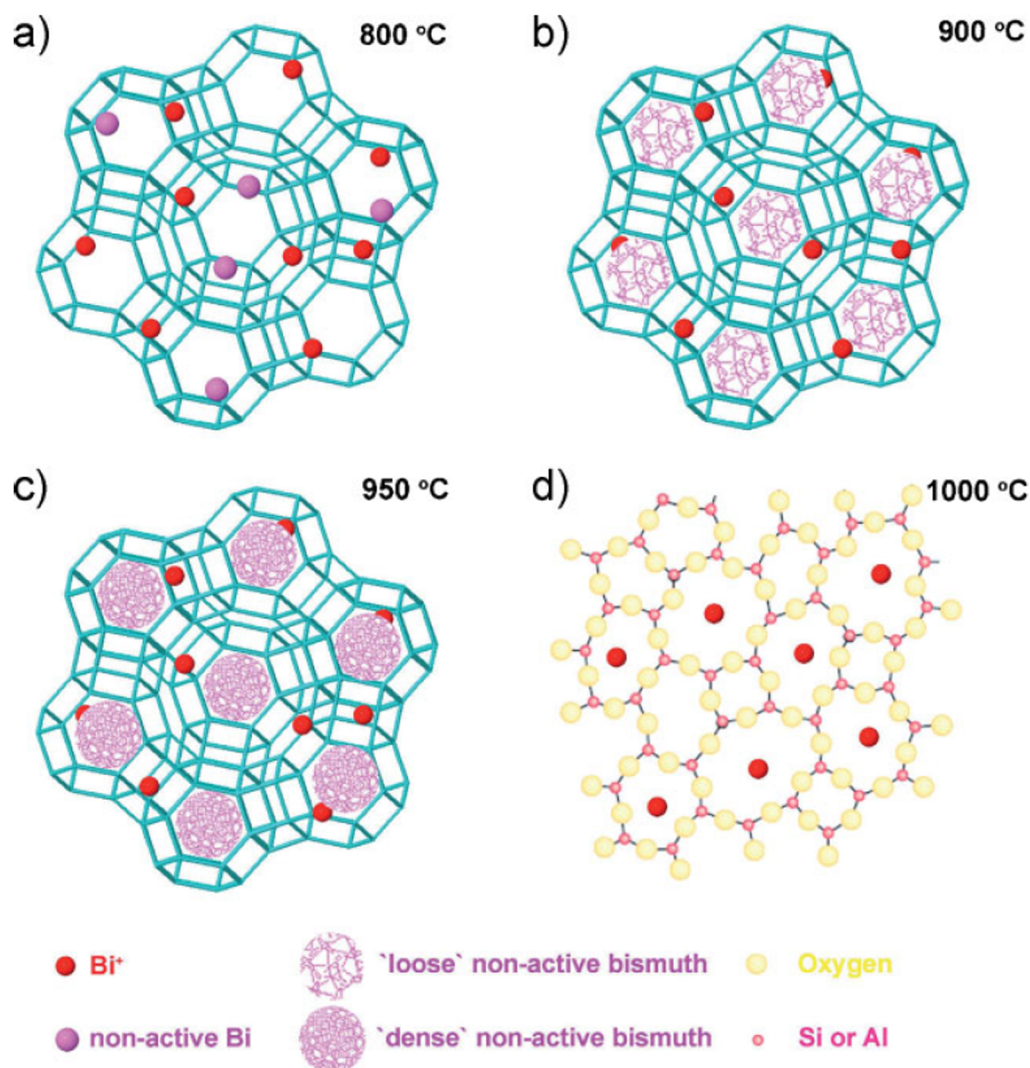


Figure 1.16: (a - c) Schematic illustration of the structure transformation of the zeolites annealed at different temperatures. (d) 2D representation of the structure of an aluminosilicate network. Note that "loose" and "dense" just represent small and large possibilities of sealing the pores of the zeolites with bismuth agglomerates [79].

of the annealed products. The $1/e$ lifetime at 300 K increases from 80 ns to 430 μ s from 800 to 1000 °C (figure 1.15 (d)). The quantum efficiency (QE) is also dependent on the annealing temperature; at 950 and 1000 °C, it is 38.1 and 72.8 %, respectively.

Interestingly, the properties of NIR emission of bismuth-doped glasses are similar to the results reported here, except that the PL property of bismuth-embedded zeolites is dependent on the annealing atmospheric conditions; the BiIRA centers can be destroyed when the zeolites are annealed in air or in a H_2/N_2 atmosphere. In Bi-doped zeolites annealed in air, Bi^{3+} ions form in the matrix, whereas in a H_2/N_2 atmosphere, bismuth

metal preferentially forms. Since Bi^{2+} ions are not infrared active, we suggest tentatively that the NIR luminescence derives from subvalent bismuth of Bi^+ .

Usually, coordinated water in optically activated materials can strongly affect the NIR emission efficiency of the emitters. Thermogravimetric (TG) analysis reveals that the water content in the annealed zeolites decreases notably with increasing annealing temperature. Note that the zeolites annealed at 900 and 950 °C contain much less water than that annealed at 800 °C. The crystallinity of the zeolites annealed 800, 900, and 950 °C does not show a large difference, which indicates that there should be other reasons for the decrease in water content. This becomes understandable if we further consider the physical properties, especially the thermal parameters, of bismuth compounds. The melting points of all inorganic bismuth compounds are below 820 °C. When the exchanged zeolites are annealed at high temperatures, on the one hand, bismuth-related dissociation reactions can easily take place; on the other hand, bismuth compounds have a chance to form agglomerates owing to bismuth migration into zeolite pores, which can partially block or totally seal the pores of the zeolites when the samples are suddenly cooled down (figure 1.16 (a)-(c)). The higher the annealing temperature, the higher the possibility of sealing the pores of the zeolites. This leads to a decrease of water content in the zeolites annealed at a relatively higher temperature. Most possibly, partial Bi^+ ions can be held in captivity totally in the sodalite cages and hexagonal prisms if the annealing temperature is high enough and water molecules have little chance to interact with them, which results in strong and long-lived NIR emission (figure 1.16 (d)).

Our group also investigated the effect of co-doping Al on the optical property of Bi doped zeolites [83]. The broadband NIR emission can be enhanced eight times in Bi-Al co-doped zeolites. The lifetimes of Bi-Al doped samples are much longer than that of bismuth doped one: with increasing aluminum and decreasing bismuth contents, the lifetime monotonously increases. The longest 1/e lifetime reaches as long as 695 μs , which is comparable to those reported in bulk glasses. The results further reveal that the NIR emission should be from subvalent bismuth infrared active centre, i.e., Bi^+ , instead of others. The existence of a charge imbalance environment caused by $[\text{AlO}_4/2]^-$ units in host materials is requisite to the formation of infrared-active Bi^+ , which is the main reason for the enhanced emission in Bi-Al doped high-silica zeolite derived nanoparticles.

1.4 Chapter Overview and Goal of this thesis

1.4.1 Photoluminescence properties of Bi doped zeolites

The goal of first part of this thesis is to reveal the structure and optical properties of Bi doped zeolites by changing doping concentration and after annealing at different at-

mosphere. In chapter 2, the dependence of doping concentration on the optical properties of Bi doped zeolites is investigated by X-ray diffraction, absorption, emission, excitation, decay time, and Raman spectroscopy. We find that the NIR emission intensity, full width at half maximum and decay time depend strongly on Bi doping concentration. The results prove the model that doped Bi acts not only as optically active centers, but also as pore-sealing substances to isolate the centers. The comparison of PL and Raman data suggests that in addition to previously proposed Bi_2O_3 , other Bi-related materials, probably Bi metal, play an important role to isolate the active centers. In chapter 3, we investigate the effect of annealing atmosphere on the optical properties of Bi doped zeolites by diffuse reflectance, steady state and time-resolved PL, and PL excitation measurements. The results reveal that zeolites can be used as an excellent host material to stabilize multiple Bi centers (Bi^{3+} , Bi^{2+} , and Bi-related NIR active centers) in the framework, which shows ultra-broadband emission from visible to NIR range. Annealing in N_2 leads to the partial conversion of Bi^{3+} ions into Bi^{2+} and Bi-related NIR active centers. Our results demonstrate that the broadband NIR emission may be attributed to the electronic transition of Bi low valence state, rather than a higher valence state.

1.4.2 Photoluminescence properties of Bi and lanthanide ions co-doped zeolites

The goal of the second part is to investigate the optical properties and energy transfer process between Bi and lanthanide ions (Er, Nd, Yb, and Eu) in zeolites. In chapter 4-6, we have shown that tunable and highly efficient broadband NIR luminescence can be realized in Er-Bi, Nd-Bi, and Yb-Bi co-doped zeolites. The intensity ratio of the two bands can be tuned by adjusting the concentration of lanthanide ions and excitation wavelength. Steady state and time-resolved PL, and PL excitation measurements indicate that two kinds of emitters coexist in the pores of zeolites, and that near infrared active bismuth simultaneously acts as a sensitizer of lanthanide ions. The findings may have potential applications in broadband fiber amplifier and biological imaging. In chapter 7, we investigate the optical properties of Eu doped zeolites by co-doping Bi. The addition of Bi^{3+} strongly enhances the red luminescence of Eu^{3+} ($^5\text{D}_0 \rightarrow ^7\text{F}_2$) in zeolites about 50 times, and the lifetime is significantly increased from 25.8 μs to 2.46 ms. The results reveal that the $\text{O}^{2-} \rightarrow \text{Eu}^{3+}$ charge transfer band and sensitization of Bi^{3+} ions distinctly enhances the excitation band of Eu^{3+} ions in the ultraviolet region. The energy transfer efficiency is estimated to be 78 %. It is expected that the present Eu-Bi co-doped zeolites have potential application in white-LEDs.

1.4.3 Simultaneously doping of different kinds of lanthanide ions in Bi doped zeolites

The goal of the third part is to simultaneously dope different kinds of lanthanide ions (Dy and Yb) in Bi doped zeolites and investigate the structural and optical properties. In chapter 8, ultraviolet-blue to NIR downconversion is investigated for the Dy³⁺ - Yb³⁺ couple in zeolites by steady-state and time-resolved photoluminescence spectra, and excitation spectra. Upon excitation of the ⁴F_{9/2} level of Dy³⁺, NIR quantum cutting could occur through a two-step energy transfer from one Dy³⁺ ion to two neighboring Yb³⁺ ions via an intermediate level. The energy transfer efficiency from the ⁴F_{9/2} level is estimated to be 42 %, and the intrinsic PL quantum efficiency of Yb³⁺ emission reaches 54 %. The findings may have potential application in enhancing the energy efficiency of the silicon-based solar cell.

References

- [1] R. M. Barrer, *Zeolites and Clays as Sorbents and Molecular Sieves*; Academic Press: London, (1978).
- [2] H. van Bekkum, E. M. Flanigen, J. C. Jansen, Eds. *Introduction to Zeolite Science and Practice*; Elsevier: Amsterdam, (1991).
- [3] P. K. Dutta, D. C. Shieh, *J. Phys. Chem.* **90**, 2331 (1986).
- [4] P. K. Dutta, D. C. Shieh, M. Puri, *J. Phys. Chem.* **91**, 2332 (1987).
- [5] S. Bordiga, D. Scarano, G. Spoto, A. Zecchina, C. Lamberti, C. O. Arean, *Vibrational Spectroscopy.* **5**, 69 (1993).
- [6] M. E. Davis, *Acc. Chem. Res.* **26**, 111 (1993).
- [7] K. Binnemans, *Chem. Rev.* **109**, 4283 (2009).
- [8] B. M. Lok, C. A. Messina, R. L. Patton, R. T. Gajek, T. R. Cannan, E. M. Flanigen, *J. Am. Chem. Soc.* **106**, 6092 (1984).
- [9] P. Enzel, T. Bein, *J. Phys. Chem.* **93**, 6270 (1989).
- [10] M. E. Davis, P. F. Lobo, *Chem. Mater.* **4**, 756 (1992).
- [11] J. A. Lercher, R. A. van Santen, H. Vinek, *Catalysis Letters.* **27**, 91 (1994).
- [12] M. E. Davis, *Micro. Mesopor. Mater.* **21**, 173 (1998).
- [13] F. J. Berry, M. Carbucicchio, A. Chiari, C. Johnson, E. A. Moore, M. Mortimer, F. F. J. Vetel, *J. Mater. Chem.* **10**, 2131 (2000).
- [14] L. F. Hazenkamp, A. M. H. Van der Veen, G. Blasse, *J. Chem. Soc. Faraday Trans.* **88**, 133 (1992).
- [15] S. B. Hong, E. W. Shin, S. H. Moon, C. H. Pyun, C. H. Kim, Y. S. Uh, *J. Phys. Chem.* **99**, 12274 (1995).

-
- [16] S. B. Hong, E. W. Shin, S. H. Moon, C. H. Pyun, C. H. Kim, Y. S. Uh, *J. Phys. Chem.* **99**, 12278 (1995).
- [17] U. Kynast, V. Weiler, *Adv. Mater.* **6**, 937 (1994).
- [18] W. Chen, R. Sammynaiken, Y. Huang, *J. Appl. Phys.* **88**, 1424 (2000).
- [19] D. Sendor, U. Kynast, *Adv. Mater.* **14**, 1570 (2002).
- [20] Y. Wada, T. Okubo, M. Ryo, T. Nakazawa, Y. Hasegawa, S. Yanagida, *J. Am. Chem. Soc.* **122**, 8583 (2000).
- [21] M. Ryo, Y. Wada, T. Okubo, T. Nakazawa, Y. Hasegawa, S. Yanagida, *J. Mater. Chem.* **12**, 1748 (2002).
- [22] J. Rocha, L. D. Carlos, *Curr. Opin. Solid State Mater. Sci.* **7**, 199 (2003).
- [23] M. Lezhnina, F. Laeri, L. Benmouhadi, U. Kynast, *Adv. Mater.* **18**, 280 (2006).
- [24] G. Calzaferri, K. Lutkouskaya, *Photochem. Photobiol. Sci.* **7**, 879 (2008).
- [25] O. A. Yeschenko, I. M. Dmitruk, S. V. Koryakov, I. P. Pundyk, Y. A. Barnakov, *Solid State Commun.* **133**, 109 (2005).
- [26] G. De Cremer, Y. Antoku, M. B. J. Roeffaers, M. Sliwa, J. Van Noyen, S. Smout, J. Hofkens, D. E. De Vos, B. F. Sels, T. Vosch, *Angew. Chem. Int. Ed.* **47**, 2813 (2008).
- [27] G. De Cremer, E. Coutino-Gonzalez, M. B. J. Roeffaers, B. Moens, J. Ollevier, M. Van der Auweraer, R. Schoonheydt, P. A. Jacobs, F. C. De Schryver, J. Hofkens, D. E. De Vos, B. F. Sels, T. Vosch, *J. Am. Chem. Soc.* **131**, 3049 (2009).
- [28] A. Monguzzi, G. Macchi, F. Meinardi, R. Tubino, M. Burger, G. Calzaferri, *Appl. Phys. Lett.* **92**, 123301 (2008).
- [29] A. Mech, A. Monguzzi, F. Meinardi, J. Mezyk, G. Macchi, R. Tubino, *J. Am. Chem. Soc.* **132**, 4574 (2010).
- [30] Y. Wang, H. Li, L. Gu, Q. Gan, Y. Li, G. Calzaferri, *Micropor. Mesopor. Mater.* **121**, 1 (2009).
- [31] H. Wu, X. Yang, X. Yu, J. Liu, H. Yang, H. Lv, K. Yin, *J. Alloys. Compd.* **480**, 867 (2009).
- [32] G. N. van den Hoven, J. H. Shin, A. Polman, S. Lombardo, S. U. Campisano, *J. Appl. Phys.* **78**, 2642 (1995).

- [33] M. Fujii, M. Yoshida, Y. Kanzawa, S. Hayashi, K. Yamamoto, *Appl. Phys. Lett.* **71**, 1198 (1997).
- [34] J. M. Sousa, O. G. Okhotnikov, *Appl. Phys. Lett.* **74**, 1528 (1999).
- [35] D. Wei, T. Li, Y. Zhao, S. Jian, *Opt. Lett.* **25**, 1150 (2000).
- [36] A. Cabasse, B. Ortac, G. Martel, A. Hideur, J. Limpert, *Opt. Express.* **16**, 19322 (2008).
- [37] L. Huang, A. Jha, S. Shen, X. Liu, *Opt. Express.* **12**, 2429 (2004).
- [38] Y. Miyazawa, T. Sugawa, Y. Fukusaku, *Optical Amplifiers and Their Applications* (Optical Society of America, Washington DC, 1991), PDP, PD1.
- [39] H. Kidorf, K. Rottwitt, M. Nissov, M. Ma, E. Rabarijaona, *Photonics Technology Letters.* **11**, 530 (1999).
- [40] C. R. S. Fludger, V. Handerek, R. J. Mears, *Journal of Lightwave Technology.* **19**, 1140 (2001).
- [41] M. N. Islam, *Journal of Selected Topics in Quantum Electronics.* **8**, 548 (2002).
- [42] K. Murata, Y. Fujimoto, T. Kanabe, H. Fujita, M. Nakatsuka, *Fusion Eng. Des.* **44**, 437 (1999).
- [43] Y. Fujimoto, M. Nakatsuka, *Appl. Phys. Lett.* **82**, 3325 (2003).
- [44] M. Peng, J. Qiu, D. Chen, X. Meng, I. Yang, X. Jiang, C. Zhu, *Opt. Lett.* **29**, 1998 (2004).
- [45] E. Dianov, V. Dvoyrin, V. Mashinsky, A. Umnikov, M. Yashkov, A. Guryanov, *Quantum Electron.* **35**, 1083 (2005).
- [46] Y. Fujimoto, M. Nakatsuka, *Jpn. J. Appl. Phys.* **40**, L279 (2001).
- [47] X. Meng, J. Qiu, M. Peng, D. Chen, Q. Zhao, X. Jiang, C. Zhu, *Opt. Express* **13**, 1628 (2005).
- [48] X. Meng, J. Qiu, M. Peng, D. Chen, Q. Zhao, X. Jiang, C. Zhu, *Opt. Express* **13**, 1635 (2005).
- [49] X. Meng, M. Peng, D. Chen, L. Yang, X. Jiang, C. Zhu, J. Qiu, *Chin. Phys. Lett.* **22**, 615 (2005).
- [50] M. Peng, X. Meng, D. Chen, J. Qiu, *Appl. Phys. Lett.* **87**, 066103 (2005).

- [51] H. Xia, X. Wang, *Appl. Phys. Lett.* **89**, 051917 (2006).
- [52] T. Suzuki, Y. Ohishi, *Appl. Phys. Lett.* **88**, 191912 (2006).
- [53] J. Ren, J. Qiu, D. Chen, C. Wang, X. Jiang, C. Zhu, *J. Mater. Res.* **22** 1954 (2007).
- [54] T. Murata, T. Mouri, *J. Non-Cryst. Solids* **353**, 2403 (2007).
- [55] G. Yang, D. Chen, J. Ren, Y. Xu, H. Zeng, Y. Yang, G. Chen, *J. Am. Ceram. Soc.* **90**, 3670 (2007).
- [56] B. Denker, B. Galagan, V. Osiko, S. Sverchkov, E. Dianov, *Appl. Phys. B* **87**, 135 (2007).
- [57] S. Zhou, G. Feng, J. Bao, H. Yang, J. Qiu, *J. Mater. Res.* **22** (6), 1435 (2007).
- [58] T. Murata, T. Mouri, *J. Non-Cryst. Solids* **353**, 2407 (2007).
- [59] M. Peng, D. Chen, J. Qiu, X. Jiang, C. Zhu, *Opt. Mater.* **29**, 556 (2007).
- [60] T. Ohkura, Y. Fujimoto, M. Nakatsuka, S. Young-Seok, *J. Am. Ceram. Soc.* **90**, 3596 (2007).
- [61] J. Ren, G. Dong, S. Xu, R. Bao, J. Qiu, *J. Phys. Chem. A* **112**, 3036 (2008).
- [62] V. Sokolov, V. Plotnichenko, E. Dianov, *Opt. Lett.* **33**, 1488 (2008).
- [63] A. Okhrimchuk, L. Butvina, E. Dianov, N. Lichkova, V. Zagorodnev, K. Boldyrev, *Opt. Lett.* **33**, 2182 (2008).
- [64] E. Kustov, L. Bulatov, V. Dvoyrin, V. Mashinsky, *Opt. Lett.* **34**, 1549 (2009).
- [65] M. Peng, L. Wondraczek, *Opt. Lett.* **34** (19), 2885 (2009).
- [66] J. Ruan, L. Su, J. Qiu, D. Chen, J. Xu, *Opt. Express* **17**, 5163 (2009).
- [67] L. Su, J. Yu, P. Zhou, H. Li, L. Zheng, Y. Yang, F. Wu, H. Xia, J. Xu, *Opt. Lett.* **34**, 2504 (2009).
- [68] I. Razdobreev, V. Ivanov, L. Bigot, M. Godlewski, E. Kustov, *Opt. Lett.* **34**, 2691 (2009).
- [69] M. Peng, G. Dong, L. Wondraczek, L. Zhang, N. Zhang, J. Qiu, *J. Non-Cryst Solids.* **357**, 2241 (2011).
- [70] R. Quimby, R. Shubochkin, T. Morse, *Opt. Lett.* **34**, 3181 (2009).

- [71] M. Hughes, T. Akada, T. Suzuki, Y. Ohishi, D. Hewak, *Opt. Express* **17**, 19345 (2009).
- [72] G. Blasse, A. Meijerink, M. Nomes, J. Zuidema, *J. Phys. Chem. Solids* **55**, 171 (1994).
- [73] G. Blasse, *J. Lumin.* **72**, 129 (1997).
- [74] A. M. Srivastava, *J. Lumin.* **78**, 239 (1998).
- [75] W. Dong, C. Zhu, *J. Phys. Chem. Solids.* **64**, 265 (2003).
- [76] Y. Xia, F. Huang, W. Wang, A. Wang, J. Shi, *J. Alloys Compd.* **476**, 534 (2009).
- [77] M. Peng, N. Da, S. Krolikowski, A. Stiegelschmitt, L. Wondraczek, *Opt. Express.* **17**, 21169 (2009).
- [78] M. Peng, B. Sprenger, M. Schmidt, H. Schwefel, L. Wondraczek, *Opt. Express* **18**, 12852 (2010).
- [79] H. Sun, A. Hosokawa, Y. Miwa, F. Shimaoka, M. Fujii, M. Mizuhata, S. Hayashi, S. Deki, *Adv. Mater.* **21**, 3694 (2009).
- [80] H. Sun, Y. Miwa, F. Shimaoka, M. Fujii, A. Hosokawa, M. Mizuhata, S. Hayashi, S. Deki, *Opt. Lett.* **34**, 1219 (2009).
- [81] H. Sun, Y. Sakka, Y. Miwa, N. Shirahata, M. Fujii, H. Gao, *Appl. Phys. Lett.* **97**, 131908 (2010).
- [82] H. Sun, M. Fujii, Y. Sakka, Z. Bai, N. Shirahata, L. Zhang, Y. Miwa, H. Gao, *Opt. Lett.* **35**, 1743 (2010).
- [83] H. Sun, T. Hasegawa, M. Fujii, F. Shimaoka, Z. Bai, M. Mizuhata, S. Hayashi, S. Deki, *Opt. Express.* **17**, 6239 (2009).

Part I

Photoluminescence properties of Bi doped zeolites

Chapter 2

Effect of doping concentration on broadband near-infrared emission of Bi doped zeolites

In this chapter, a series of Bi doped zeolites are prepared by an ion-exchange process by changing doping concentration in a wide range, and the optical properties are investigated. The near-infrared photoluminescence (PL) intensity, full width at half maximum and decay time depend strongly on Bi doping concentration. The PL intensity increases 178 times when the concentration is changed from 0.3 to 1.5 at.%. At the same time, the lifetime increases from 83 to 527 μ s. The results prove the model that doped Bi acts not only as optically active centers, but also as pore-sealing substances to isolate the centers. The comparison of PL and Raman data suggests that in addition to previously proposed Bi_2O_3 , other Bi-related materials, probably Bi metal, play an important role to isolate the active centers.

2.1 Introduction

With the rapid development of optical telecommunication, there exists an urgent requirement to develop broadband fiber amplifiers and laser sources to achieve more efficient wavelength division multiplexing transmission network with higher capacity and faster bit rate. Recently, the telecommunication transmission window has been extended to the range from 1.2 to 1.7 μm by the elimination of OH in silica fibers. As a result, exploring a new luminescent material which can cover the whole telecommunication window has attracted great attention [1-8]. More recently, Fujimoto and Nakatsuka reported a

broadband near-infrared (NIR) emission from Bi-doped silica glass and realized its optical amplification at 1300 nm with 800 nm excitation [1,2]. Subsequently, the broadband NIR emissions of Bi were investigated in different host materials, such as glasses [3,4], crystals [5,6], and zeolites [7,8].

Zeolites are microporous crystalline aluminosilicates with nanosized pores. Their framework is composed of SiO_4 and AlO_4 tetrahedra units by sharing oxygen between every two consecutive units, and cations located inside channels or cavities to balance negative charges in the framework. For a long time, zeolites played indispensable roles in many technological and economical applications, such as catalysis, ion exchange, and separations [9,10]. Recently, zeolites acting as host materials of optically active guests have attracted much attention for constructing novel materials designed at nanosized levels, because of their low-frequency vibrational framework, regularly spaced nanochannels and nanopores, and inexpensive price [11-27]. At present, visible luminescence with very high efficiencies from rare-earth-functionalized zeolites has been reported [11,12]. However, it is not easy to observe efficient NIR emission in zeolites, due to the strong nonradiative relaxation of the excited energies by water molecules within the pores of the zeolites host [13,14]. Until now, several strategies have been reported to overcome this difficulty [7,15-19]. Very recently, Sun et al. [7] reported efficient broadband NIR luminescence from Bi doped zeolites. They proposed that effective isolation of Bi-related active centers from environment by Bi_2O_3 agglomerates results in the efficient NIR luminescence [27]. In this process, the Bi concentration is a very important parameter to achieve the maximum luminescence efficiency because doped Bi acts not only as NIR luminescence centers but also as pore-sealing substances. However, the effect of doping concentration on optical properties in Bi doped zeolites has not been investigated in detail.

In this work, we investigate the optical properties of Bi doped zeolites by changing doping concentration in a very wide range. The measurement results show that NIR photoluminescence (PL) intensity, full width at half maximum (FWHM) and decay time are strongly dependent on Bi concentration in zeolites. Highly efficient NIR emission from Bi-related active centers can be realized by increasing Bi concentration to 1.2 at.%, and further increase causes the shortening of lifetime. It is also proposed that Bi_2O_3 and bismuth metal agglomerates are formed in zeolites, and separate Bi-related active centers from quenchers.

2.2 Experimental details

The samples used in this study were synthesized by an ion-exchange method. The NH_4 form of faujasite (FAU) type zeolite was purchased from Tosoh Co. Japan (Zeolite Y, $\text{SiO}_2/\text{Al}_2\text{O}_3 = 7$, grain size 700 - 1000 nm). Zeolites were stirred in a 10 - 80 mM aqueous

solution of Bi^{3+} prepared from $\text{Bi}(\text{NO}_3)_3 \cdot 5\text{H}_2\text{O}$ for 24 h to exchange NH_4 ions with Bi^{3+} ions. The products were removed by centrifugation, then washed with deionized water, and dried in air at 120 °C. The Bi doped zeolites were calcined at 900 °C for 1 h in N_2 atmospheric condition. All samples were exposed to the laboratory atmosphere prior to measurements.

The prepared products were characterized by an X-ray diffractometer (Rigaku-TTR/S2, $\lambda = 1.54056 \text{ \AA}$), and the crystallinity of all samples is estimated from the ratio of the sums of the intensities of the peaks (111), (311), (331), (511), (440), (533), and (642) of the doped zeolites and the undoped-zeolites, by following a usual procedure [28,29]. Bi concentration was determined by energy-dispersive X-ray spectroscopy (EDS). Hereafter, the samples were denoted as Bi-X, where X is bismuth atomic concentrations in the final products. PL measurements were carried out with the excitation of a 488 nm line from an Ar^+ laser and a 355 nm line from a He-Cd laser. The signal was analyzed by a single grating monochromator and detected by liquid-nitrogen-cooled InGaAs and CCD detectors. PL excitation spectrum was obtained by a NIR PL spectrophotometer (Bunkoh-Keiki Co. Ltd., Tokyo, Japan) equipped with an InGaAs detector. The absorption spectrum was measured by a Jasco V-570 UV-VIS-NIR spectrophotometer. Time-resolved luminescence measurements were performed by detecting the modulated luminescence signal with a photomultiplier tube (Hamamatsu, R5509-72), and then analyzing the signal with a photon-counting multichannel scaler. The excitation source for decay time measurements was 488 nm light from an optical parametric oscillator (OPO) pumped by the third harmonic of a Nd:YAG laser (pulse width 5 ns, repetition frequency 20Hz). Raman spectra were recorded by using a SPEX 1877 triple spectrometer under the excitation of a 514.5 nm line from the Ar^+ laser. All the measurements were carried out at room temperature.

2.3 Results and discussion

The color of the powder samples turned gradually from white to shallow pink with increasing concentration of Bi ions. Figure 2.1 shows the XRD patterns of undoped-zeolites and Bi doped zeolites (Bi-0.9). The comparison of two spectra indicates that no new diffraction peak develops after doping and thermal treatment. However, a broad background appears and the peak intensity decreases in Bi doped zeolites. The crystallinity of all samples is calculated to be 92 % (Bi-0.3), 78 % (Bi-0.6), 67 % (Bi-0.9), 61 % (Bi-1.2), and 54 % (Bi-1.5). The results reveal a decreasing trend of crystallinity as the doping concentration increases. However, the zeolite structure is still maintained even in the highest doping concentration sample.

The NIR PL spectra of Bi doped zeolites excited at 488 nm are shown in figure 2.2

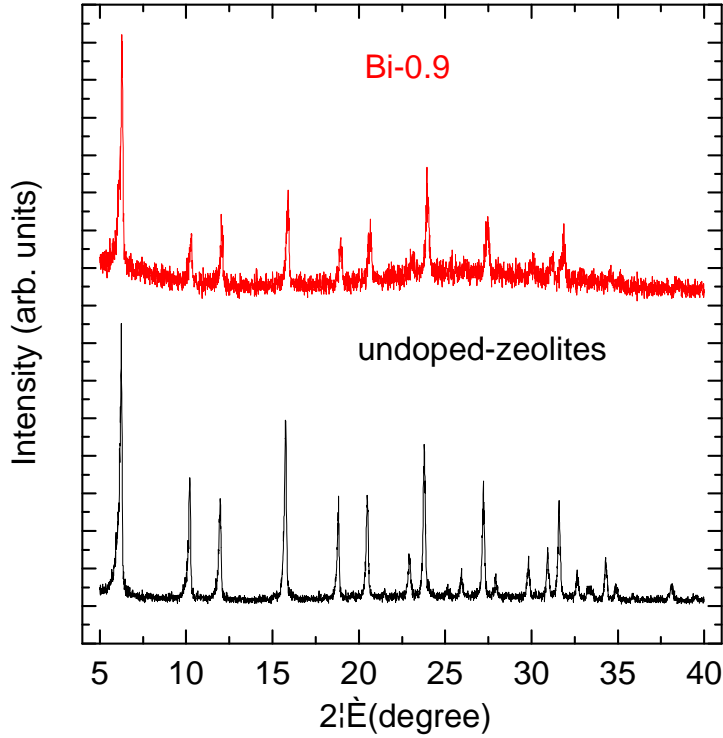


Figure 2.1: X-ray diffraction patterns of undoped-zeolites and Bi doped zeolites (Bi-0.9).

(a). All samples show broad NIR emission in the range of 930 - 1480 nm with the peak wavelength of 1145 nm. The broad PL is usually assigned to Bi^+ , but it is not finally proved [5,8]. Thus, we ascribe the origin of the luminescence to Bi-related active centers here. Figure 2.2 b shows PL intensity at 1145 nm as a function of Bi concentration. The PL intensity is normalized with respect to that of Bi-0.3. By increasing Bi concentration, PL intensity significantly increases; it increases about one order of magnitude from Bi-0.3 to Bi-0.6. Above the concentration, the intensity increases even steeper. When the Bi concentration reaches 1.5 at.%, the PL intensity increases 178 times comparing with that in Bi-0.3 sample. Figure 2.2 (b) also shows the dependence of FWHM on Bi concentration. The FWHM increases gradually until the Bi concentration reaches 1.2 at.%, and then significantly increases to 212 nm in the Bi-1.5 sample.

The increase of FWHM with increasing Bi concentration can be explained as follows. As reported in the literature, the spectral properties of Bi ions are very sensitive to their local environment [3]. FAU-type zeolites consist of three kinds of units (α -cages, the

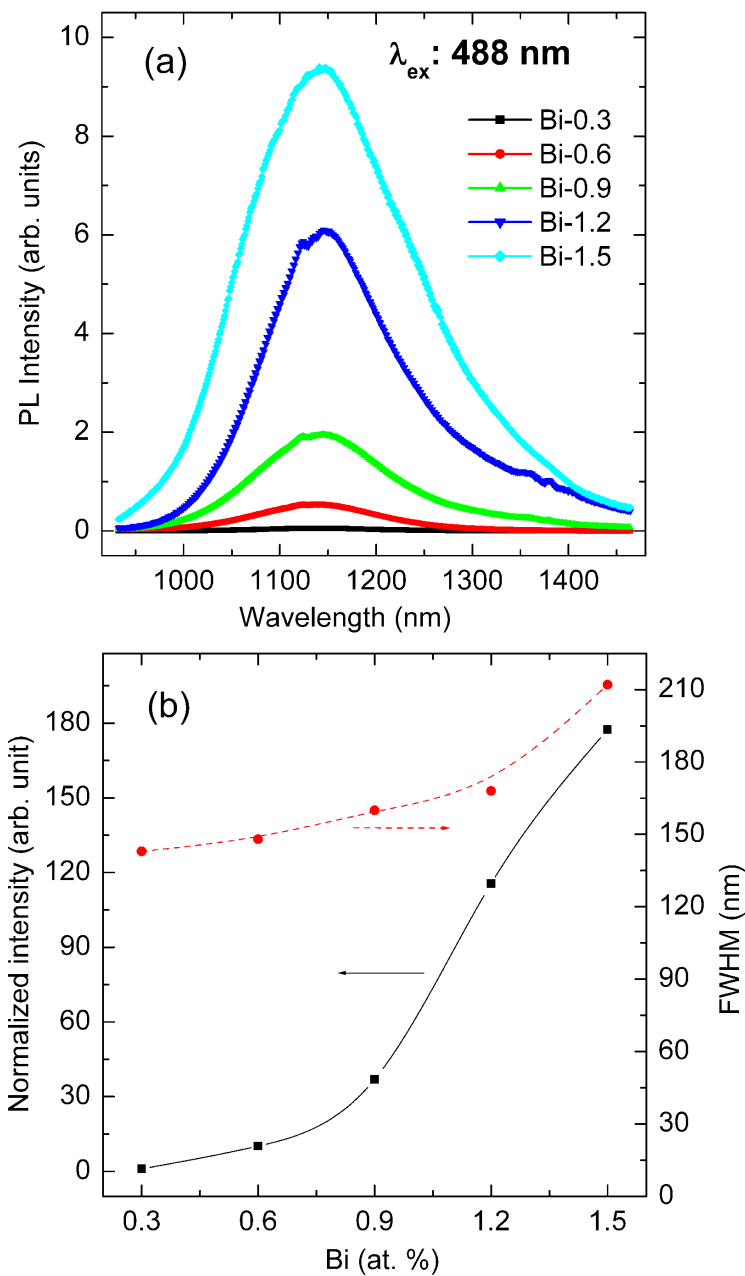


Figure 2.2: (a) PL spectra of Bi doped zeolites in the NIR range, excited at 488 nm. (b) The normalized intensity at 1145 nm (left scale) and full width at half maximum (right scale) as a function of Bi concentration. Note that the arrows were drawn for guiding the eye.

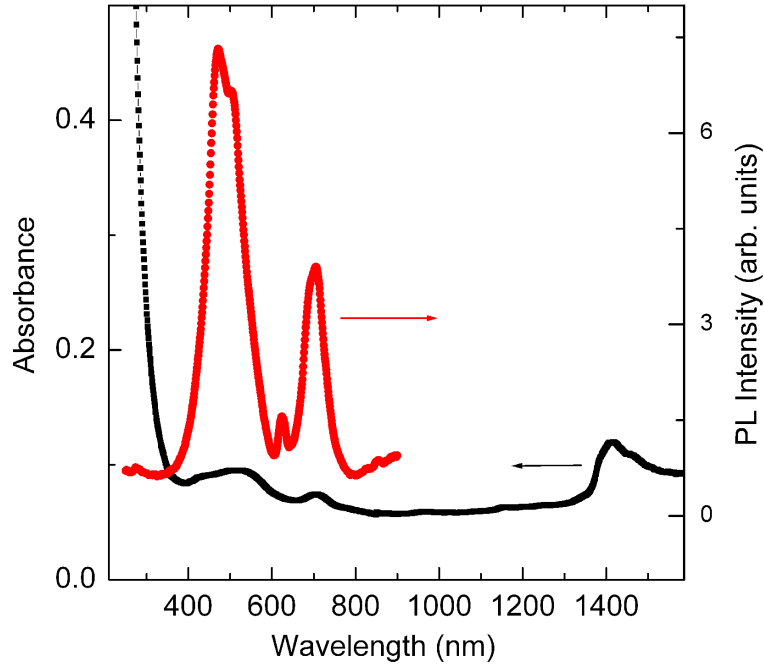


Figure 2.3: Absorption spectrum of Bi-1.2 sample (left scale), and the excitation spectra of the corresponding sample detected at 1145 nm (right scale). Note that the arrows were drawn for guiding the eye.

sodalite cages, and the double six-ring hexagonal prisms), and have several sites (such as SI, SI', SII, SII', and SIII sites) for cations [14]. It is possible that some ion-exchange sites are favourable for Bi ions, and thus Bi locates at these positions for low concentration samples. By increasing doping concentration, Bi ions occupy other sites with different crystal field strength, which results in the broader emission band of Bi ions.

The absorption spectrum of Bi-1.2 sample is shown in figure 2.3. Three absorption bands at 500 nm, 700 nm, and 1400 nm are observed. There have been reports on Bi doped silica glasses in which absorption spectra were composed of three bands occurring at 500 nm, 700 nm, and 800 nm [3]. Therefore, in our sample, the absorption bands at 500 nm and 700 nm can be assigned to Bi-related active centers. The strong absorption at 1400 nm is considered to be due to the coordinated water in zeolites. The excitation spectrum of the corresponding sample is also shown in figure 2.3. Two strong excitation bands at 470 nm and 700 nm are detected, which almost coincide with the absorption spectrum. In addition, a weak peak at 620 nm is observed.

Figure 2.4 (a) shows the PL decay curves of Bi doped zeolites detected at 1145 nm. These curves could not be fitted by single-exponential decay, thus the mean lifetime (τ_m)

is calculated by

$$\tau_m = \int_{t_0}^{\infty} [I(t)/I_0]d(t), \quad (2.1)$$

Where $I(t)$ is the luminescence intensity as a function of time t and I_0 is the maximum of $I(t)$ that occurs at the initial time t_0 . As shown in the figure, the longest lifetime reaches $542 \mu\text{s}$, which is comparable to those reported for Bi doped glasses and crystals [1,4,5]. It can be seen that the decay curves of Bi doped zeolites show a fast drop at the beginning, followed by a single-exponential slow component. To further study the relation between the fast and slow components, we fitted all curves by double-exponential decay

$$I(t) = A_{fast} \exp\left(-\frac{t}{\tau_{fast}}\right) + A_{slow} \exp\left(-\frac{t}{\tau_{slow}}\right), \quad (2.2)$$

Figure 2.4 (b) presents the τ_{fast} and τ_{slow} . The τ_{slow} is almost constant ($662 \mu\text{s}$) until Bi concentration reaches 1.2 at.%, and slightly decreases to $596 \mu\text{s}$ at the highest Bi concentration sample. The very long lifetime of the slow component suggests that it is an intrinsic radiative lifetime of Bi-related active centers in zeolites. The reason for the decrease of τ_{slow} at high concentration will be discussed later. In contrast to this, the τ_{fast} increases significantly from 3 to $80 \mu\text{s}$ by increasing Bi concentration. Figure 2.4 (c) shows the evolution of A_{fast} and A_{slow} for different Bi concentration samples. With the increase of Bi concentration, an anticorrelation is observed between A_{fast} and A_{slow} .

The PL decay data suggest that Bi-related active centers in zeolites can be classified into two categories and the ratio of the two groups depends on the Bi concentration. The first one is Bi active centers which are almost completely isolated from non-radiative relaxation processes and have very long luminescence lifetime. The other group is the Bi active centers contributing to the fast component of decay curves. With increasing Bi concentration, the lifetime becomes longer and the ratio of these centers decreases. These results indicate that the fast decay component is controlled by non-radiative relaxation processes and they are effectively suppressed by increasing Bi concentration. This is consistent with the significant enhancement of the PL intensity with the increase of Bi concentration.

The most probable origin of the nonradiative relaxation process in the present system is the excitation of the high-frequency vibrational modes of coordinated water in the zeolite cages. As is known, the coordinated water mainly exists in the supercages, thus it is probable that the Bi-related active centers in supercages mainly contribute to the fast decay component. Since the PL intensity increases and the fast decay component decreases with increasing Bi concentration, Bi not only acts as NIR luminescence centers but also as substances to protect Bi active centers from coordinated water.

In previous papers, our group proposed a model that Bi ions migrate into the pores of zeolites by ion-exchange process, and after subsequent high temperature annealing,

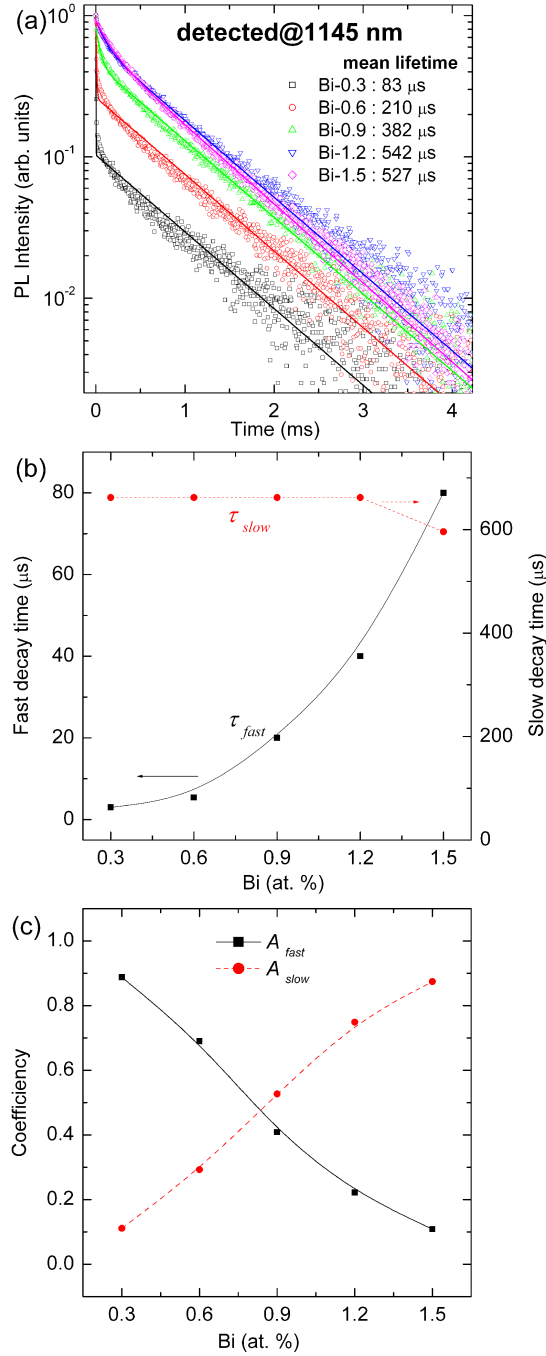


Figure 2.4: (a) PL decay curves of Bi doped samples detected at 1145 nm. All curves are fitted by double-exponential decay equation, and fitted results are also shown, respectively. (b) The dependence of the τ_{fast} and the τ_{slow} on Bi doping concentration. (c) The dependence of the A_{fast} and A_{slow} on Bi doping concentration.

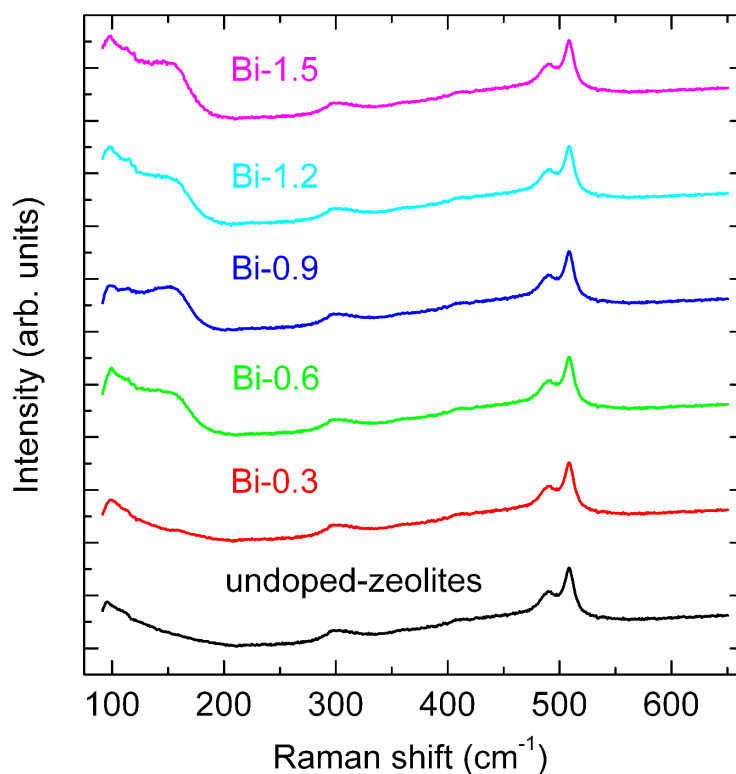


Figure 2.5: Raman spectra of Bi doped zeolites with different doping concentration. Raman spectrum of undoped-zeolites is shown as a reference.

parts of Bi ions are converted to Bi-related active centers, and the other parts form Bi_2O_3 agglomerates, due to the low melting point of bismuth compounds [7,27]. The Bi_2O_3 agglomerates act as a blockage to seal the pores of zeolites, which can avoid the admission of coordinated water into the pores of zeolites. To verify the model, we measured the doping concentration dependence of Raman spectra in Bi doped zeolites. As shown in figure 2.5, all samples show characteristic scattering bands of zeolites in the range of 200 - 600 cm^{-1} , which can be assigned to the Si-O-Si or Si-O-Al bending modes [30,31]. In addition, a new broad band at 150 cm^{-1} appears when the Bi concentration is equal or larger than 0.6 at.%, which can be assigned to Bi_2O_3 [27,32]. It can be seen that the change of Raman spectra in this Bi concentration range is very small, which suggests the tiny difference of the Bi_2O_3 amount in these samples.

It is reported that the emission bands of Bi^{3+} occurs in the ultraviolet, green, or even red wavelength regions with variation of host materials [33]. To confirm the Raman data, we measured the emission spectra of Bi doped zeolites in the visible range, excited by 325 nm. As shown in figure 2.6 (a), all samples show a broad emission band in the range of 400 - 750 nm, which can be assigned to the electronic transition of Bi^{3+} . It is also observed that the peak position slightly shifts from 500 nm to 526 nm with increasing Bi

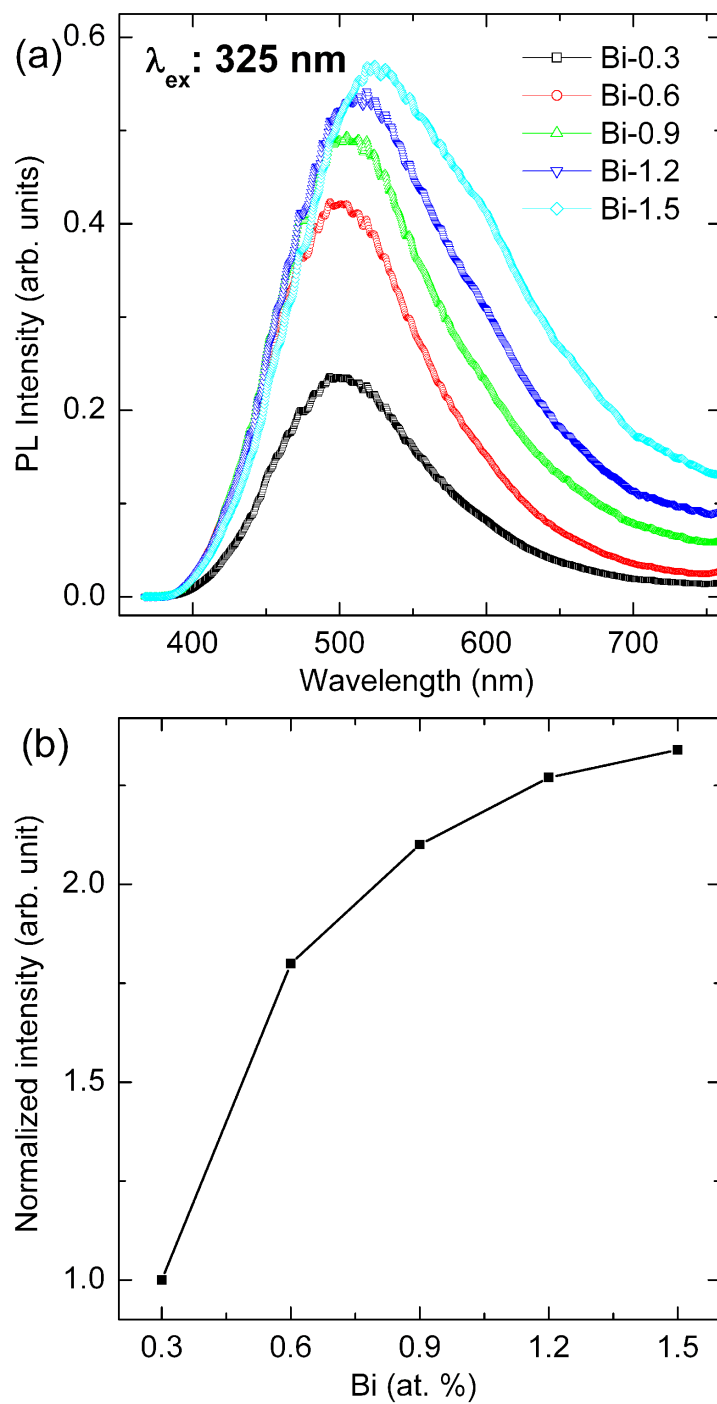


Figure 2.6: (a) PL spectra of Bi doped zeolites in the visible range, excited at 325 nm. (b) The normalized intensity as a function of Bi concentration.

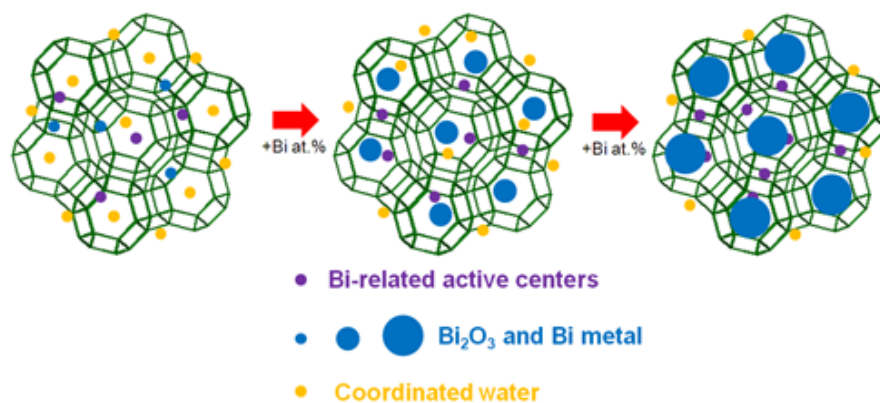


Figure 2.7: Schematic illustration of Bi doped zeolites at different doping concentration.

concentration from 0.3 at.% to 1.5 at.%. Figure 2.6 (b) shows the dependence of visible PL intensity on Bi concentration. The PL intensity is normalized with respect to that of Bi-0.3. As is shown, the Bi^{3+} emission intensity is not linearly increased by increasing Bi concentration. The PL intensity seems to be saturated slowly, suggesting the small change of Bi_2O_3 amount in high Bi concentration samples, which is consistent with the Raman data.

When the Bi concentration is 0.3 at.%, the amount of Bi is too small, so that Bi_2O_3 amount is not enough to isolate Bi-related active centers from coordinated water. When the Bi concentration is equal or larger than 0.6 at.%, the NIR PL intensity increases steeply and the fast component in decay curves is gradually suppressed. In contrast to this, the increase of the visible PL from Bi_2O_3 is very small. The results combined with the Raman data strongly suggests that Bi exists not only as Bi_2O_3 , but also as another form in the high doping concentration samples, which also can act as a blockage substance. As is known, Bi_2O_3 can be partially converted into atomic bismuth metal at high temperature [34]. Based on measurement results, we surmise that the mixtures of Bi_2O_3 and bismuth metal are contributable to seal the pores of zeolites, which is shown as figure 2.7. When the Bi concentration exceeds 1.2 at.%, the lifetime of the slow component becomes shorter, which is probably due to concentration quenching effect or deactivation by Bi metal.

2.4 Conclusion

The mechanism of efficient NIR emission from Bi doped zeolites was studied by analyzing PL and Raman scattering data for the samples with different Bi concentrations. The NIR PL intensity increases significantly with increases Bi concentration; it increases 178 times when the concentration is changed from 0.3 to 1.5 at.%. The significant increase of the intensity is accompanied by the lengthening of the lifetime. The observed

Bi concentration dependence of the PL data clearly indicates that doped Bi acts not only as optically active centers, but also as pore-sealing substances to isolate the centers. Therefore, in this system, Bi concentration is a very important parameter to have the maximum luminescence efficiency. The comparison of PL and Raman data suggests that in addition to previously proposed Bi_2O_3 , other Bi-related materials, probably Bi metal, play an important role to isolate the active centers.

References

- [1] Y. Fujimoto, M. Nakatsuka, *Jpn. J. Appl. Phys.* **40**, L279 (2001).
- [2] Y. Fujimoto, M. Nakatsuka, *Appl. Phys. Lett.* **82**, 3325 (2003).
- [3] X. Meng, J. Qiu, M. Peng, D. Chen, Q. Zhao, X. Jiang, C. Zhu, *Opt. Express* **13**, 1635 (2005).
- [4] T. Suzuki, Y. Ohishi, *Appl. Phys. Lett.* **88**, 191912 (2006).
- [5] L. Su, J. Yu, P. Zhou, H. Li, L. Zheng, Y. Yang, F. Wu, H. Xia, J. Xu, *Opt. Lett.* **34**, 2504 (2009).
- [6] M. Peng, B. Sprenger, M. Schmidt, H. L. Schwefel, L. Wondraczek, *Opt. Express* **18**, 12852 (2010).
- [7] H. Sun, A. Hosokawa, Y. Miwa, F. Shimaoka, M. Fujii, M. Mizuhata, S. Hayashi, S. Deki, *Adv. Mater.* **21**, 3694 (2009).
- [8] H. Sun, Y. Miwa, F. Shimaoka, M. Fujii, A. Hosokawa, M. Mizuhata, S. Hayashi, S. Deki, *Opt. Lett.* **34**, 1219 (2009).
- [9] M. E. Davis, *Acc. Chem. Res.* **26**, 111 (1993).
- [10] L. Tosheva, V. P. Valtchev, *Chem. Mater.* **17**, 2494 (2005).
- [11] U. Kynast, V. Weiler, *Adv. Mater.* **6**, 937 (1994).
- [12] J. Rocha, L. D. Carlos, *Curr. Opin. Solid State Mater. Sci.* **7**, 199 (2003).
- [13] Y. Wada, T. Okubo, M. Ryo, T. Nakazawa, Y. Hasegawa, S. Yanagida, *J. Am. Chem. Soc.* **122**, 8583 (2000).
- [14] M. Ryo, Y. Wada, T. Okubo, T. Nakazawa, Y. Hasegawa, S. Yanagida, *J. Mater. Chem.* **12**, 1748 (2002).
- [15] M. Lezhnina, F. Laeri, L. Benmouhadi, U. Kynast, *Adv. Mater.* **18**, 280 (2006).
- [16] G. Calzaferri, K. Lutkouskaya, *Photochem. Photobiol. Sci.* **7**, 879 (2008).

- [17] A. Monguzzi, G. Macchi, F. Meinardi, R. Tubino, M. Burger, G. Calzaferri, *Appl. Phys. Lett.* **92**, 123301 (2008).
- [18] A. Mech, A. Monguzzi, F. Meinardi, J. Mezyk, G. Macchi, R. Tubino, *J. Am. Chem. Soc.* **132**, 4574 (2010).
- [19] O. A. Yeschenko, I. M. Dmitruk, S. V. Koryakov, I. P. Pundyk, Y. A. Barnakov, *Solid State Commun.* **133**, 109 (2005).
- [20] G. De Cremer, Y. Antoku, M. B. J. Roeffaers, M. Sliwa, J. Van Noyen, S. Smout, J. Hofkens, D. E. De Vos, B. F. Sels, T. Vosch, *Angew. Chem. Int. Ed.* **47**, 2813 (2008).
- [21] G. De Cremer, E. Coutino-Gonzalez, M. B. J. Roeffaers, B. Moens, J. Ollevier, M. Van der Auweraer, R. Schoonheydt, P. A. Jacobs, F. C. De Schryver, J. Hofkens, D. E. De Vos, B. F. Sels, T. Vosch, *J. Am. Chem. Soc.* **131**, 3049 (2009).
- [22] Y. Wang, H. Li, L. Gu, Q. Gan, Y. Li, G. Calzaferri, *Micropor. Mesopor. Mater.* **121**, 1 (2009).
- [23] H. Wu, X. Yang, X. Yu, J. Liu, H. Yang, H. Lv, K. Yin, *J. Alloys. Compd.* **480**, 867 (2009).
- [24] G. De Cremer, B. F. Sels, J. Hotta, M. B. J. Roeffaers, E. Bartholomeeusen, E. Coutino-Gonzalez, V. Valtchev, D. E. De Vos, T. Vosch, J. Hofkens, *Adv. Mater.* **22**, 957 (2010).
- [25] G. De Cremer, E. Coutino-Gonzalez, M. B. J. Roeffaers, D. E. De Vos, J. Hofkens, T. Vosch, B. F. Sels, *ChemPhysChem.* **11**, 1627 (2010).
- [26] H. Sun, Y. Sakka, Y. Miwa, N. Shirahata, M. Fujii, H. Gao, *Appl. Phys. Lett.* **97**, 131908 (2010).
- [27] A. Corma, C. Corell, J. Perez-Pariente, *zeolites.* **15**, 2 (1995).
- [28] A. Carvalho, M. Carvalho, J. Pires, *zeolites.* **19**, 382 (1997).
- [29] P. K. Dutta, D. C. Shieh, M. Puri, *J. Phys. Chem.* **91**, 2332 (1987).
- [30] K. S. Smirnov, D. Bougeard, *J. Phys. Chem.* **97**, 9434 (1993).
- [31] V. N. Denisov, A. N. Ivlev, A. S. Lipin, B. N. Mavrin, V. G. Orlov, *J. Phys.: Condens. Matter* **9**, 4967 (1997).
- [32] G. Blasse, A. Brill, *J. Chem. Phys.* **48**, 217 (1968).
- [33] M. Peng, D. Chen, J. Qiu, X. Jiang, C. Zhu, *Opt. Mater.* **29**, 556 (2007).

Chapter 3

Controlling the optical properties by annealing atmosphere - Co-existence of Bi with multiple valence states in zeolites

In this chapter, we investigate the effect of annealing atmosphere on the optical properties of Bi doped zeolites by diffuse reflectance, steady state and time-resolved photoluminescence (PL), and PL excitation measurements. The results reveal that zeolites can be used as an excellent host material to stabilize multiple Bi centers (Bi^{3+} , Bi^{2+} , and Bi-related near-infrared (NIR) active centers) in the framework, which shows ultra-broadband emission from visible to NIR range. Annealing in N_2 leads to the partial conversion of Bi^{3+} ions into Bi^{2+} and Bi-related NIR active centers. Our results demonstrate that the broadband NIR emission may be attributed to the electronic transition of Bi low valence state, rather than a higher valence state.

3.1 Introduction

In the past decades, Bi ions have attracted a great deal of attention for the potential applications in phosphor, laser, and optical communication [1-12]. As is known, Bi ions can exist in materials with different valence states, such as 0, +1, +2, +3, and +5, which show the characteristic emissions in different wavelength region. For instance, Xia et al. [3] reported that an intense emission at 443 nm can be obtained in Bi^{3+} -doped $CaSb_2O_6$ phosphor as a potential blue candidate for white-LED and other display devices. Peng et

al. [6] successfully synthesized Bi²⁺-doped MBPO₅ (M = Ba²⁺, Sr²⁺, Ca²⁺), and observed orange and red emissions with improved color quality. Recently, many groups reported that Bi-doped glasses and crystals show ultra-broad near-infrared (NIR) luminescence in the wavelength region from 1000 nm to 1600 nm with FWHM over 200 nm covering the whole telecommunications window [7-12]. It is an interesting work to explore a host material to accommodate these Bi multiple valence states in a single framework for various applications.

Zeolites are crystalline microporous aluminosilicates, constituted by a tri-dimensional arrangement of SiO₄ and AlO₄ tetrahedra, linked by oxygen atoms forming different construction units and large frameworks. It is well known that zeolites possess some unique features of low-frequency vibrational framework, regularly spaced nanochannels and nanopores, and ion-exchange capacity [13-15]. These particular structural properties make it very promising as host materials of optically active centers for constructing novel materials designed at nanosized levels [14-24]. Recently, it is reported that highly efficient NIR photoluminescence (PL) from Bi doped zeolites can be realized after annealing in an inert atmosphere, and the quantum efficiencies are strongly dependent on the annealing temperature and the Bi doping concentration [21,23]. As is known, annealing atmosphere is an important parameter for the optical properties of Bi doped zeolites, since the variation of Bi valence states is very sensitive to annealing condition [25]. Therefore, it is necessary to investigate the effect of annealing atmosphere on the optical properties of Bi doped zeolites for practical applications.

In this work, we prepare Bi doped zeolites by an ion-exchange process and subsequent high temperature annealing in air and N₂. Diffuse reflectance, steady state and time-resolved PL, and PL excitation (PLE) spectra have been measured to investigate the optical properties of Bi doped zeolites. The results reveal that zeolites can be used as an excellent host material to stabilize multiple Bi centers (Bi³⁺, Bi²⁺, and Bi-related NIR active centers) in the framework, which shows ultra-broadband emission from visible to NIR range. The origin of the broadband NIR emission is discussed.

3.2 Experimental details

The samples studied in this work were synthesized by the method described previously [21,22]. Zeolites were stirred in a 50 mM aqueous solution of Bi³⁺ prepared from Bi(NO₃)₃·5H₂O for 24 h to exchange NH₄ ions with Bi³⁺ ions. The products were removed by centrifugation, then washed with deionized water, and dried in air at 120 °C. The Bi doped zeolites were calcined at 900 °C for 1 h in air and N₂, respectively. All samples were exposed to the laboratory atmosphere prior to measurements.

The prepared products were characterized by a X-ray diffractometer (Rigaku-TTR/S2,

=1.54056 Å), and an energy-dispersive X-ray spectroscopy (EDX). Diffuse reflectance spectra were recorded by a UV-visible-NIR scanning spectrophotometer (UV-3101PC) by using barium sulphate as a reference. PL and PLE spectra in the range of 370 - 930 nm were obtained by a CCD detector upon exciting with a Xe lamp. PL spectra in the range of 930 - 1630 nm were measured by the excitation of a 488 nm line from an Ar⁺ laser. The signal was analyzed by a single grating monochromator and detected by a liquid-nitrogen-cooled InGaAs detector. Excitation spectrum at 1145 nm was obtained by a NIR PL spectrophotometer (Bunkoh-Keiki Co. Ltd., Tokyo, Japan) equipped with an InGaAs detector. Time-resolved luminescence measurements were performed by detecting the modulated luminescence signal with a photomultiplier tube (Hamamatsu, R5509-72), and then analyzing the signal with a photon-counting multichannel scaler. The excitation sources for decay time measurements were 355 nm and 488 nm lights from an optical parametric oscillator (OPO) pumped by the third harmonic of a Nd:YAG laser (pulse width 5 ns, repetition frequency 20Hz). All measurements were performed at room temperature.

3.3 Results and discussion

The Bi doped zeolites show different colors after annealing in air and N₂. After annealing in air, the powder is white, while annealing in N₂, the sample becomes shallow pink. Figure 3.1 shows the XRD patterns of undoped-zeolites, Bi-air, and Bi-N₂ samples. The comparison of these spectra indicates that, although the doping and thermal treatment result in the decreases of the peak intensity in the doped samples, the zeolite structure is still maintained. It should be noted that there is one weak peak at $2\theta = 21.9$ for the doped zeolites, which can be attributed to the (101) reflection of the Cristobalite silica (JCPDS No. 11-0695). The EDX spectrum of Bi-N₂ sample is shown in figure 3.2. The atomic compositions of the sample are determined to be 30.37 % (Si), 6.23 % (Al), 62.28 % (O), and 1.12 % (Bi). The atomic ratio of Bi/Al is calculated to be about 18 %.

Figure 3.3 shows the diffuse reflectance spectra of Bi-air and Bi-N₂ samples. Only one absorption band at 1400 nm is observed in Bi-air sample, while three absorption bands at 500 nm, 700 nm and 1400 nm are detected in Bi-N₂ sample. As is known, a typical feature of zeolites is that they can easily absorb water in air [16]. Therefore, the band at 1400 nm in our samples is ascribed to the absorption of the coordinated water. The absorption bands at 500 nm and 700 nm are commonly observed in Bi-doped glasses, which can be assigned to Bi-related NIR active centers [7,8]. The difference between the two spectra is shown in the inset of figure 3.3. Besides the bands at 500 nm and 700 nm, a strong band at 300 nm can be confirmed, which is the typical absorption of Bi³⁺ ions. The results reveal that the Bi³⁺ absorption in Bi-air sample is much stronger than that

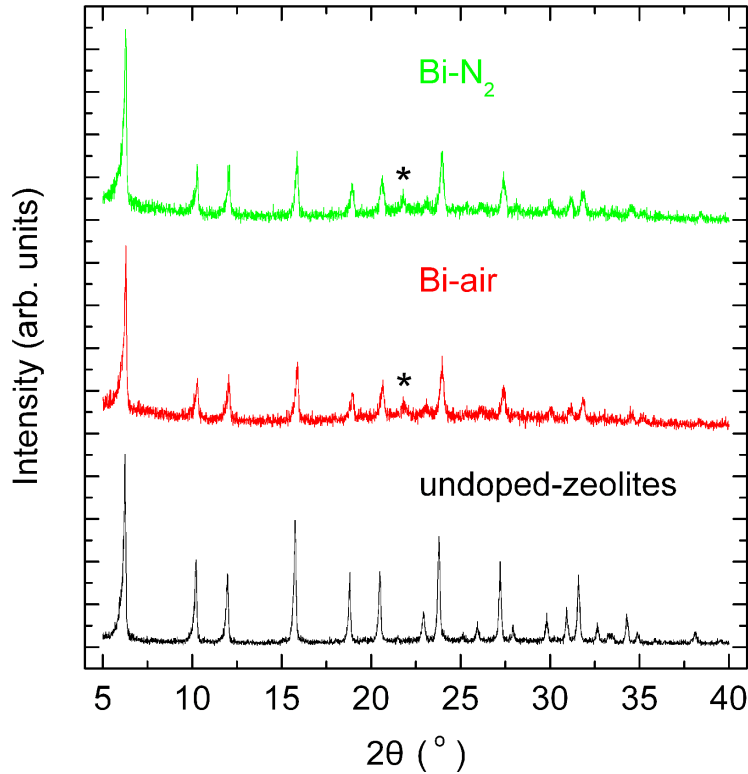


Figure 3.1: X-ray diffraction patterns of undoped-zeolites, Bi-air, and Bi-N₂ samples. The peaks marked by the * symbol indicate the (101) reflection of the Cristobalite silica (JCPDS No. 11-0695).

of Bi-N₂ sample.

The PL spectra of Bi-air and Bi-N₂ samples in the range of 370 - 930 nm are shown in figure 3.4 (a). In the Bi-air sample, a strong emission band at 520 nm and a weak emission band at 800 nm are observed. Interestingly, in the Bi-N₂ sample, the emission band at 520 nm is decreased, while the emission band at 800 nm is significantly enhanced. It is important to point out that, in the measurements, the Bi-air and Bi-N₂ samples show white light, which are bright enough to be observed by the naked eye even at the excitation power as low as 2.5 mW. To clarify the origin of these two bands, the excitation spectra of Bi-air sample detected at 520 nm and Bi-N₂ sample detected at 800 nm are recorded, which is shown in figure 3.4 (b). The Bi-air sample detected at 520 nm shows an excitation band at about 320 nm. Based on the PL and PLE spectra, the 520 nm emission can be assigned to the electronic transition of Bi³⁺ ions [1-3]. In the previous works, the characteristic Raman band of Bi₂O₃ was observed in Bi doped zeolites, which indicates that Bi³⁺ ions exist as Bi₂O₃ clusters in zeolites [23,24]. On the other hand, the excitation spectrum at 800 nm for Bi-N₂ sample is characterized by the presence of two

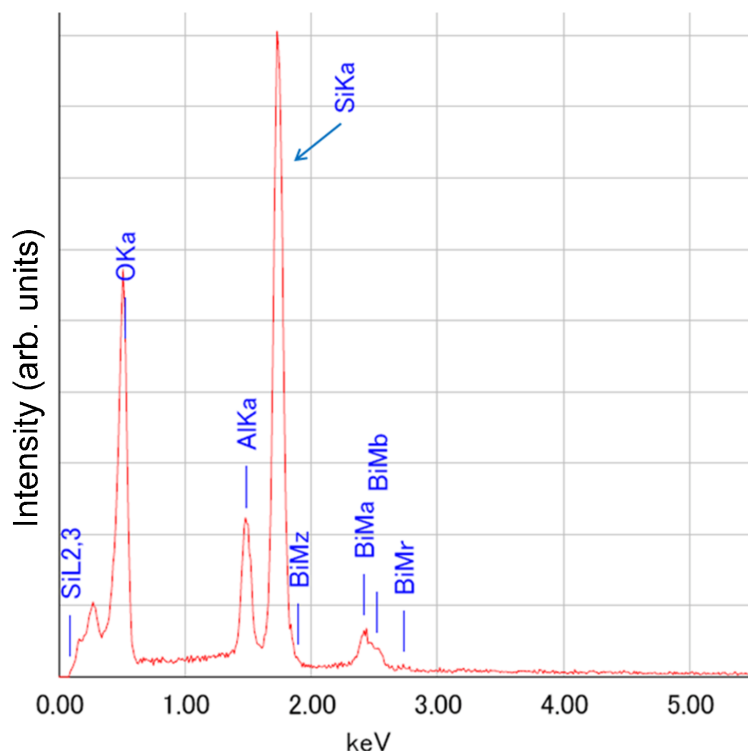


Figure 3.2: EDX spectrum of Bi-N₂ sample.

bands at 380 nm and 710 nm. According to the results of Srivastava et al. [4] and Peng et al. [6], the 800 nm emission most likely arises from the Bi²⁺ centers. Figure 3.4 (c) shows the decay curves of Bi-air and Bi-N₂ samples detected at 520 nm and 800 nm. The 1/e lifetimes are about 1.5 μ s (at 520 nm) and 8.7 μ s (at 800 nm) in Bi-air sample, and 1.6 μ s (at 520 nm) and 10 μ s (at 800 nm) in Bi-N₂ sample. The lifetimes detected at 520 nm and 800 nm are similar between the two samples, and these values are comparable to those reported in Bi doped glasses and crystals [6,25].

In the low-power excitation regime, the luminescence intensity is proportional to the amount of active centers. Therefore, the PL intensities of Bi³⁺ and Bi²⁺ ions in figure 3.4 (a) are determined by the amount of Bi³⁺ and Bi²⁺ ions in the samples. The above results reveal that the Bi³⁺ absorption and emission in Bi-air sample is much stronger than that of Bi-N₂ sample, which clearly proves that the amount of Bi³⁺ ions is decreased after annealing in N₂. On the other hand, the Bi²⁺ emission intensity in Bi-N₂ sample is almost three times stronger than that in Bi-air sample, which indicates that the amount of Bi²⁺ ions is significantly increased after annealing in N₂. It should be mentioned that Bi²⁺-doped materials are presently limited to a few types of materials, such as strontium borates and alkaline earth borophosphates, because of the difficulties of stabilizing the divalent Bi ions [4-6]. Our results demonstrate that high temperature annealing leads to

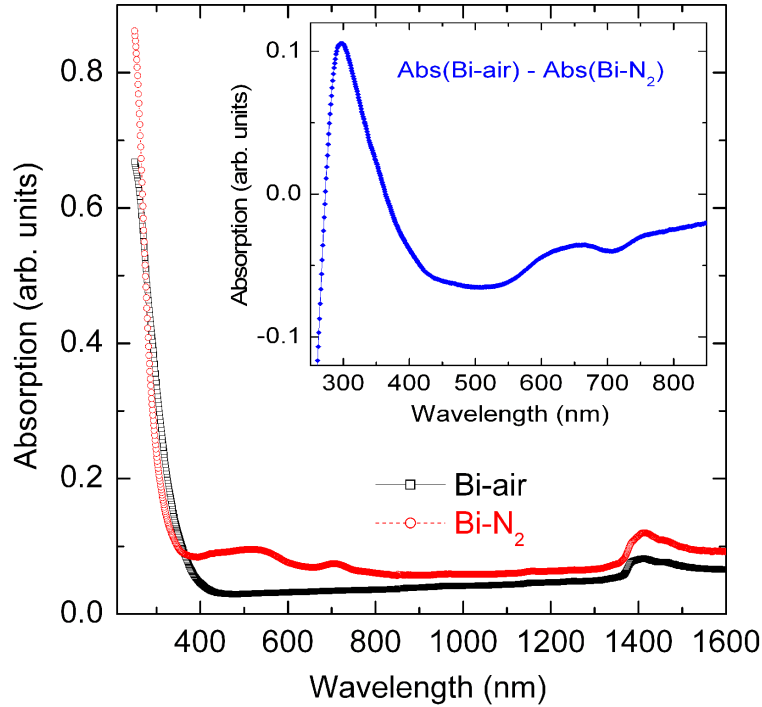
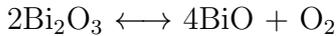


Figure 3.3: Diffuse reflectance spectra of Bi-air and Bi-N₂ samples in the wavelength region from 250 nm to 1600 nm. The inset shows the difference between the two spectra in the range of 250 - 850 nm.

the partial reduction of Bi ions from +3 to +2 valence state, and this process becomes more efficient when annealing in the inert atmosphere. It is reported that Bi₂O₃ can be partially converted into BiO at relatively high temperature, which coincides with our results [26]. The variation between Bi³⁺ and Bi²⁺ valence states in zeolites can be expressed as the following reaction:



High temperature annealing can decompose Bi₂O₃ into BiO, and on the other hand, annealing in air results in the oxidation of BiO into Bi₂O₃. The reversible reaction can reach a dynamic balance depending on annealing temperature and annealing atmosphere. Therefore, Bi₂O₃ and BiO clusters are stabilized in the pores of zeolites.

Figure 3.5 (a) shows the emission spectra of Bi-air and Bi-N₂ samples in the range of 930 - 1630 nm. For the Bi-air sample, no infrared emission is detectable in this region. In contrast, we observe a broad NIR emission centered at 1145 nm in the Bi-N₂ sample. The origin of this broadband NIR emission is still unclear, so we tentatively assign it to Bi-related NIR active centers. The broadband emission covers the range of 970 - 1600 nm, and the full-width at half maximum is about 184 nm. The excitation spectrum detected at 1145 nm is shown in figure 3.5 (b). We observed two strong excitation bands

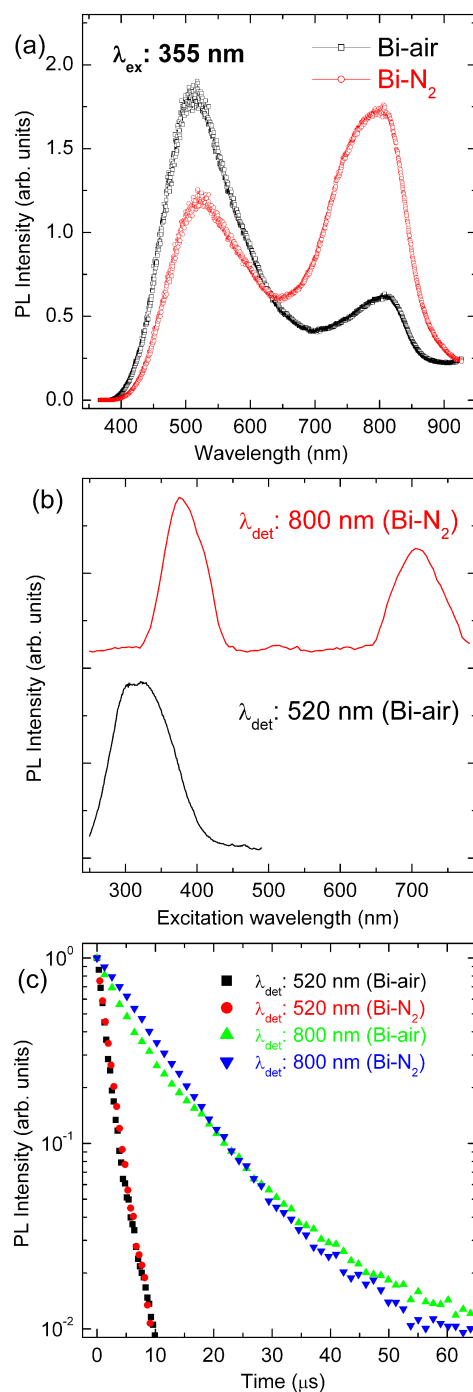


Figure 3.4: (a) Photoluminescence spectra of Bi-air and Bi-N₂ samples in the range of 370 - 930 nm. The excitation wavelength is 355 nm. (b) Excitation spectra of Bi-air sample detected at 520 nm and Bi-N₂ sample detected at 800 nm, respectively. (c) Decay curves of Bi-air and Bi-N₂ samples detected at 520 nm and 800 nm.

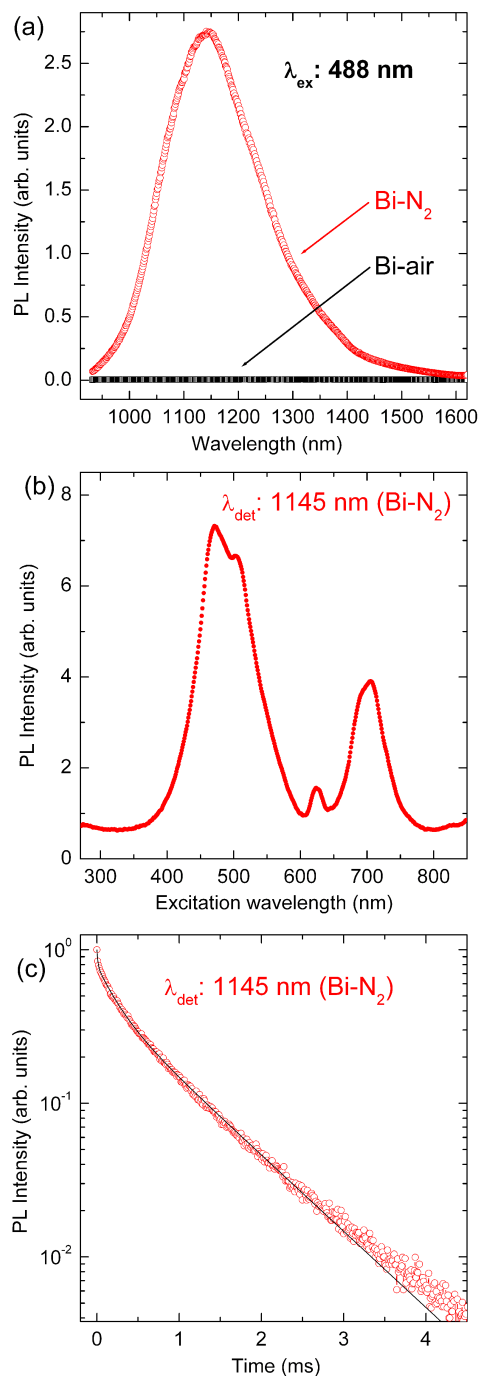


Figure 3.5: (a) Photoluminescence spectra of Bi-air and Bi- N_2 samples in the range of 930 - 1630 nm. The excitation wavelength is 488 nm. (b) Excitation spectrum and (c) decay curve of Bi- N_2 sample detected at 1145 nm. The fitting result of decay curve is $I(t) = 0.237 \exp(-t/58) + 0.748 \exp(-t/870)$.

at 470 nm and 700 nm and a weak peak at 620 nm. Figure 3.5 (c) shows the decay curve of the emission at 1145 nm. The decay curve shows a fast drop at the beginning, followed by a first-order exponential slow component. To further study the fast and slow components, the curve is fitted by a double-exponential function. The lifetimes of fast and slow components are estimated to be 58 μ s and 870 μ s, respectively, and the contribution of slow component is about 75 %. It is reasonable to assume that Bi-related active centers in zeolites can be classified into two parts. One part is the NIR active centers which are almost completely isolated from non-radiative relaxation processes and have very long luminescence lifetime. The other part is the NIR active centers strongly quenched by non-radiative relaxation processes. Due to particular morphology, this type of zeolites always contains a large amount of coordinated water, which strongly quenches NIR emission [15-19]. However, the large contribution of slow component suggests that most of the active centers are well isolated from the coordinated water in our sample.

As is known, FAU-type zeolites consist of three kinds of units (α -cages, the sodalite cages, and the double six-ring hexagonal prisms), and have several sites (such as SI, SI', SII, SII', and SIII sites) for cations [16]. Therefore, Bi^{3+} ions can migrate into the pores of zeolites by the ion-exchange process. Based on the results, Bi-related NIR active centers are formed in our sample after annealing in N_2 . It is noteworthy that the melting points of all inorganic bismuth compounds are below 820 $^\circ\text{C}$ [27]. High-temperature annealing leads to the formation of Bi_2O_3 and BiO clusters, which act as a blockage material to seal the pores of zeolites. As a result, the Bi-related NIR active centers can be protected from the quenching effect of the coordinated water, and have chance to show very long lifetime in zeolites. The quantum efficiency of the NIR emission has been previously estimated [21].

In the previous publications, the NIR emission has been attributed to electronic transition of Bi^{5+} [7], Bi^{2+} [11], Bi^+ [8], or Bi clusters [9]. However, the origin is still controversial. According to our results, the emission and excitation properties of Bi-related NIR active centers are completely different from those of Bi^{2+} ion. Therefore, Bi^{2+} can be ruled out from the origin of broadband NIR emission. On the other hand, it is known that the Bi^{5+} containing compounds become extremely unstable at temperature higher than 300 $^\circ\text{C}$ [28], such that Bi^{5+} is less likely to exist in our sample after annealed at 900 $^\circ\text{C}$. The results of measurements show that annealing at oxidation atmosphere results in the destruction of Bi-related NIR active centers, which strongly suggests that the broadband NIR emission is related to Bi low-valence state (Bi^+ or Bi clusters), rather than a higher valence state.

3.4 Conclusion

In conclusion, the effect of annealing atmosphere on the optical properties of Bi doped zeolites is studied by diffuse reflectance, steady state and time-resolved PL, and PLE spectra. It is revealed that Bi doped zeolites can be exploited as a tunable ultra-broadband light-source by controlling annealing condition, which covers the broad visible and NIR range. Annealing in N₂ leads to the partial conversion of Bi³⁺ ions into Bi²⁺ and Bi-related NIR active centers. Most of Bi-related NIR active centers are well isolated from the coordinated water in zeolites due to sealing the pores of zeolites by Bi₂O₃ and BiO clusters. Our results demonstrate that the broadband infrared emission may be attributed to the electronic transition of Bi low valence state, rather than a higher valence state.

References

- [1] M. J. Weber, R. R. Monchamp, *J. Appl. Phys.* **44**, 5495 (1973).
- [2] W. Dong, C. Zhu, *J. Phys. Chem. Solids* **64**, 265 (2003).
- [3] Y. Xia, F. Huang, W. Wang, A. Wang, J. Shi, *J. Alloy. Comp.* **476**, 534 (2009).
- [4] A. M. Srivastava, *J. Lumin.* **78**, 239 (1998).
- [5] Q. Zeng, T. Zhang, Z. Pei, Q. Su, *J. Mater. Sci. Technol.* **15**, 281 (1999).
- [6] M. Peng, N. Da, S. Krolikowski, A. Stiegelschmitt, L. Wondraczek, *Opt. Express* **17**, 21169 (2009).
- [7] Y. Fujimoto, M. Nakatsuka, *Jpn. J. Appl. Phys.* **40**, L279 (2001).
- [8] X. Meng, J. Qiu, M. Peng, D. Chen, Q. Zhao, X. Jiang, C. Zhu, *Opt. Express* **13**, 1635 (2005).
- [9] M. Peng, J. Qiu, D. Chen, X. Ment, C. Zhu, *Opt. Lett.* **30**, 2433 (2005).
- [10] T. Suzuki, Y. Ohishi, *Appl. Phys. Lett.* **88**, 191912 (2006).
- [11] J. Ren, J. Qiu, D. Chen, C. Wang, X. Jiang, C. Zhu, *J. Mater. Res.* **22**, 1954 (2007).
- [12] L. Su, J. Yu, P. Zhou, H. Li, L. Zheng, Y. Yang, F. Wu, H. Xia, J. Xu, *Opt. Lett.* **34**, 2504 (2009).
- [13] U. Kynast, V. Weiler, *Adv. Mater.* **6**, 937 (1994).
- [14] J. Rocha, L. D. Carlos, *Curr. Opin. Solid State Mater. Sci.* **7**, 199 (2003).
- [15] Y. Wada, T. Okubo, M. Ryo, T. Nakazawa, Y. Hasegawa, S. Yanagida, *J. Am. Chem. Soc.* **122**, 8583 (2000).
- [16] K. Binnemans, *Chem. Rev.* **109**, 4283 (2009).
- [17] M. Lezhnina, F. Laeri, L. Benmouhadi, U. Kynast, *Adv. Mater.* **18**, 280 (2006).
- [18] G. Calzaferri, K. Lutkouskaya, *Photochem. Photobiol. Sci.* **7**, 879 (2008).

- [19] A. Monguzzi, G. Macchi, F. Meinardi, R. Tubino, M. Burger, G. Calzaferri, *Appl. Phys. Lett.* **92**, 123301 (2008).
- [20] G. De Cremer, Y. Antoku, M. B. J. Roeffaers, M. Sliwa, J. Van Noyen, S. Smout, J. Hofkens, D. E. De Vos, B. F. Sels, T. Vosch, *Angew. Chem. Int. Ed.* **47**, 2813 (2008).
- [21] H. Sun, A. Hosokawa, Y. Miwa, F. Shimaoka, M. Fujii, M. Mizuhata, S. Hayashi, S. Deki, *Adv. Mater.* **21**, 3694 (2009).
- [22] A. Mech, A. Monguzzi, F. Meinardi, J. Mezyk, G. Macchi, R. Tubino, *J. Am. Chem. Soc.* **132**, 4574 (2010).
- [23] Z. Bai, M. Fujii, T. Hasegawa, K. Imakita, Y. Miwa, M. Mizuhata, S. Hayashi, *Micropor. Mesopor. Mater.* **145**, 21 (2011).
- [24] H. Sun, Y. Sakka, Y. Miwa, N. Shirahata, M. Fujii, H. Gao, *Appl. Phys. Lett.* **97**, 131908 (2010).
- [25] S. Zhou, N. Jiang, B. Zhu, H. Yang, S. Ye, G. Lakshminarayana, J. Hao, J. Qiu, *Adv. Funct. Mater.* **18**, 1407 (2008).
- [26] J. Ren, L. Yang, J. Qiu, D. Chen, X. Jiang, C. Zhu, *Solid State Commun.* **140**, 38 (2006).
- [27] D. L. Perry, S. L. Phillips, *Handbook of Inorganic Compounds* (CRC, Boca Raton, 1995).
- [28] M. Peng, G. Dong, L. Wondraczek, L. Zhang, N. Zhang, J. Qiu, *J. Non-Cryst. Solids* **357**, 2241 (2011).

Part II

**Photoluminescence properties of Bi
and lanthanide ions co-doped zeolites**

Chapter 4

Efficient near-infrared luminescence and energy transfer in erbium/bismuth co-doped zeolites

In this chapter, we have shown that tunable and highly efficient broadband near-infrared luminescence can be realized in Er/Bi co-doped zeolites. The emission covers the ranges of 930 - 1450 nm and 1450 - 1630 nm. The intensity ratio of the two bands can be tuned by adjusting the concentration of Er and excitation wavelength. Steady state and time-resolved photoluminescence (PL), and PL excitation measurements indicate that two kinds of emitters coexist in the pores of zeolites, and that near infrared active bismuth simultaneously acts as a sensitizer of erbium. The present results demonstrate an important rational strategy for the design of a tunable near-infrared emitting zeolite-based nanosystem.

4.1 Introduction

Zeolites are microporous crystalline solids with well-defined structures containing silicon, aluminium and oxygen in their frameworks and cations, water or other molecules within their pores. Due to their particular morphological features, zeolites have very high surface areas and have been widely used in applications such as catalysis, ion exchange, and separations [1, 2]. Recently, zeolites acting as a host material of optically active guest have attracted much attention for constructing novel materials designed at nanosized levels [3-10]. Visible luminescence with very high efficiencies from rare-earth-functionalized zeolites has been reported [6, 7]. In contrast, it is difficult to realize highly efficient

near-infrared (NIR) emission in zeolites, because of the existence of coordinated water in cages, causing fast relaxation of its excitation energy through nonradiative vibrational deactivation [8-10]. Thus, the critical thing to increase NIR emission efficiency in zeolites is to separate active ions from coordinate water. Up till now, several strategies have been reported by Wada et al.[8], Lezhnina et al.[9], and Sun et al.[11] to reach this purpose. All these methods concentrated on singly active ions doped NIR emitting zeolites. To the best of our knowledge, there are no reports on multi-type active ions codoped zeolites emitting in the NIR range.

Recently, we observed very broad NIR emission of “ bismuth-related active centers (BiRAC) ” from the Bi doped zeolites annealed in an inert gas atmosphere [11, 12]. Furthermore, we realized efficient NIR luminescence of Er^{3+} by using Er/Bi co-doped zeolites annealed in air [13]. However, we had not realized NIR emission of Er^{3+} and BiRAC simultaneously until now. One of the purposes of this work is to make them optical active simultaneously and realize NIR emission in wider wavelength range. Another purpose is to improve the excitation efficiency of Er^{3+} by co-doping other optical active centers. As is known, excitation efficiency of Er^{3+} is very low due to its forbidden intra-4f transition. Moreover, the intrinsically sharp and discontinuous absorption bands of Er^{3+} require lasers as excitation source to realize some functional applications of Er doped materials. Thus, it is an interesting topic to realize sensitization of Er^{3+} by using active centers with broad absorption bands. Very recently, Monguzzi et al. proposed the sensitization of Er^{3+} by using a suitable organic molecule acting as an antenna [10]. Though these hybrid composites provide new opportunities to create novel multifunctional materials, the complicated preparation process and air-instability of these materials limit their practical applications.

In this chapter, we prepared Er singly doped and Er/Bi co-doped FAU-type nanocrystalline zeolites by a method consisting of a simple ion-exchange process and subsequent high-temperature annealing under N_2 atmospheric condition. We realized two efficient near infrared emission bands corresponding to BiRAC and Er^{3+} intra-4f transition in Er/Bi co-doped samples. A clear correlation between the intensities of the two peaks can be observed. To further investigate this phenomenon, we performed photoluminescence excitation and decay-time measurements. The measurement results provide clear evidence of energy transfer from Bi to Er.

4.2 Experimental details

Zeolites was stirred in x mM (x= 0.1, 0.5, 1) aqueous solution of Er^{3+} prepared from $\text{Er}(\text{NO}_3)_3 \cdot 5\text{H}_2\text{O}$ at 80 °C for 120 h to exchange NH_4 ions with Er^{3+} ions. The products were removed by centrifugation, then washed with deionized water, and dried in air at

120 °C. The Er embedded zeolites were further stirred in a 0.06 M aqueous solution of Bi^{3+} prepared from $\text{Bi}(\text{NO}_3)_3 \cdot 5\text{H}_2\text{O}$ at 80 °C for 144 h to dope Bi. The products were removed by centrifugation, then washed with deionized water, and dried in air at 120 °C. The Er/Bi co-doped zeolites were calcined at 920 °C for 1 h in N_2 atmospheric condition. For comparison, we also prepared Er(0.5mM) singly doped zeolites. All samples were exposed to the laboratory atmosphere prior to measurements.

The prepared products were first characterized by X-ray diffractometer (Rigaku-TTR/S2, $\lambda = 1.54056 \text{ \AA}$), which shows that the zeolites structure keeps well after thermal treatment. Field emission scanning electron microscopy (FE-SEM) measurement reveals that the morphology and monodispersity of the nanoparticles remain unchanged. Furthermore, energy dispersive X-ray spectroscopy (EDS) results showed that Er and Bi concentration was well-controlled by this experimental procedure. Photoluminescence (PL) measurements were carried out with the excitation of a 488 nm and 457.9 nm lines of an Ar^+ laser. PL excitation measurements were performed under the excitation with 440 - 540 nm light from an optical parametric oscillator (OPO) pumped by the third harmonic of a Nd:YAG laser. The signal was analyzed by a single grating monochromator and detected by a liquid-nitrogen-cooled InGaAs detector. Time-resolved luminescence measurements were performed by detecting the modulated luminescence signal with a photomultiplier tube (Hamamatsu, R5509-72), and then analyzing the signal with a photon-counting multichannel scaler. The excitation source for the lifetime measurements was the 488 nm light from the OPO (pulse width 5 ns, repetition frequency 20Hz). All the measurements were carried out at room temperature.

4.3 Results and discussion

Figure 4.1 (a) and (b) show PL spectra of Er, Bi singly and co-doped samples excited at 488.0 and 457.9 nm, respectively. The Bi concentration is kept almost the same for all the Bi doped samples. In Bi singly doped sample, we observe a broad emission band centered at 1145 nm and covering the 930 - 1630 nm range. The broad PL is usually assigned to Bi^+ , but it is not finally proved [14]. Thus, we ascribe the origin of the luminescence to BiRAC here. For Er singly doped zeolites, a weak PL peak can be seen at 1532 nm due to the intra-4f shell electronic transitions ($^4\text{I}_{13/2} \rightarrow ^4\text{I}_{15/2}$) of Er^{3+} when it is excited at 488 nm. This wavelength can directly excite Er^{3+} from the ground state to the $^4\text{F}_{7/2}$ state. When the singly doped sample is excited at 457.9 nm, no PL is observed because Er^{3+} has no absorption at this wavelength. Interestingly, in co-doped samples, remarkably strong Er^{3+} -related PL is observed even when it is excited at 457.9 nm. Furthermore, in addition to the 1532 nm band from Er^{3+} , co-doped samples show broad PL from BiRAC. The full widths at half maximum (FWHM) of the luminescence

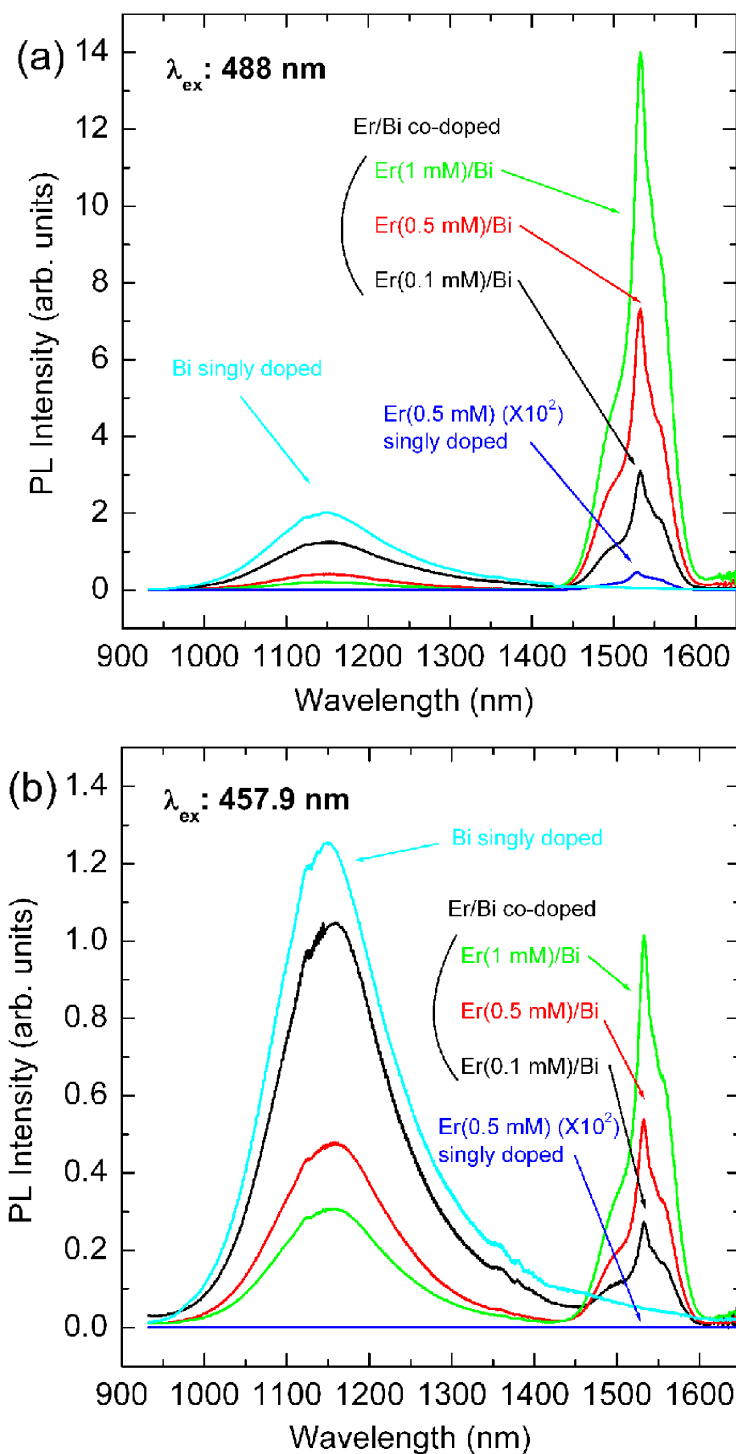


Figure 4.1: PL spectra of Er, Bi singly and co-doped zeolites, excited by (a) 488 nm and (b) 457.9 nm. The PL spectra of Er singly doped sample are multiplied by a factor of 10^2 .

of Er and Bi in all samples are 50 and 162 nm, respectively. It is obvious that in the series of co-doped samples, with the increase of Er concentration, the emission intensity of Er^{3+} monotonically increases while the BiRAC emission intensity decreases with the introduction of Er. The phenomenon suggests that the luminescence can be controlled through adjusting the dopant concentration.

Figure 4.2 shows photoluminescence excitation (PLE) spectra detected at 1532 nm for a co-doped sample and an Er singly doped sample. The Er concentration of these two samples is the same. All spectra are characterized by the presence of three sharp peaks at 452 nm, 488 nm, and 520 nm, which are assigned to the $^4\text{I}_{15/2} \rightarrow ^4\text{F}_{5/2}$, $^4\text{I}_{15/2} \rightarrow ^4\text{F}_{7/2}$, $^4\text{I}_{15/2} \rightarrow ^2\text{H}_{11/2}$ transitions of Er^{3+} , respectively. As expected, in the singly doped sample, Er^{3+} can only be excited at these wavelengths. On the other hand, the PLE spectrum of the co-doped sample exhibits a continuous background superimposed on the direct excitation peak. The broad background of the PLE spectrum suggests that, in addition to the direct excitation, Er^{3+} in co-doped samples is indirectly excited by an energy transfer process. It is noteworthy that FAU-type zeolite is transparent in the visible range, and thus does not act as a sensitizer for Er^{3+} . Therefore, the most probable candidate of the energy

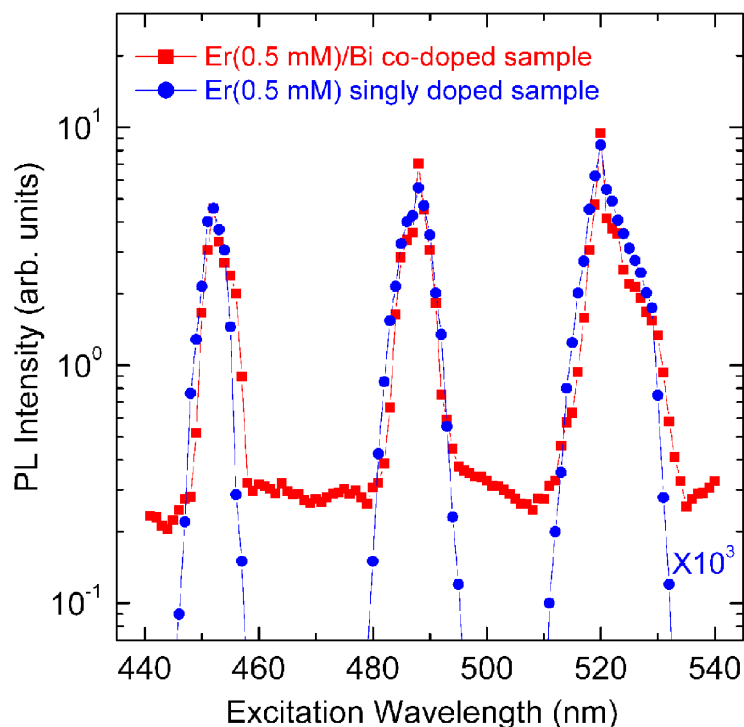


Figure 4.2: PL excitation spectra of $\text{Er}(0.5 \text{ mM})/\text{Bi}$ co-doped zeolites and $\text{Er}(0.5 \text{ mM})$ singly doped zeolites detected at 1532 nm. The PLE spectrum of singly doped sample is multiplied by a factor of 10^3 .

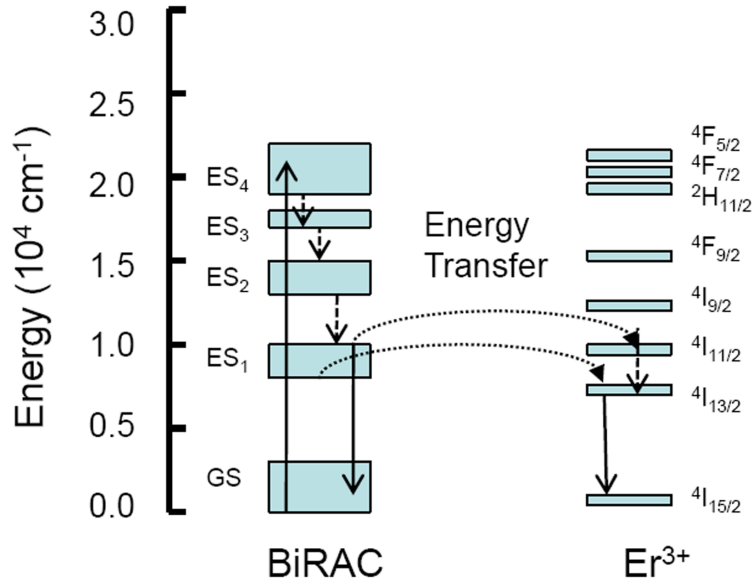


Figure 4.3: Energy level diagram of Er/Bi co-doped zeolites which exhibits BiRAC \rightarrow Er³⁺ energy transfer. ES, excited state; GS, ground state.

donor is BiRAC. Recently, Xu et al. reported that the introduction of Bi³⁺ can broaden the excitation band of Er³⁺ in the ultra violet region [17]. In fact, in figure 4.1, we can see an anti-correlation between the emission intensity of Er³⁺ and BiRAC. Similar behavior has commonly been observed for donor to acceptor energy transfer systems [18].

The analysis of figure 4.2 allows us to draw a meaningful conclusion concerning the performance of Er/Bi co-doped zeolites in comparison to Er singly doped sample. This system is represented by the fact that it can also work under off-resonance excitation conditions. As is known, the f-f transitions show narrow bandwidths because the processes are confined to the inner shells and they are insensitive to the local environment, so excitation spectrum of Er³⁺ is sharp and discontinuous. In contrast, we observed that the BiRAC have a broad excitation band in the visible region. For energy transfer process, it requires an overlap of the emission region of the sensitizer and the absorption region of the acceptor. As shown in figure 4.3, the BiRAC emission band covers the 930 - 1630 nm range, excellently overlapping with the excitation bands of Er³⁺, especially the 4I_{15/2} \rightarrow 4I_{11/2} (980 nm) and 4I_{15/2} \rightarrow 4I_{13/2} (1532 nm) transitions. Based on the results of measurements, Er³⁺ in the co-doped system can be efficiently excited within the broad visible region, so optical pumping using flash lamp or white LED rather than laser becomes feasible using this broadband sensitization (figure 4.4).

Figure 4.5 (a) shows the decay curves detected at 1145nm, i.e., emission from BiRAC. The 1/e lifetime reaches as long as 532 μ s for Bi singly doped sample and it becomes

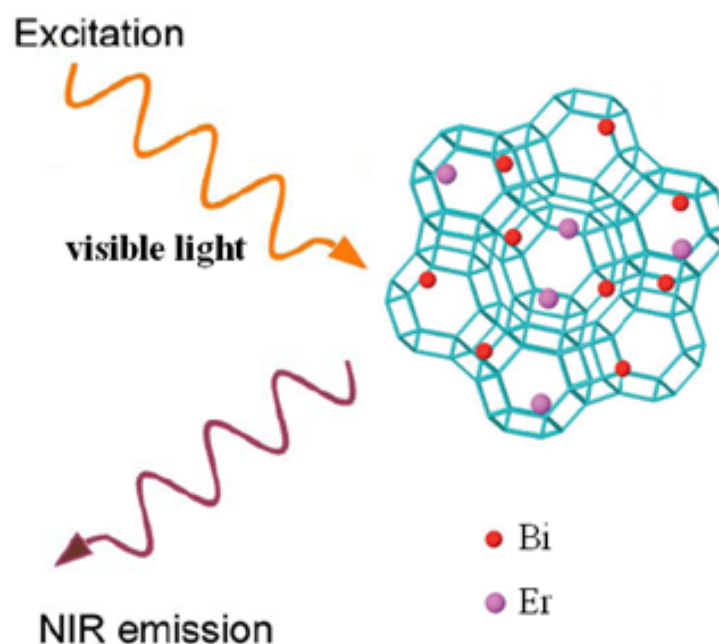


Figure 4.4: Schematic illustrations of the excitation and emission properties of Er/Bi co-doped zeolites.

shorter by the introduction of Er. The obtained lifetimes are comparable to those reported for Bi doped glasses and crystals [19-21]. Figure 4.5 (b) shows decay curves detected at 1532 nm, i.e., emission from Er^{3+} . In the Er singly doped sample, the lifetime is much shorter than the transition intrinsic lifetime of Er^{3+} . This is due to nonradiative relaxation of Er^{3+} by strong coupling of the excitation to high-frequency vibrations of coordinated water. In co-doped zeolites, the lifetime is significantly increased to about 5 ms. This suggests that Er^{3+} is well separated from coordinated water. As shown in figure 4.6, based on low melting points of Bi compounds and high temperature annealing, we think that Bi compounds form agglomerates to seal the pores of zeolites, and Er^{3+} and partial BiRAC can be held in captivity totally in the pores and then water molecules have little chance to interact with them, which results in strong and long-lived NIR emission [16].

In figure 4.5 (c), PL dynamics of all co-doped samples just after excitation are shown. In the decay curves of BiRAC (1145 nm), fast and slow components can be seen. With increasing Er concentration, the fast component becomes more dominant and the lifetimes become shorter. We believe that the shortening of the lifetime is the direct evidence that Er^{3+} is excited indirectly by the energy transfer from BiRAC. In the decay curves of Er^{3+} (1532 nm), the intensity does not decay simply after excitation. It rises slowly after the excitation and reaches maximum after 50 μs . This delayed PL is due to the combined action of the relaxation of excited Er^{3+} to first excited state and the energy transfer

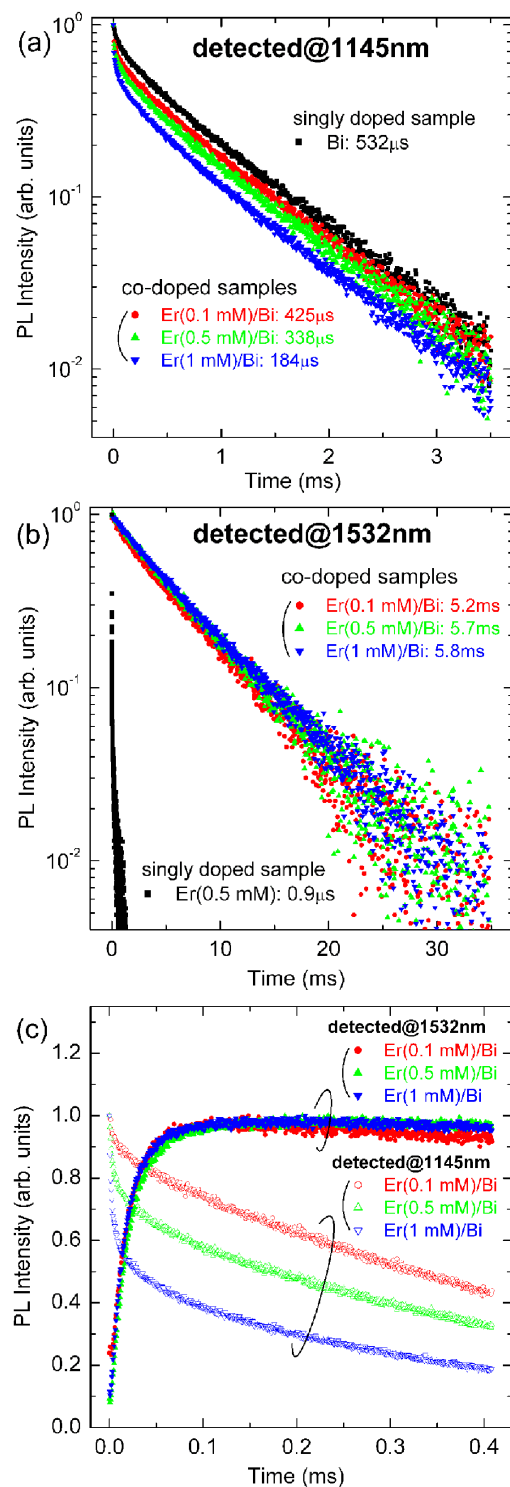


Figure 4.5: PL decay curves of all samples detected at (a) 1145 nm and (b) 1532 nm. (c) shows the time dependence of PL intensity just after excitation.

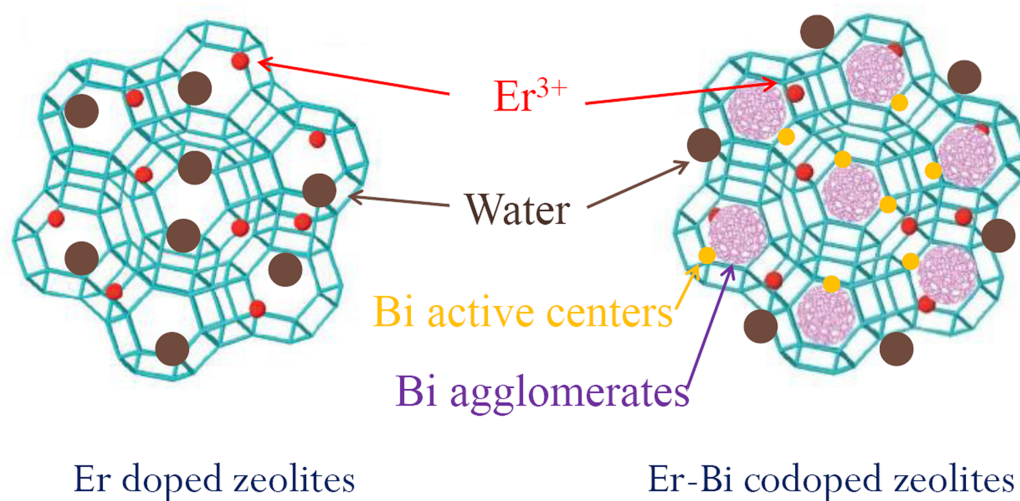


Figure 4.6: Schematic illustrations of the blocking property of Bi agglomerates.

process from BiRAC.

4.4 Conclusion

In conclusion, Er/Bi co-doped zeolites were prepared by an ion-exchange method and their PL properties were investigated. We observed two efficient, tunable and long-lived emission bands covering 930 - 1450 nm and 1450 - 1630 nm, corresponding to BiRAC and Er^{3+} intra-4f transition, respectively. The intensity ratio of the two bands can be tuned by adjusting the concentration of erbium. The introduction of Bi distinctly broadened the excitation band of Er^{3+} in the visible region. The steady state and time-resolved PL results proved that efficient energy transfer process occurs in Er/Bi co-doped zeolites. The peculiar optical properties make them promising for potential application in NIR optical devices.

References

- [1] M. E. Davis, *Acc. Chem. Res.* **26**, 111 (1993).
- [2] L. Tosheva, V. P. Valtchev, *Chem. Mater.* **17**, 2494 (2005).
- [3] U. Kynast, V. Weiler, *Adv. Mater.* **6**, 937 (1994).
- [4] T. Justel, D. U. Wiechert, C. Lau, D. Sendor, U. Kynast, *Adv. Funct. Mater.* **11**, 105 (2001).
- [5] J. Rocha, L. D. Carlos, *Curr. Opin. Solid State Mater. Sci.* **7**, 199 (2003).
- [6] G. Calzaferri, K. Lutkouskaya, *Photochem. Photobiol. Sci.* **7**, 879 (2008).
- [7] D. Bruhwiler, G. Calzaferri, T. Torres, J. H. Ramm, N. Gartmann, L. Dieu, I. Lopez-Duarte, M. V. Martinez-Diaz, *J. Mater. Chem.* **19**, 8040 (2009).
- [8] K. Binnemans, *Chem. Rev.* **109**, 4283 (2009).
- [9] Y. Wang, H. Li, Y. Feng, H. Zhang, G. Calzaferri, T. Ren, *Angew. Chem. Int. Ed.* **49**, 1434 (2010).
- [10] Y. Wada, T. Okubo, M. Ryo, T. Nakazawa, Y. Hasegawa, S. Yanagida, *J. Am. Chem. Soc.* **122**, 8583 (2000).
- [11] M. Ryo, Y. Wada, T. Okubo, T. Nakazawa, Y. Hasegawa, S. Yanagida, *J. Mater. Chem.* **12**, 1748 (2002).
- [12] M. Lezhnina, F. Laeri, L. Benmouhadi, U. Kynast, *Adv. Mater.* **18**, 280 (2006).
- [13] A. Monguzzi, G. Macchi, F. Meinardi, R. Tubino, M. Burger, G. Calzaferri, *Appl. Phys. Lett.* **92**, 123301 (2008).
- [14] H. Sun, A. Hosokawa, Y. Miwa, F. Shimaoka, M. Fujii, M. Mizuhata, S. Hayashi, S. Deki, *Adv. Mater.* **21**, 3694 (2009).
- [15] H. Sun, Y. Miwa, F. Shimaoka, M. Fujii, A. Hosokawa, M. Mizuhata, S. Hayashi, S. Deki, *Opt. Lett.* **34**, 1219 (2009).

- [16] H. Sun, T. Hasegawa, M. Fujii, F. Shimaoka, Z. Bai, M. Mizuhata, S. Hayashi, S. Deki, Appl. Phys. Lett. **94**, 141106 (2009).
- [17] Q. Xu, B. Lin, Y. Mao, J. Lumin. **128**, 1965 (2008).
- [18] M. Fujii, M. Yoshida, Y. Kanzawa, S. Hayashi, K. Yamamoto, Appl. Phys. Lett. **71**, 1198 (1997).
- [19] Y. Fujimoto, M. Nakatsuka, Appl. Phys. Lett. **82**, 3325 (2003).
- [20] X. Meng, J. Qiu, M. Peng, D. Chen, Q. Zhao, X. Jiang, C. Zhu, Opt. Express. **13**, 1635 (2005).
- [21] V. O. Sokolov, V. G. Plotnichenko, E. M. Dianov, Opt. Lett. **33**, 1488 (2008).

Chapter 5

Efficient near-infrared emission from neodymium by broadband sensitization of bismuth in zeolites

In this chapter, Nd-Bi co-doped zeolites were prepared by an ion-exchange process, and the optical properties were investigated by photoluminescence (PL) and PL excitation spectra, and decay time measurements. The results show that the near-infrared (NIR) emission of Nd^{3+} ions is significantly enhanced by the introduction of bismuth in co-doped samples, and the lifetime reaches 246 μs . Furthermore, it is revealed that NIR active Bi acts as a sensitizer of Nd^{3+} ions. The energy transfer efficiency is also estimated. The peculiar optical properties make them promising for potential application in biological probes.

5.1 Introduction

Zeolites are constructed from SiO_4 and AlO_4 tetrahedra linked to each other by sharing all of the oxygen atoms. For a long time, zeolites have been used as a major class of porous inorganic oxides that have wide applications in industry for separation and catalysis [1, 2]. In addition to common industrial applications of zeolites, there has been a tremendous surge in the application as host materials of optically active guests in the past decade, because the well-defined and well-organized cavities provided by zeolites host serve as an ideal environment to organize the optically active guests well dispersed in their framework [3-11]. However, near-infrared (NIR) emitters (such as Er^{3+} , Yb^{3+} , and Nd^{3+}) hardly show efficient emission in zeolites, because of the fast relaxation of their excitation energy via high-frequency vibration of O-H and/or C-H bonds [4, 8]. In order to obtain strong

emission using zeolites as the host, separating the NIR active centers from coordinated water is necessary. Recently, Sun et al. reported that bismuth is an excellent blockage material to realize highly efficient NIR emission in zeolites [9, 10].

Optical coherence tomography (OCT) is a noninvasive technology currently used to perform in vivo high-resolution, cross-sectional imaging of microstructure in biological tissues [12, 13]. For traditional OCT light sources, at 800 nm and 1.3 μm , the OCT resolution is seriously degraded with deeper imaging depths due to the dispersion by water in tissues. It is reported that the ultrahigh resolution of OCT can be achieved by choosing a light source with a center wavelength near 1.0 μm [14, 15]. Nd^{3+} is an ideal candidate for this purpose, because it displays strong emission bands at ~ 1064 nm. However, similar to the situation in other rare-earth ions, optical absorption of Nd^{3+} is too weak due to the forbidden nature of the intra-4f transitions. To overcome this deficiency, sensitization of Nd^{3+} emission by a sensitizer is an attractive way to obtain efficient emission. Very recently, it was found that Bi-related active centers can be exploited as sensitizers of rare earth ions such as Er^{3+} [16].

In this letter, we realize strong and long-lived Nd^{3+} emission in zeolites by means of co-doping bismuth. The emission cover the range of 970 - 1450 nm, corresponding to the electronic transitions of Nd^{3+} ions and Bi-related active centers, respectively. The NIR emission of Nd^{3+} ions is significantly enhanced by the introduction of bismuth in co-doped samples, and the lifetime reaches 246 μs . Steady state and time-resolved photoluminescence (PL), and PL excitation (PLE) measurements demonstrate the energy transfer from Bi-related active centers to Nd^{3+} .

5.2 Experimental details

Zeolites were stirred in x mM (x=0.5, 3, 6) aqueous solution of Nd^{3+} prepared from $\text{Nd}(\text{NO}_3)_3 \cdot 6\text{H}_2\text{O}$ at 80 $^\circ\text{C}$ for 96 h to exchange NH_4 ions with Nd^{3+} ions. The products were removed by centrifugation, then washed with deionized water, and dried in air at 120 $^\circ\text{C}$. The Nd embedded zeolites were further stirred in a 60 mM aqueous solution of Bi^{3+} prepared from $\text{Bi}(\text{NO}_3)_3 \cdot 5\text{H}_2\text{O}$ at 80 $^\circ\text{C}$ for 120 h to dope Bi. The products were removed by centrifugation, then washed with deionized water, and dried in air at 120 $^\circ\text{C}$. The Nd-Bi codoped zeolites were calcined at 920 $^\circ\text{C}$ for 1 h in N_2 atmospheric condition. For comparison, we also prepared Nd(3mM) and Bi(60mM) singly doped zeolites. All samples were exposed to the laboratory atmosphere prior to measurements.

The structural properties of prepared products were characterized by an X-ray diffractometer (Rigaku-TTR/S2, $\lambda = 1.54056$ \AA) and a field emission scanning electron microscopy (FE-SEM). Neodymium and bismuth concentrations were determined by energy-dispersive X-ray spectroscopy (EDS). The atomic concentrations of Nd and Bi in the final

products were shown in table 5.1. PL and PLE spectra were measured by using an Ar⁺ laser and an optical parametric oscillator (OPO) pumped by the third harmonic of a Nd:YAG laser. The signal was analyzed by a single grating monochromator and detected by a liquid-nitrogen-cooled InGaAs detector. Time-resolved luminescence measurements were performed by detecting the modulated luminescence signal with a photomultiplier tube, and then analyzing the signal with a photon-counting multichannel scaler. The excitation source for the lifetime measurements was 530 nm light from the OPO (pulse width 5 ns, repetition frequency 20Hz). All the measurements were carried out at room temperature.

Table 5.1: Atomic ratios (at. %) of Nd and Bi to (Yb+Bi+Si+Al+O) in the final products

Sample	Nd (at. %)	Bi (at. %)
Nd(3mM)	0.21	-
Nd(0.5mM)-Bi(60mM)	0.04	1.28
Nd(3mM)-Bi(60mM)	0.17	1.37
Nd(6mM)-Bi(60mM)	0.28	1.34
Bi(60mM)	-	1.30

5.3 Results and discussion

Figure 5.1 shows the XRD patterns of undoped-zeolites, Nd, Bi, singly and co-doped [Nd(3mM)-Bi(60mM)] zeolites. The diffraction patterns of doped samples are identical to that of undoped-zeolites, which means that the zeolites structure is well maintained after doping and thermal treatment. The FE-SEM images of corresponding samples are shown in figure 5.2 (a)-(c). The morphology and monodispersity of these samples remain almost unchanged.

The PL spectra of Nd, Bi singly and co-doped samples excited at 514.5 nm are shown in figure 5.3. The measurements are performed under the same testing condition. In the Nd singly doped sample, two emission bands centred at 1064 and 1332 nm are observed, which are attributed to the typical ${}^4F_{3/2} \rightarrow {}^4I_{11/2} + {}^4I_{13/2}$ transitions of the Nd³⁺ ions. For the Bi singly doped sample, a broad near-infrared emission centred at 1145 nm is observed, which could be ascribed to Bi-related active centers. The broadband emission covers the range of 970 - 1450 nm, and the full-width at half maximum is about 162 nm. In the co-doped samples, strong emissions from Nd³⁺ and Bi-related active centers are observed simultaneously. It can be seen that the Nd³⁺ emission in the co-doped samples are much stronger than that of the singly doped sample, more than two orders of magnitude. It is interesting to note that, in the series of co-doped samples, with the increase of Nd

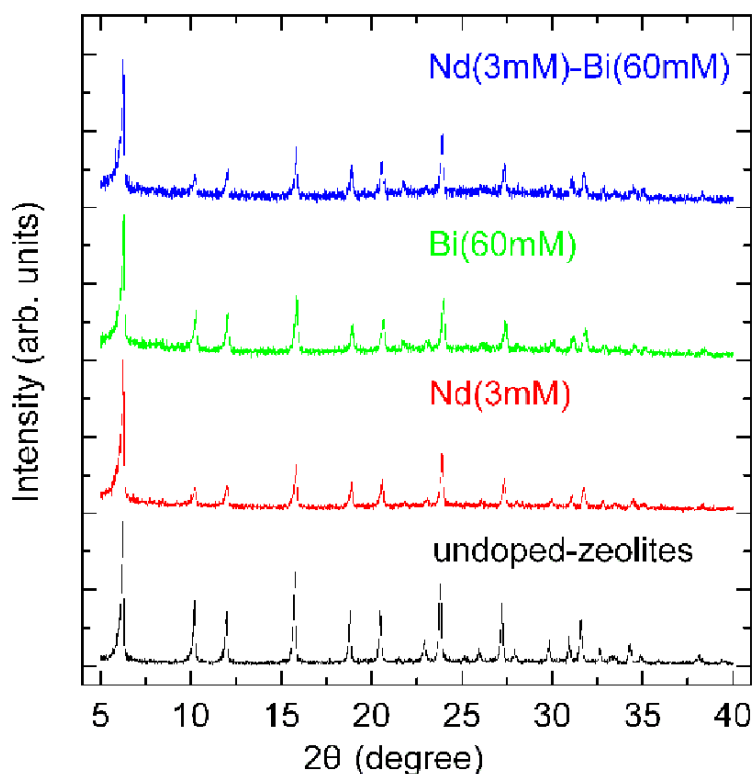


Figure 5.1: X-ray diffraction patterns of undoped-zeolites, Nd(3mM) singly doped, Bi(60mM) singly doped, and Nd(3mM)-Bi(60mM) co-doped zeolites.

concentration, the emission intensity of Bi-related active centers monotonically decreases compared with that in Bi singly doped sample, while the Nd³⁺ emission intensity increases. This suggests that the energy transfer from Bi-related active centers to Nd³⁺ results in the gradual decrease of emission from Bi-related active centers.

To clarify the energy transfer process between Nd³⁺ and Bi-related active centers, PLE spectra are measured. The PLE spectra of Nd(3mM) and Nd(3mM)-Bi(60mM) samples

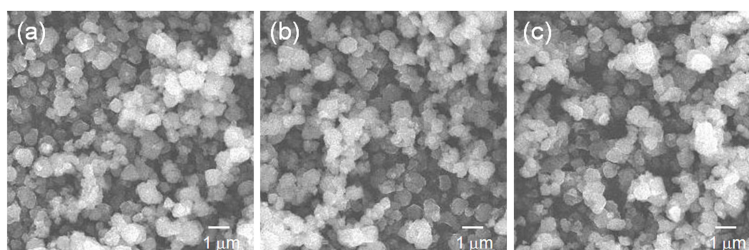


Figure 5.2: FE-SEM images of (a) Nd(3mM), (b) Bi(60mM) and (c) Nd(3mM)-Bi(60mM) samples.

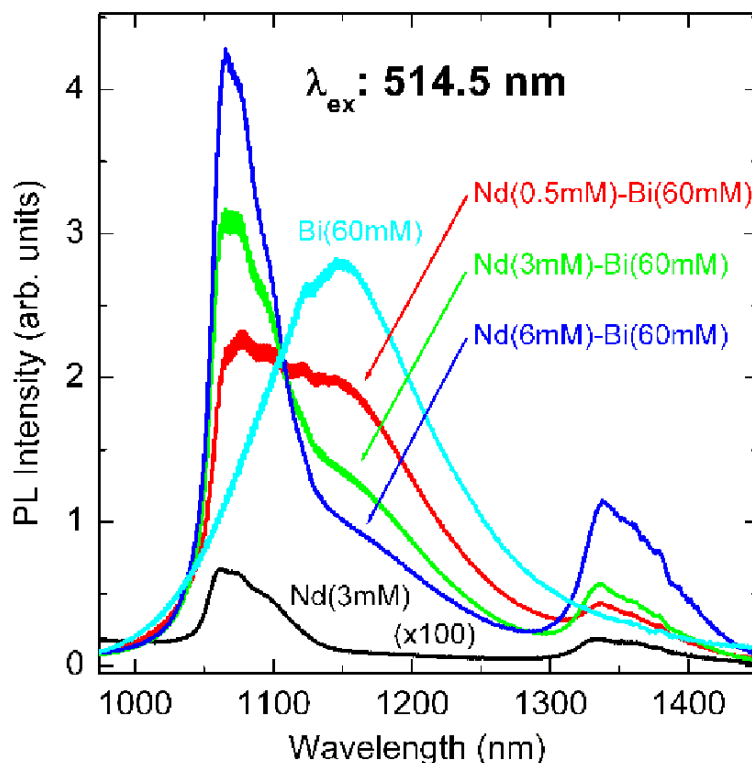


Figure 5.3: PL spectra of Nd, Bi singly and codoped zeolites excited at 514.5 nm. The PL spectrum of Nd singly doped sample is multiplied by a factor of 100.

detected at 1064 nm, and Bi(60mM) sample detected at 1145 nm are shown in figure 5.4. The PLE spectrum of Nd singly doped sample displays two discrete excitation bands at 476 and 530 nm, corresponding to the $^4I_{9/2}$ to $^4K_{15/2} + ^2D_{3/2} + ^2G_{9/2} + ^4G_{11/2}$ and $^2K_{13/2} + ^4G_{7/2} + ^4G_{9/2}$ transitions, respectively [17]. It is noteworthy that no Nd^{3+} emission can be detected under other excitation wavelengths. In contrast, the co-doped sample shows a continuous excitation spectrum, which means that Nd^{3+} ions in the co-doped sample are not only excited by direct absorption, but also excited by an indirect process. The indirect excitation of Nd^{3+} ions in the co-doped sample indicates that an energy transfer process occurs in zeolites. It should be mentioned that FAU-type zeolite is transparent in the visible region, so it could not be the energy donor for Nd^{3+} . On the other hand, the Bi singly doped sample exhibits a broad excitation band centred at ~ 500 nm (in figure 5.4), which coincides with those reported for Bi-doped glasses [18]. Therefore, Bi-related active centers are most likely to act as a sensitizer of Nd^{3+} .

Figure 5.5 (a) shows PL decay curves detected at 1064 nm. In the Nd singly doped sample, the lifetime is much shorter than the transition intrinsic lifetime of Nd^{3+} (less than 1 μs). This is due to nonradiative relaxation of Nd^{3+} by strong coupling of the excitation to high-frequency vibrations of coordinated water. The decay curves of co-doped samples

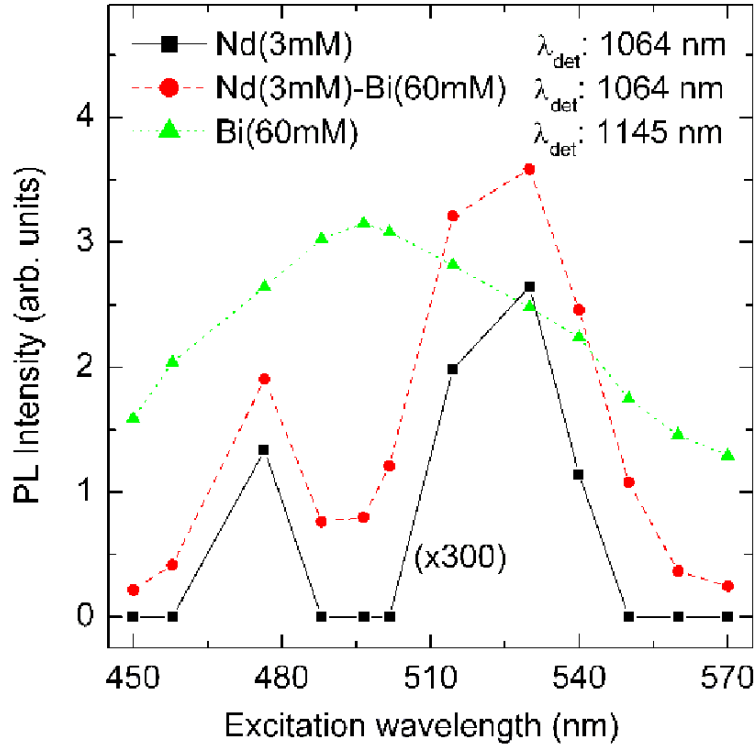


Figure 5.4: PL excitation spectra of Nd(3mM) and Nd(3mM)-Bi(60mM) samples detected at 1064 nm, and Bi(60mM) sample detected at 1145 nm. The PLE spectrum of Nd singly doped sample is multiplied by a factor of 300.

show a fast drop at the beginning, followed by a single-exponential slow component. With increasing Nd concentration, the slow component becomes more dominant. It is noteworthy that the Nd^{3+} emission at 1064 nm overlaps with the broadband emission of Bi-related active centers, such that there are two components with different lifetimes in all curves. The occurrence of the fast drop in the decay curves is the result of relaxation of Bi-related active centers excited state. The slow component is due to Nd^{3+} and the longest lifetime reaches 246 μs . The long lifetime of Nd^{3+} in co-doped samples suggests that Nd^{3+} is well separated from coordinated water in zeolites. One possible explanation of this is that bismuth forms bismuth oxide agglomerates to seal the pores of zeolites [19], and then water molecules have little chance to interact with Nd^{3+} ions. Another possibility is that Nd^{3+} ions are imbedded within bismuth oxide agglomerates in the pores of zeolites. Further work is necessary to fully prove these models. The lifetime of the Nd^{3+} becomes shorter in the highest Nd concentration sample, which could be ascribed to the energy migration between neighboring Nd^{3+} ions.

Figure 5.5 (b) shows the decay curves detected at 1145 nm. The decay curve of Bi singly doped sample can be well fitted by a single-exponential function, and the lifetime reaches

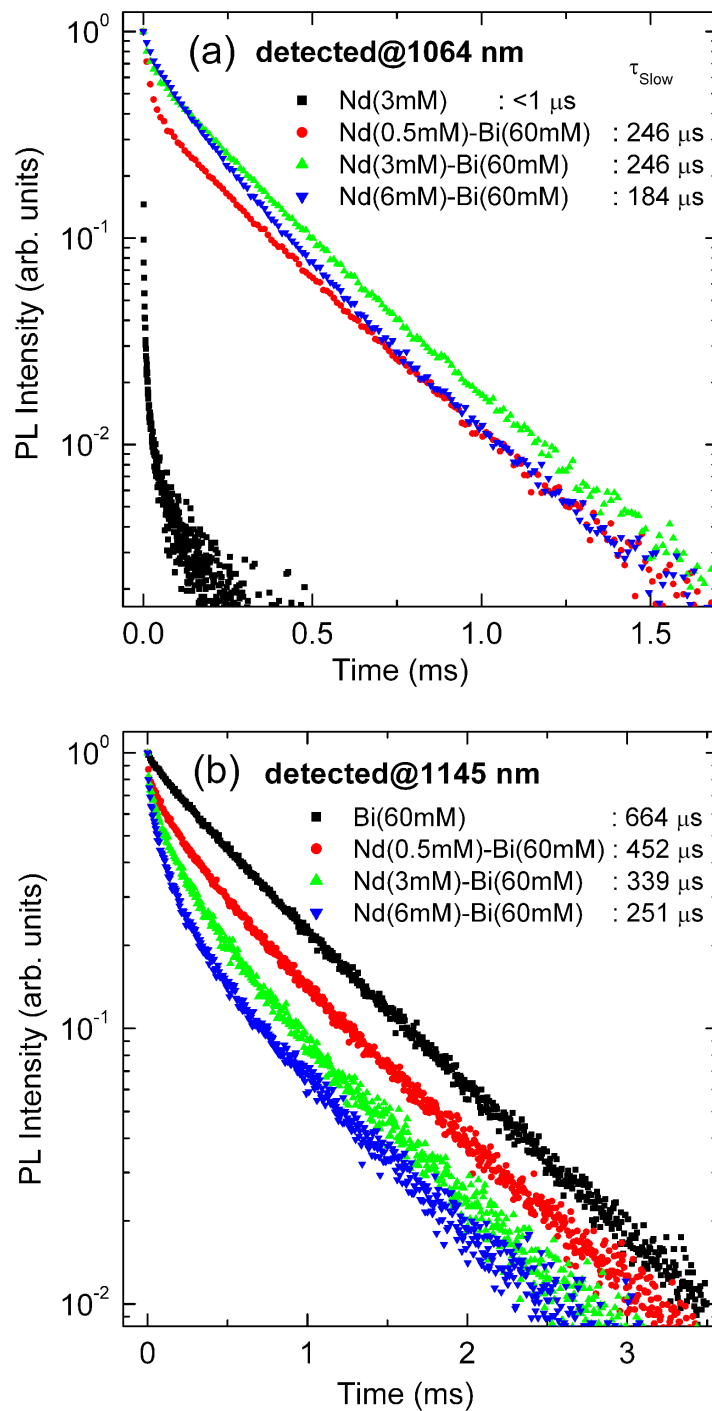


Figure 5.5: PL decay curves of all samples detected at (a) 1064 and (b) 1145 nm.

as long as 664 μs . The curves of co-doped samples can be fitted by double-exponential decay, and the mean lifetime (τ_m) was calculated by

$$\tau_m = \int_{t_0}^{\infty} [I(t)/I_0]d(t), \quad (5.1)$$

Where $I(t)$ is the luminescence intensity as a function of time t and I_0 is the maximum of $I(t)$ that occurs at the initial time t_0 . The lifetimes of Bi-related active centers decrease rapidly with the increase of Nd^{3+} concentrations, which is also a strong evidence of energy transfer from Bi-related active centers to Nd^{3+} . Similar behavior is commonly observed for nonradiative energy transfer processes. The energy transfer efficiency (η) can be estimated by

$$\eta = 1 - \frac{\tau_{Nd-Bi}}{\tau_{Bi}}, \quad (5.2)$$

Where τ_{Nd-Bi} and τ_{Bi} are the lifetimes of Bi-related active centers in co-doped and singly doped samples, respectively. The is calculated to be 32 % [Nd(0.5mM)-Bi(60mM)], 49 % [Nd(3mM)-Bi(60mM)], and 62 % [Nd(6mM)-Bi(60mM)], respectively.

It is well known that energy transfer process strongly depends on the spectral overlap between the emission band of the sensitizer and the absorption band of the acceptor. The emission band of Bi-related active centers covers the 970 - 1450 nm range, matching well with the excitation bands of Nd^{3+} , especially the ${}^4\text{I}_{11/2} \rightarrow {}^4\text{F}_{3/2}$ (1064 nm) and ${}^4\text{I}_{13/2} \rightarrow {}^4\text{F}_{3/2}$ (1332 nm) transitions. Thus, an efficient energy transfer process can be obtained in Nd-Bi co-doped zeolites.

5.4 Conclusion

In summary, Nd-Bi co-doped zeolites were prepared by an ion-exchange process, and the optical properties were investigated. The NIR emission of Nd^{3+} ions is significantly enhanced by the introduction of bismuth in co-doped samples, and the lifetime reaches 246 μs . The energy transfer from Bi-related active centers to Nd^{3+} was demonstrated by steady state and time-resolved PL, and PLE measurements. The energy transfer efficiency is also estimated. The results show that these nanosized materials have potential applications in biological probes.

References

- [1] M. E. Davis, *Acc. Chem. Res.* **26**, 111 (1993).
- [2] L. Tosheva, V. P. Valtchev, *Chem. Mater.* **17**, 2494 (2005).
- [3] U. Kynast, V. Weiler, *Adv. Mater.* **6**, 937 (1994).
- [4] Y. Wada, T. Okubo, M. Ryo, T. Nakazawa, Y. Hasegawa, S. Yanagida, *J. Am. Chem. Soc.* **122**, 8583 (2000).
- [5] J. Rocha, L. D. Carlos, *Curr. Opin. Solid State Mater. Sci.* **7**, 199 (2003).
- [6] M. Lezhnina, F. Laeri, L. Benmouhadi, U. Kynast, *Adv. Mater.* **18**, 280 (2006).
- [7] G. Calzaferri, K. Lutkouskaya, *Photochem. Photobiol. Sci.* **7**, 879 (2008).
- [8] K. Binnemans, *Chem. Rev.* **109**, 4283 (2009).
- [9] H. Sun, A. Hosokawa, Y. Miwa, F. Shimaoka, M. Fujii, M. Mizuhata, S. Hayashi, S. Deki, *Adv. Mater.* **21**, 3694 (2009).
- [10] H. Sun, T. Hasegawa, M. Fujii, F. Shimaoka, Z. Bai, M. Mizuhata, S. Hayashi, S. Deki, *Appl. Phys. Lett.* **94**, 141106 (2009).
- [11] A. Mech, A. Monguzzi, F. Meinardi, J. Mezyk, G. Macchi, R. Tubino, *J. Am. Chem. Soc.* **132**, 4574 (2010).
- [12] D. Huang, E. Swanson, C. P. Lin, J. S. Schuman, W. G. Stinson, W. Chang, M. R. Hee, T. Flotte, K. Gregory, C. A. Puliafito, J. G. Fujimoto, *Science* **254**, 1178 (1991).
- [13] W. Drexler, U. Morgner, F. X. Kartner, C. Pitris, S. A. Boppart, X. D. Li, E. P. Ippen, J. G. Fujimoto, *Opt. Lett.* **24**, 1221 (1999).
- [14] Y. Wang, J. Nelson, Z. Chen, B. Reiser, R. Chuck, R. Windeler, *Opt. Express* **11**, 1411 (2003).
- [15] S. Fuchi, A. Sakano, Y. Takeda, *Jpn. J. Appl. Phys.* **47**, 7932 (2008).

- [16] Z. Bai, H. Sun, T. Hasegawa, M. Fujii, F. Shimaoka, Y. Miwa, M. Mizuhata, S. Hayashi, *Opt. Lett.* **35**, 1926 (2010).
- [17] Y. Chen, Y. Huang, M. Huang, R. Chen, Z. Luo, *J. Am. Ceram. Soc.*, **88**, 19 (2005).
- [18] Y. Fujimoto, M. Nakatsuka, *Jpn. J. Appl. Phys.* **40**, 279 (2001).
- [19] H. Sun, Y. Sakka, Y. Miwa, N. Shirahata, M. Fujii, H. Gao, *Appl. Phys. Lett.* **97**, 131908 (2010).

Chapter 6

Bismuth sensitized efficient near-infrared luminescence from ytterbium in zeolites

In this chapter, Yb-Bi co-doped zeolites were prepared by a method consisting of a simple ion-exchange process and subsequent high-temperature annealing. We observe two strong near-infrared (NIR) emission bands overlapping in the range of 930 - 1480 nm, corresponding to the electronic transitions of bismuth-related active centres (BiRAC) and Yb³⁺ ions, respectively. In the obtained products, the excitation wavelength of Yb³⁺ is extended to the range of 420 - 850 nm, and the lifetime reaches 665 μ s. In the zeolite matrix, Bi ions exist as BiRAC and Bi compounds agglomerates. The former one act as a sensitizer of Yb³⁺ ions, and the latter one act as a blockage to seal the pores of zeolites, which enable Yb³⁺ ions to show efficient NIR emission even the zeolites contain large amount of coordinated water. The excellent optical and structural properties make these NIR emitting nanoparticles promising in application as biological probes.

6.1 Introduction

Nowadays, near-infrared (NIR) luminescence of rare-earth ions plays an important role in laser, optical telecommunication, and many other applications [1]. Er³⁺, Nd³⁺, and Yb³⁺ are the most investigated NIR emitting rare-earth ions. Among them, Yb³⁺ shows some unique optical properties, since Yb³⁺ has a very simple electronic level scheme involving only two manifolds, which makes it free from some undesired effects such as

excited state absorption, up-conversion, and cross relaxation [2]. As is known, human tissue is relatively transparent at around 0.8 - 1 μm [3]. Rare-earth ions, which are luminescent in this window, such as Yb^{3+} at 980 nm, are ideal candidates for in vivo biological probes, since they display sharp emission bands that can be easily discriminated from background fluorescence, and exhibit long luminescent lifetimes, which increase assay sensitivity through time-resolved measurements [4-6]. However, the single and narrow absorption band of Yb^{3+} means that the direct excitation is not ideal. It is far more common and convenient to stimulate the Yb^{3+} luminescence by exploiting energy transfer from a suitable sensitizer. Petit et al [7] reported continuous-wave room temperature and tunable laser operation of a co-doped Nd^{3+} , Yb^{3+} : CaF_2 bulk crystal around 1 μm after pumping Nd^{3+} around 800 nm. Shavaleev et al [8] reported that, the complexes $[\text{Yb}(\text{ligand})_2(\mu\text{-ligand})_2\text{Na}]$ display efficient Yb^{3+} emission upon excitation maximum at 450 nm, which results from a ligand-to-ytterbium energy transfer. Recently, it was found that " bismuth-related active centres (BiRAC) " can be exploited as sensitizers of rare earth ions such as Er^{3+} [9]. Therefore, we also expect that there may be effective sensitization of Yb^{3+} ions by an energy transfer process from BiRAC due to the excellent energy level overlap of Yb^{3+} and BiRAC.

Zeolites play indispensable roles in many technological and economical applications, such as catalysis, ion exchange, and separations. Recently, zeolites acting as host materials of optically active guests have attracted much attention for constructing functional materials designed at nanosized levels, because of their low vibrational framework, ion exchange capacity, well defined cavities and transparency in the UV-visible-NIR region [9-19]. Furthermore, our recent work reveals that the optically functionalized zeolites can be used as a new type of nanosized NIR photoluminescence (PL) biological probe, which show high efficiency and high photostability [20]. At present, optical properties of NIR emitting rare-earth ions, such as Er^{3+} and Nd^{3+} ions, have been intensely investigated in zeolites [9,15-18]. However, to the best of our knowledge, there has been no report on Yb^{3+} doped zeolites until now.

In this work, we prepare Yb and Bi singly and co-doped zeolites by an ion-exchange process and subsequent high temperature annealing. Steady state and time-resolved emission spectra, and excitation spectra are measured, and the energy transfer from BiRAC to Yb^{3+} ions is confirmed. The energy transfer mechanism is discussed, and the intrinsic quantum yield of the sensitized Yb^{3+} luminescence is estimated.

6.2 Experimental details

Zeolites were stirred in x mM (x=1, 10, 60) aqueous solution of Yb^{3+} prepared from $\text{YbCl}_3 \cdot 6\text{H}_2\text{O}$ at 80 $^\circ\text{C}$ for 120 h to exchange NH_4 ions with Yb^{3+} ions. The products

were removed by centrifugation, then washed with deionized water, and dried in air at 120 °C. The Yb embedded zeolites were further stirred in a 60 mM aqueous solution of Bi^{3+} prepared from $\text{Bi}(\text{NO}_3)_3 \cdot 5\text{H}_2\text{O}$ at 80 °C for 144 h to dope Bi. The products were removed by centrifugation, then washed with deionized water, and dried in air at 120 °C. The Yb-Bi co-doped zeolites were calcined at 900 °C for 1 h in N_2 atmospheric condition. Hereafter, the co-doped samples were denoted as Z-xYb-yBi, where x and y are ytterbium and bismuth concentrations (mM) in the experimental solution. For comparison, we also prepared Z-10Yb and Z-60Bi singly doped samples. All samples were exposed to the laboratory atmosphere prior to measurements.

The structural properties of prepared products were characterized by an X-ray diffractometer (Rigaku-TTR/S2, $\lambda = 1.54056 \text{ \AA}$) and a field emission scanning electron microscopy (FE-SEM). Ytterbium and bismuth concentrations were determined by inductively coupled plasma atomic emission spectroscopy (ICP-AES) and energy-dispersive X-ray spectroscopy (EDS), respectively. The atomic concentrations of Yb and Bi in the final products were shown in table 6.1. PL measurements were carried out with the excitation of 488 nm line from an Ar^+ laser. The excitation sources for PL excitation (PLE) measurements were 420 - 670 nm light from an optical parametric oscillator (OPO) pumped by the third harmonic of a Nd:YAG laser, 690 nm light from a laser diode, 720 - 850 nm light from a Ti:sapphire laser. The signal was analyzed by a single grating monochromator and detected by a liquid-nitrogen-cooled InGaAs detector. Time-resolved luminescence measurements were performed by detecting the modulated luminescence signal with a photomultiplier tube (Hamamatsu, R5509-72), and then analyzing the signal with a photon-counting multichannel scaler. The excitation source for the lifetime measurements was 488 nm light from the OPO (pulse width 5 ns, repetition frequency 20Hz). All the measurements were carried out at room temperature.

6.3 Results and discussion

Figure 6.1 shows the XRD patterns of Z-10Yb, Z-60Bi, and Z-10Yb-60Bi samples. The data of the diffraction peaks agree well with the standard values for the Zeolite Y

Table 6.1: The atomic concentrations of Yb and Bi in the final products

Sample	Yb at. %	Bi at. %
Z-10Yb	0.46	-
Z-1Yb-60Bi	0.03	1.28
Z-10Yb-60Bi	0.15	1.32
Z-60Yb-60Bi	0.45	1.30
Z-60Bi	-	1.30

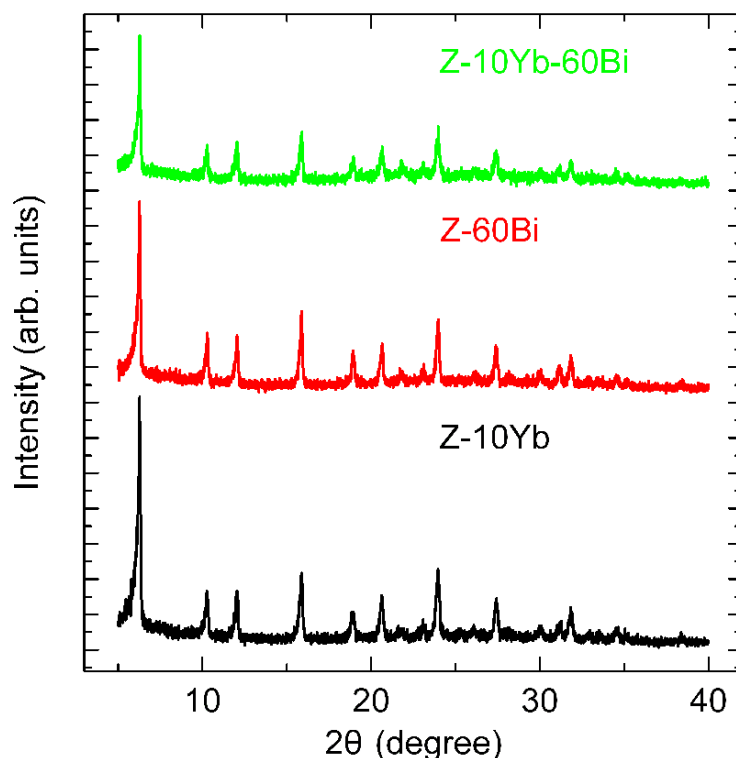


Figure 6.1: X-ray diffraction patterns of Z-10Yb, Z-60Bi, and Z-10Yb-60Bi samples.

(JCPDS No. 45-0112), indicating that the obtained samples are single phase and the co-doped ytterbium and bismuth do not cause any significant change. The FE-SEM images of corresponding samples are shown in figure 6.2 (a)-(c). The morphology and monodispersity of these samples remain almost unchanged.

The PL spectra of Yb, Bi singly and co-doped samples excited at 488 nm are shown in figure 6.3. In the Bi singly doped sample, we observe a broad NIR emission centered at 1145 nm, which could be ascribed to BiRAC. The broadband emission covers the range of 930 - 1480 nm, and the full-width at half maximum is about 160 nm. For Yb singly doped

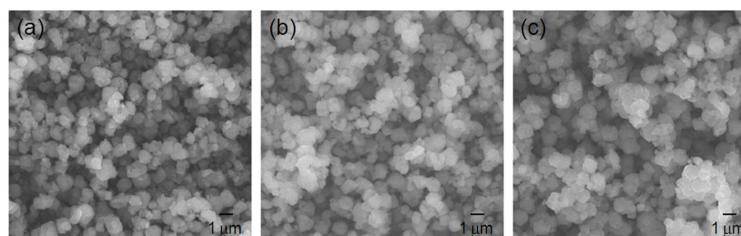


Figure 6.2: FE-SEM images of (a) Z-10Yb, (b) Z-60Bi, and (c) Z-10Yb-60Bi samples.

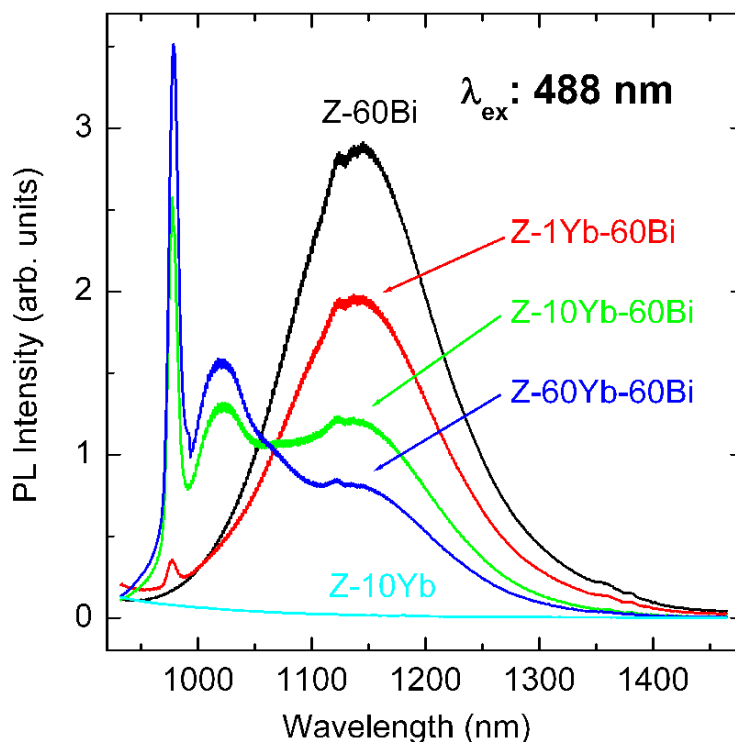


Figure 6.3: PL spectra of Yb, Bi singly and co-doped zeolites, excited at 488 nm.

sample, no NIR emission is detectable, because there is no Yb^{3+} level enabling the direct excitation of ytterbium emission with 488 nm light. Interestingly, in co-doped samples, we observe remarkably strong Yb^{3+} -related emissions at 980 and 1022 nm, corresponding to the transitions from the lowest Stark level of the Yb^{3+} : $^2\text{F}_{7/2}$ multiplet to two different Stark levels of the $^2\text{F}_{5/2}$ multiplet. Furthermore, in addition to the emission band from Yb^{3+} , co-doped samples show broad PL from BiRAC. It is obvious that in the series of co-doped samples, with the increase of Yb concentration, the emission intensity of Yb^{3+} monotonically increases, while the BiRAC emission intensity decreases. It can be considered that the energy transfer from BiRAC to Yb^{3+} results in the strong Yb^{3+} emission and the decrease of BiRAC emission under the excitation of 488 nm.

In order to further investigate the energy transfer between BiRAC and Yb^{3+} , PLE spectra are measured. The measurements are performed under the same testing condition. The PLE spectra of Z-10Yb and Z-10Yb-60Bi samples detected at 980 nm, and Z-60Bi sample detected at 1145 nm are shown in figure 6.4. In the Yb singly doped sample, Yb^{3+} has no excitation band in the range of 420 - 850 nm. The excitation spectrum of BiRAC is characterized by the presence of three broad bands centered at 520 nm, 690 nm, and 820 nm. It was reported that bismuth-doped silica glasses have the absorption bands at 500 nm, 700 nm and 800 nm [21], which almost consists with the excitation spectrum of

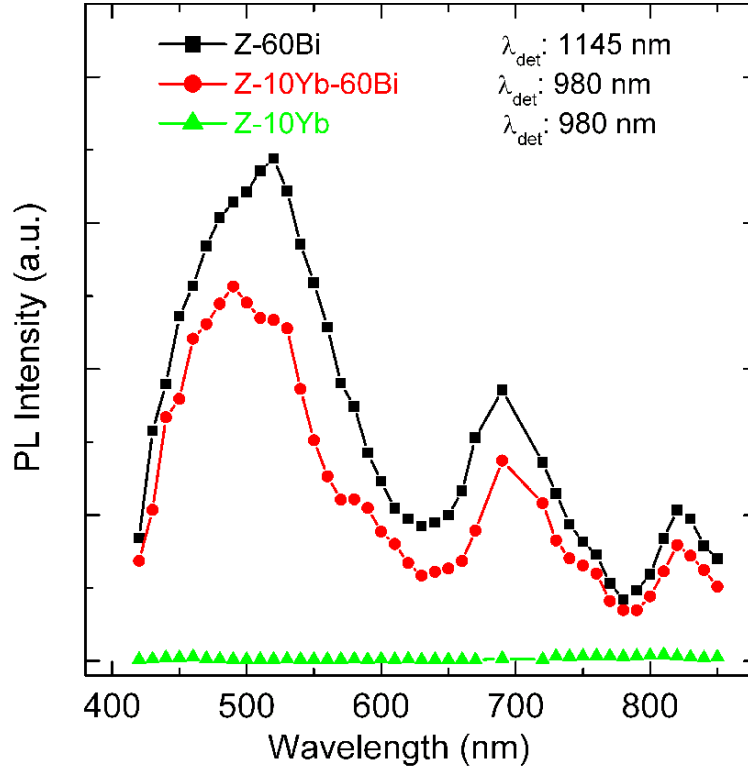


Figure 6.4: PL excitation spectra of Z-10Yb and Z-10Yb-60Bi samples detected at 980 nm, and Z-60Bi sample detected at 1145 nm.

Bi doped zeolites used for our experiment. The PLE spectrum of the co-doped sample detected at 980 nm exhibits a similar excitation spectrum with BiRAC. The two similar excitation spectra prove that Yb^{3+} in codoped samples is indirectly excited by an energy transfer process from BiRAC.

For energy transfer process, it requires an overlap of the emission region of the sensitizer and the absorption region of the acceptor. Figure 6.5 shows the possible energy transfer process between Yb^{3+} ions and BiRAC. As can be seen, there is an excellent overlap between the emission band of BiRAC assigned to the $\text{ES}_1 \rightarrow \text{GS}$ transition and the absorption band of Yb^{3+} due to the ${}^2\text{F}_{7/2} \rightarrow {}^2\text{F}_{5/2}$ transition. BiRAC can be excited by photons in the range of 420 - 850 nm to reach upper excited state (such as ES_2 , ES_3 , and ES_4) and then relax nonradiatively to ES_1 . The energy transfer occurs from the ES_1 excited state of BiRAC to the ${}^2\text{F}_{5/2}$ excited state of Yb^{3+} , which stimulates the occurrence of the strong NIR emission of Yb^{3+} . The results of measurements reveal that Yb^{3+} in the co-doped system can be efficiently excited within the broad visible-NIR region, so optical pumping using flash lamp or white LED rather than laser becomes feasible using this broadband sensitization.

Figure 6.6 (a) shows the decay curves detected at 980 nm. All of them show a fast drop

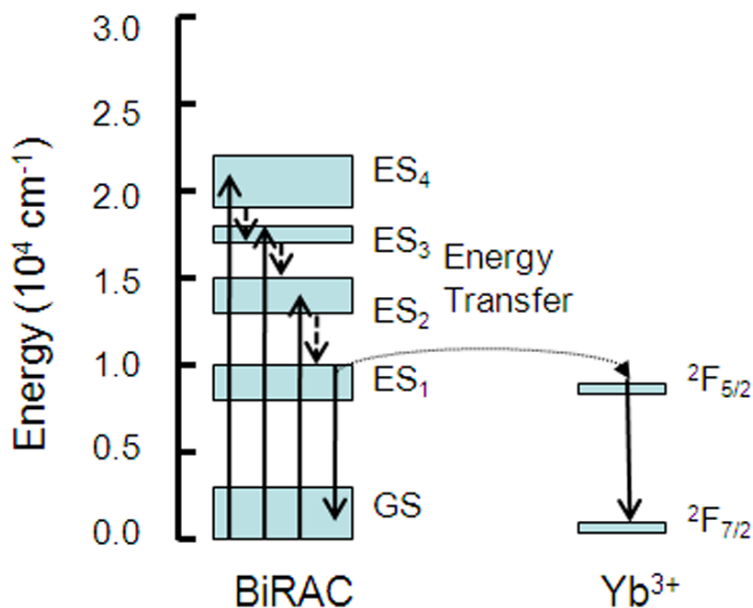


Figure 6.5: Energy level diagram of Yb-Bi codoped zeolites which exhibits BiRAC \rightarrow Yb³⁺ energy transfer. ES, excited state; GS, ground state.

at the beginning, followed by a single-exponential slow component. With increasing Yb concentration, the slow component becomes more dominant. It is noteworthy that the Yb³⁺ emission at 980 nm overlaps with the edge of the broadband emission of BiRAC, such that there are two components with different lifetimes in all curves. The occurrence of the fast drop in the decay curves is the result of relaxation of BiRAC excited state. The slow component is due to Yb³⁺ and the longest lifetime reaches up to 665 μ s. The lifetime of the Yb³⁺ becomes shorter in the highest Yb concentration. This is probably due to the energy migration between neighboring Yb³⁺ ions.

The intrinsic quantum yield (Φ) of the sensitized Yb³⁺ luminescence can be estimated using the following relationship between the experimentally determined lifetime of Yb³⁺ (τ_{exp}) and its radiative lifetime (τ_{rad}):

$$\Phi = \frac{\tau_{exp}}{\tau_{rad}}, \quad (6.1)$$

Using a typical value of 1.2 ms for Yb³⁺, we estimate the intrinsic quantum yield to be 55.4 %. Due to the particular morphology, this type of zeolite always contain large amount of coordinated water. In general, high efficient NIR emission in zeolites is difficult to achieve, because of the existence of coordinated water in cages, causing fast relaxation of its excitation energy through nonradiative vibrational deactivation.

Based on our model [18,19], we think that Yb³⁺ and Bi ions migrate into the pores of zeolites by ion-exchange process, and after subsequent high temperature annealing, parts

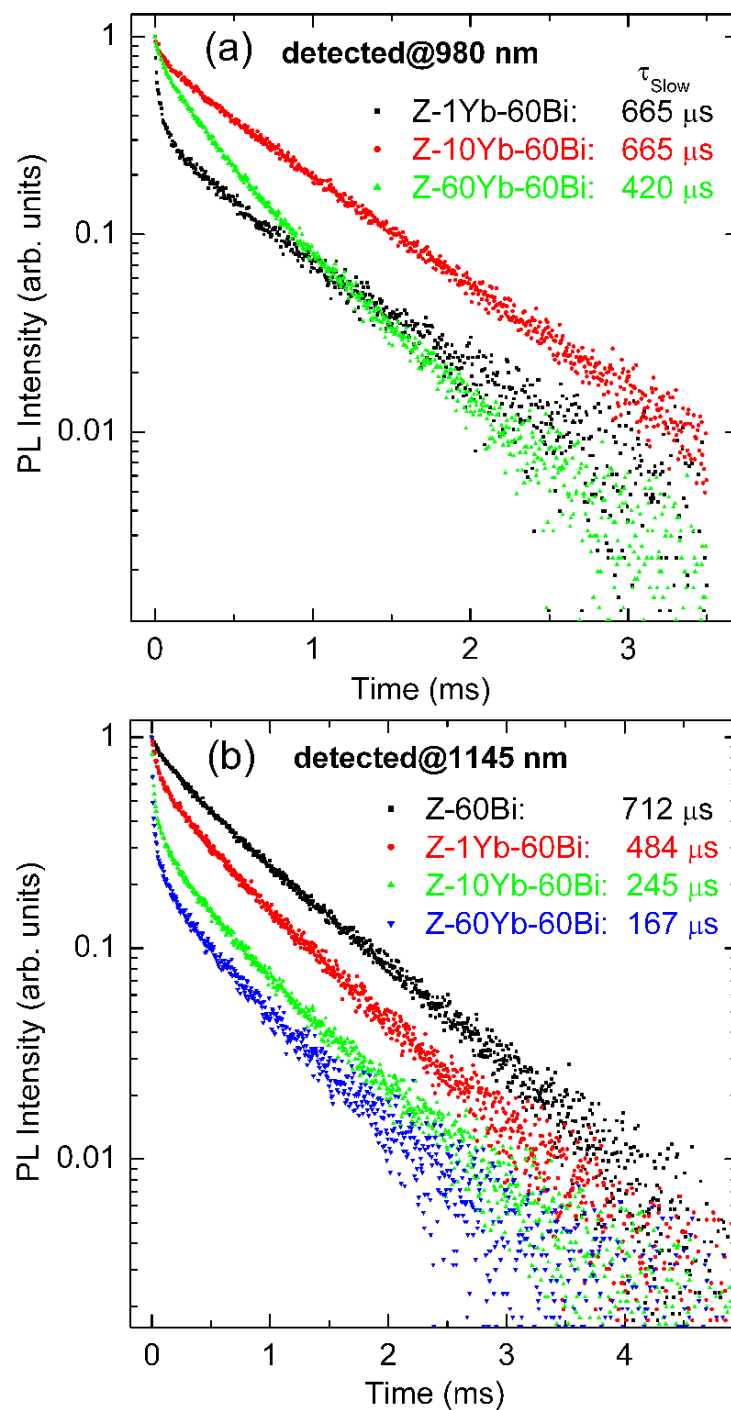


Figure 6.6: (a) PL decay curves of co-doped samples detected at 980 nm. (b) PL decay curves of co-doped samples and Bi singly doped sample detected at 1145 nm.

of Bi ions are converted to BiRAC, and the other parts form Bi compounds agglomerates, due to the low melting point of bismuth compounds. The agglomerates act as a blockage to seal the pores of zeolites, which can avoid the admission of coordinated water into the pores of zeolites. Therefore, Yb^{3+} ions can be held in captivity totally in the pores, and then have chance to show strong and long-lived NIR emission, even the zeolites contain large amount of water. Due to the mature fabrication technology, the size and morphology of zeolites can be well controlled. Based on the excellent blocking property of Bi compounds agglomerates, broadband sensitization of BiRAC, and efficient NIR emission of Yb^{3+} ions, it is expected that these NIR emitting nanoparticles can show strong NIR emission even when dispersed in blood as biological probes.

Figure 6.6 (b) shows the decay curves detected at 1145 nm, i.e., emission from BiRAC. The decay curve of Bi singly doped sample can be well fitted by a single-exponential function, and the lifetime reaches as long as 712 μs . The curves of co-doped samples can be fitted by double-exponential decay, and the mean lifetime (τ_m) was calculated by

$$\tau_m = \int_{t_0}^{\infty} [I(t)/I_0]d(t), \quad (6.2)$$

Where $I(t)$ is the luminescence intensity as a function of time t and I_0 is the maximum of $I(t)$ that occurs at the initial time t_0 . The lifetimes of BiRAC decrease rapidly with the increase of Yb^{3+} concentrations, which is also a strong evidence of energy transfer from BiRAC to Yb^{3+} . Similar behavior is commonly observed for nonradiative energy transfer processes. The energy transfer efficiency (η) can be estimated by

$$\eta = 1 - \frac{\tau_{\text{Yb-Bi}}}{\tau_{\text{Bi}}}, \quad (6.3)$$

Where $\tau_{\text{Yb-Bi}}$ and τ_{Bi} are the lifetimes of BiRAC in co-doped and singly doped samples, respectively. η is calculated to be 32 % (Z-1Yb-60Bi), 66 % (Z-10Yb-60Bi), and 77 % (Z-60Yb-60Bi).

6.4 Conclusion

Yb-Bi co-doped zeolites were prepared by an ion-exchange method and their optical properties were investigated. We observed two strong emission bands overlapping in the range of 930 - 1480 nm under the visible-NIR light excitation, corresponding to the electronic transitions of BiRAC and Yb^{3+} ions, respectively. The energy transfer between BiRAC and Yb^{3+} has been demonstrated from steady state and time-resolved emission spectra, and excitation spectra. The excitation wavelength of Yb^{3+} is extended to the range of 420 - 850 nm, and the lifetime reaches 665 μs . The energy transfer mechanism is discussed and the energy transfer efficiency is estimated. The excellent optical and

structural properties make these NIR emitting nanoparticles promising in application as biological probes.

The results obtained in this work are similar to those of our previous work on Er-Bi co-doped zeolites [9]. In that case, Er^{3+} exhibits long-lived NIR PL ($1.54 \mu\text{m}$) due probably to the isolation from coordinated water by Bi compounds and the sensitization by BiRAC. The observation of similar behaviour between Er-Bi and Yb-Bi co-doped zeolites strongly suggest that the present system can be extended to different kinds of rare-earth ions and can be used in a variety of fields that require visible to NIR light sources.

References

- [1] J. Meng, j. Li, Z. Shi, K. Cheah, *Appl. Phys. Lett.* **93**, 221908 (2008).
- [2] W. Li, H. Pan, L. Ding, H. Zeng, W. Lu, G. Zhao, C. Yan, L. Su, J. Xu, *Appl. Phys. Lett.* **88**, 221117 (2006).
- [3] M. D. Ward, *Coord. Chem. Rev.* **251**, 1663 (2007).
- [4] M. I. Gaiduk, V. V. Grigoryants, A. F. Mironov, V. D. Rumyantseva, V. I. Chissoy, G. M. Sukhin, *J. Photochem. Photobiol. B.* **7**, 15 (1990).
- [5] J. Zhang, P. D. Badger, S. J. Geib, S. Petoud, *Angew. Chem. Int. Ed.* **44**, 2508 (2005).
- [6] F. Jiang, C. Poon, W. Wong, H. Koon, N. Mak, C. Choi, D. W. J. Kwong, Y. Liu, *ChemBioChem.* **9**, 1034 (2008).
- [7] V. Petit, P. Camy, J. L. Doualan, R. Moncorge, *Appl. Phys. Lett.* **88**, 051111 (2006).
- [8] N. M. Shavaleev, R. Scopelliti, F. Gumy, J. G. Bunzli, *Inorg. Chem.* **48**, 7937 (2009).
- [9] Z. Bai, H. Sun, T. Hasegawa, M. Fujii, F. Shimaoka, Y. Miwa, M. Mizuhata, S. Hayashi, *Opt. Lett.* **35**, 1926 (2010).
- [10] J. He, Y. Ba, C. I. Ratcliffe, J. A. Ripmeester, D. D. Klug, J. S. Tse, *Appl. Phys. Lett.* **74**, 830 (1999).
- [11] W. Chen, R. Sammynaiken, Y. Huang, *J. Appl. Phys.* **88**, 1424 (2000).
- [12] J. Rocha, L. D. Carlos, *Curr. Opin. Solid State Mater. Sci.* **7**, 199 (2003).
- [13] M. Flores-Acosta, R. Perez-Salas, R. Aceves, M. Sotelo-Lerma, R. Ramirez-Bon, *Solid State Commun.* **136**, 567 (2005).
- [14] G. Calzaferri, K. Lutkouskaya, *Photochem. Photobiol. Sci.* **7**, 879 (2008).
- [15] M. Ryo, Y. Wada, T. Okubo, T. Nakazawa, Y. Hasegawa, S. Yanagida, *J. Mater. Chem.* **12**, 1748 (2002).

- [16] M. Lezhnina, F. Laeri, L. Benmouhadi, U. Kynast, *Adv. Mater.* **18**, 280 (2006).
- [17] K. Binnemans, *Chem. Rev.* **109**, 4283 (2009).
- [18] H. Sun, T. Hasegawa, M. Fujii, F. Shimaoka, Z. Bai, M. Mizuhata, S. Hayashi, S. Deki, *Appl. Phys. Lett.* **94**, 141106 (2009).
- [19] H. Sun, A. Hosokawa, Y. Miwa, F. Shimaoka, M. Fujii, M. Mizuhata, S. Hayashi, S. Deki, *Adv. Mater.* **21**, 3694 (2009).
- [20] H. Sun, J. Yang, M. Fujii, Y. Sakka, Y. Zhu, T. Asahara, N. Shirahata, M. Li, Z. Bai, J. Li, H. Gao, *Small.* **7**, 199 (2011).
- [21] X. Meng, J. Qiu, M. Peng, D. Chen, Q. Zhao, X. Jiang, C. Zhu, *Opt. Express* **13**, 1635 (2005).

Chapter 7

Enhanced red luminescence and energy transfer in Eu-Bi co-doped zeolites for white LEDs

In this chapter, we investigate the optical properties of Eu doped zeolites by co-doping Bi. The addition of Bi^{3+} strongly enhances the red luminescence of Eu^{3+} (${}^5D_0 \rightarrow {}^7F_2$) in zeolites about 50 times, and the lifetime is significantly increased from 25.8 μs to 2.46 ms. The results reveal that the $O^{2-} \rightarrow Eu^{3+}$ charge transfer band and sensitization of Bi^{3+} ions distinctly enhances the excitation band of Eu^{3+} ions in the ultraviolet region. The energy transfer efficiency is estimated to be 78 %. It is expected that the present Eu-Bi co-doped zeolites have potential application in white-LEDs.

7.1 Introduction

In recent years, there is a great interest in generation of white light sources for a variety of applications, such as lighting and displays and so on [1,2]. One of the effective ways for generating white light is mixing three monochromatic sources (blue, green, and red) [3]. Rare-earth ions are the suitable candidates for this purpose owing to their abundant energy levels enable them to emit narrow intra-4f transitions over the entire ultraviolet (UV) to infrared spectral range [3,4]. Among them, the optical properties of Eu^{3+} ions doped into various host materials have been extensively studied since the Eu^{3+} ion is a preferable choice for red emitting phosphors in white light emitting diodes (LEDs) [4]. However, the optical absorption of the Eu^{3+} ion is too weak due to the forbidden nature

of intra-4f transitions [5]. Sensitization by an energy transfer process is an attractive way to obtain efficient red emission from Eu^{3+} ions.

Zeolites are very promising host materials of optically active centers for constructing novel materials, because their wall consists of Si-O-Al and Si-O-Si framework with low vibration quanta and their pores can be used for separately locating the cations [6]. In addition, zeolites are thermally stable at relatively high temperatures and optically transparent in the region from UV to near infrared, which is very promising for optical applications [7,8]. In the past decade, considerable works have been devoted on the luminescent properties of Eu doped zeolites [9-14]. However, the low quantum yield is a serious problem for practical applications, because of the fast relaxation of its excitation energy via high-frequency vibration of O-H bond [9-11]. Borgmann et al.[9] demonstrated that efficient red emission can be realized by collapsing the open zeolitic material in to more dense aluminosilicates, which is attributed to the reduction of OH species in the materials. Chen et al.[10] reported that the luminescence from Eu^{3+} in zeolites is enhanced greatly when the sample is treated at 800 °C, due to loss of water and the migration of the ions from the supercages to the sodalite cages. Though these methods can enhance the emission of Eu doped zeolites to some extent, the quantum yields are still very low comparing with other host materials, such as glasses and crystals.

Here, we report that co-doping Bi into Eu doped zeolites is a facile access to efficient red emitting microporous materials. We observe enhanced red luminescence in Eu-Bi co-doped zeolites, and the lifetime reaches as long as 2.46 ms. The introduction of Bi^{3+} ions distinctly enhances the excitation band of Eu^{3+} ions in the UV region.

7.2 Experimental details

Zeolites were stirred in 5 mM aqueous solution of Eu^{3+} prepared from $\text{EuCl}_3 \cdot 6\text{H}_2\text{O}$ at 80 °C for 24 h to exchange NH_4 ions with Eu^{3+} ions. The products were removed by centrifugation, then washed with deionized water, and dried in air at 120 °C. The Eu embedded zeolites were further stirred in a 60 mM aqueous solution of Bi^{3+} prepared from $\text{Bi}(\text{NO}_3)_3 \cdot 5\text{H}_2\text{O}$ at 80 °C for 24 h to dope Bi. The products were removed by centrifugation, then washed with deionized water, and dried in air at 120 °C. The Eu-Bi co-doped zeolites were calcined at 900 °C for 1 h in air. For comparison, we also prepared Eu(5 mM) and Bi(60 mM) singly doped samples. Hereafter, the Eu, Bi singly and co-doped samples were denoted as Z-Eu, Z-Bi, and Z-Eu-Bi. All samples were exposed to the laboratory atmosphere prior to measurements.

The structural properties of prepared products were characterized by an X-ray diffractometer (Rigaku-TTR/S2, $\lambda = 1.54056 \text{ \AA}$) and a field emission scanning electron microscopy (FE-SEM). Eu and Bi concentrations were determined by energy-dispersive X-

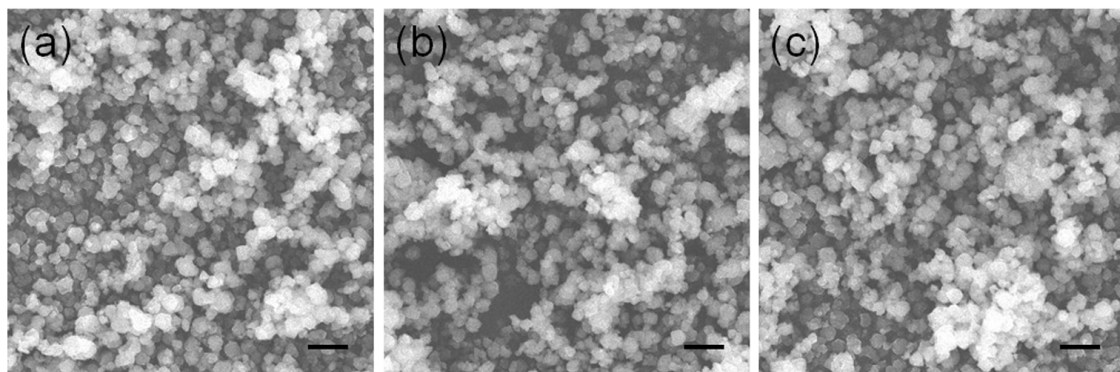


Figure 7.1: FE-SEM images of (a) Z-Eu, (b) Z-Bi, and (c) Z-Eu-Bi samples. Scale bars: 2 μm .

ray spectroscopy (EDS). Photoluminescence (PL) measurements were carried out with the excitation of 325 nm light from a He-Cd laser. The signal was analyzed by a single grating monochromator and detected by a liquid-nitrogen-cooled CCD detector. PL excitation spectrum was obtained by a PL spectrophotometer (JASCO FP6500) equipped with a CCD detector. Time-resolved luminescence measurements were performed by detecting the modulated luminescence signal with a photomultiplier tube (Hamamatsu, R943-02), and then analyzing the signal with a photon-counting multichannel scaler. The excitation source for decay time measurements was 355 nm light from a Nd:YAG laser (pulse width 5 ns, repetition frequency 20Hz).

7.3 Results and discussion

The X-ray diffraction patterns of all samples reveal that the obtained samples are single phase and the doping Eu and/or Bi do not cause any significant change (not shown here). Figure 7.1 (a)-(c) show the FE-SEM images of Z-Eu, Z-Bi, and Z-Eu-Bi samples. The morphology and monodispersity of these samples remain almost unchanged. The atomic concentrations of Eu and Bi in the final products are shown in table 7.1. It can be seen that Eu and Bi concentrations are well controlled by the experimental procedure.

Table 7.1: The atomic concentrations of Eu and Bi in the final products.

Sample	Eu at. %	Bi at. %
Z-Eu	0.16	-
Z-Bi	-	1.26
Z-Eu-Bi	0.14	1.23

Figure 7.2 shows the PL spectra of Eu, Bi singly and co-doped zeolites excited at 325 nm. In Bi singly doped sample, a broad emission band centered at 560 nm is detected. Similar emission band is commonly observed in Bi doped materials, which corresponds to the $^3P_1 \rightarrow ^1S_0$ transition of Bi^{3+} [15]. It is also reported that high temperature annealing process in air may introduce several types of defects in zeolites, such as oxygen vacancies, which shows broad emission in visible region [16]. Therefore, both Bi^{3+} and oxygen vacancies are the potential origins of the broad emission. For Eu singly doped sample, a strong emission peak at 621 nm and several weak peaks at 580 nm, 592 nm, 654 nm, and 703 nm are observed, which arise from the $^5D_0 \rightarrow ^7F_J$ ($J = 1-4$) transitions of Eu^{3+} . Interestingly, in the co-doped sample, the PL intensities from Eu^{3+} are significantly enhanced about 50 times, and at the same time, the Eu^{3+} emission peaks are superimposed on a broad and weak emission band. It is also observed that the addition of Bi^{3+} results in the change of the shape of Eu^{3+} luminescence; the strongest luminescence peak shifts from 621 nm to 613 nm, the relative PL intensity at 580 nm is enhanced, and a new additional peak at 598 nm appears.

The PL excitation spectra of Z-Eu and Z-Eu-Bi samples detected at 613 nm are presented in figure 7.3. The spectra are normalized at 394 nm. In the Z-Eu sample, several

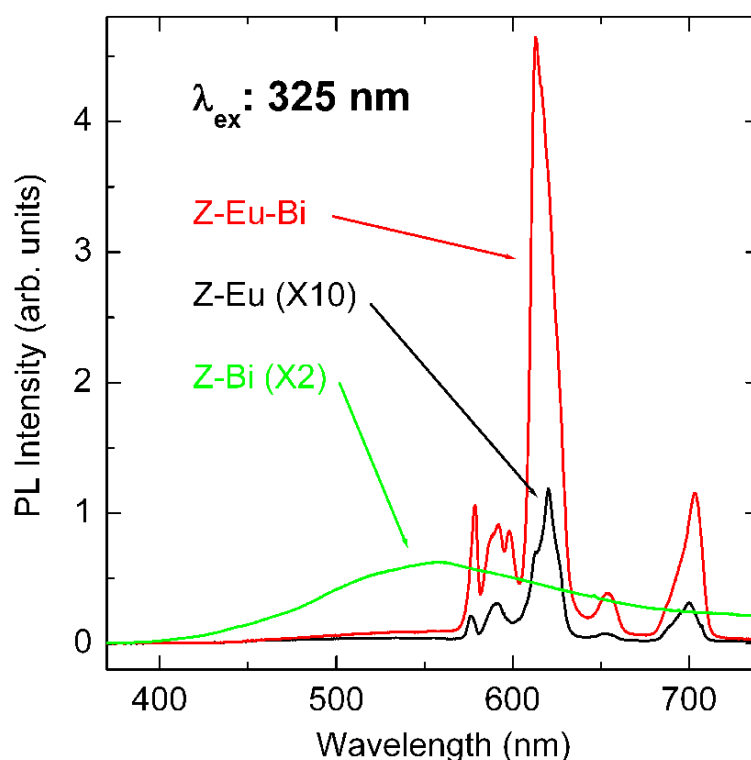


Figure 7.2: PL spectra of Eu, Bi singly and co-doped zeolites, excited at 325 nm. The PL spectra of Z-Eu and Z-Bi samples are multiplied by factors of 10 and 2, respectively.

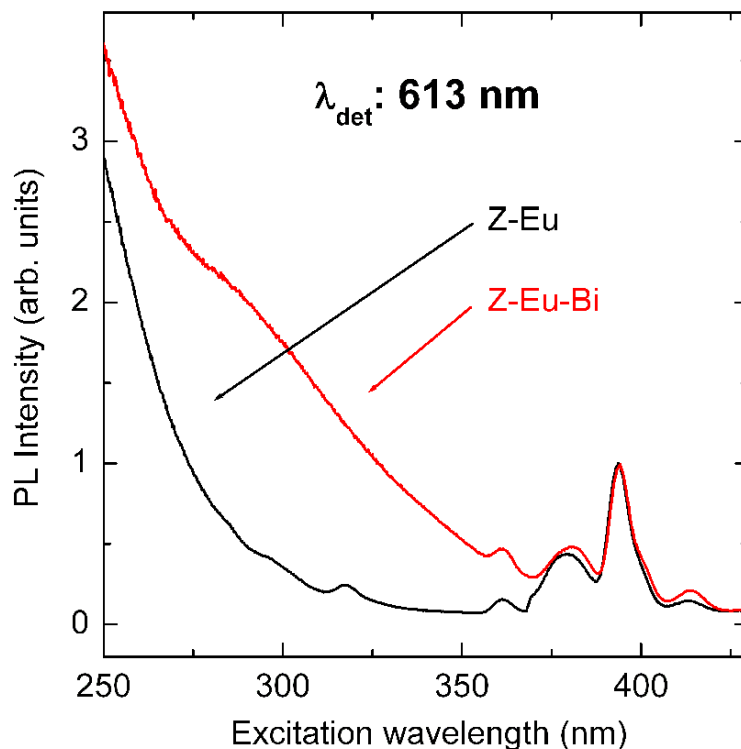


Figure 7.3: PL excitation spectra of Z-Eu and Z-Eu-Bi samples detected at 613 nm. The spectra are normalized at 394 nm.

sharp peaks in the range of 310 - 420 nm are observed, which are related to the intra-4f transitions of Eu^{3+} ions. It should be noted that the spectrum is continuously increased in the shorter wavelength region, which probably caused by the $\text{O}^{2-} \rightarrow \text{Eu}^{3+}$ charge transfer band [4,5]. The spectral shape of the co-doped sample is very similar to that of the Eu singly sample in the longer wavelength region above 370 nm. However, we can see that the excitation is greatly enhanced below 370 nm region by the addition of Bi^{3+} ions. It is well known that Bi^{3+} ions have strong absorption in the near UV region [15]. Therefore, it is reasonable to consider that the enhanced excitation in the UV region is due to the energy transfer from Bi^{3+} ions. Based on the measurements results, Eu^{3+} ions in the co-doped sample can be efficiently excited by broad ultraviolet light, due to the $\text{O}^{2-} \rightarrow \text{Eu}^{3+}$ charge transfer band and the sensitization of Bi^{3+} ions. Therefore, optical pumping using flash lamps or LEDs rather than laser becomes feasible using this broadband sensitization.

The decay curves detected at 560 nm in the Z-Bi and Z-Eu-Bi samples are shown in figure 4 (a). We observe nearly single exponential luminescence decays in both samples, and the addition of Eu results in the rapid decreases of the lifetime from 7.36 μs to 1.65 μs . Such kind of phenomenon is commonly observed for nonradiative energy transfer process [17]. Therefore, the shortening of the lifetime is a strong evidence of the energy transfer

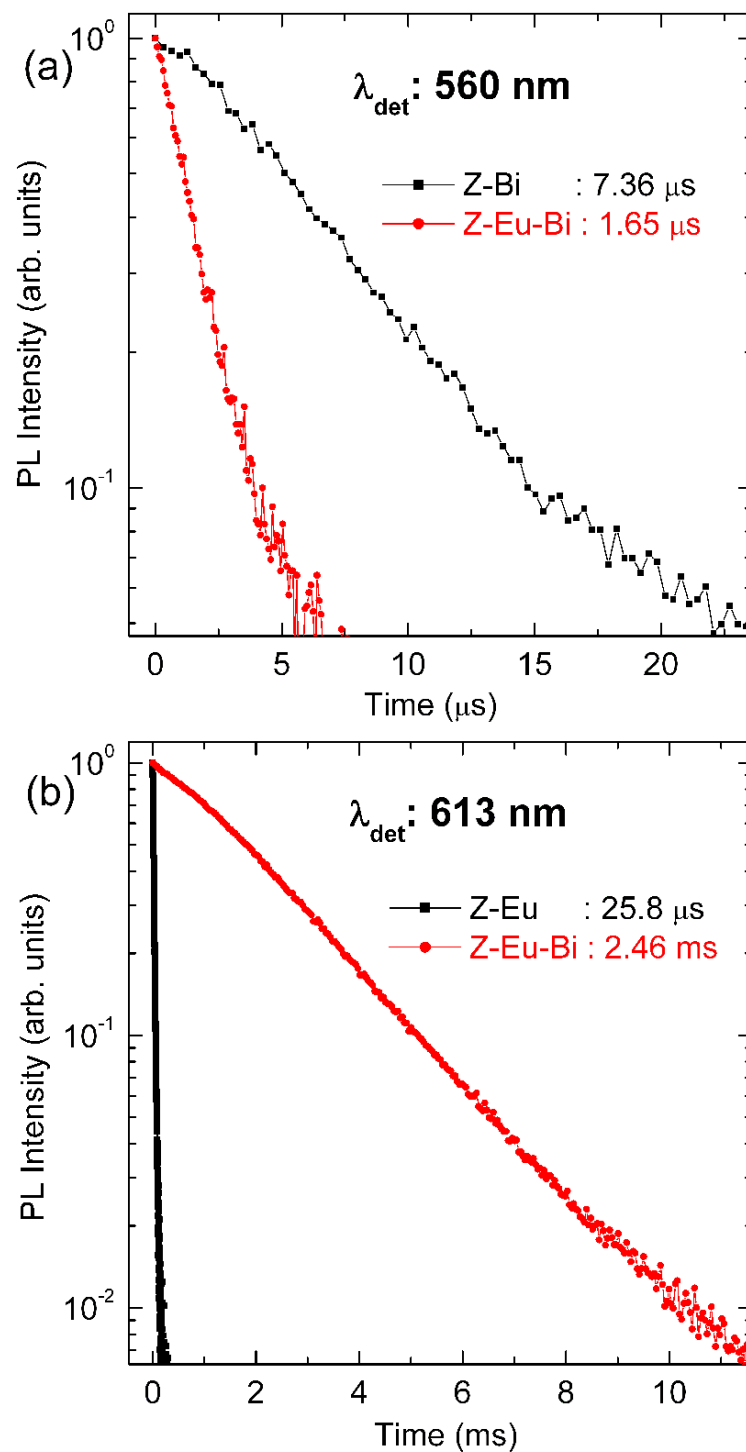


Figure 7.4: (a) PL decay curves of Z-Bi and Z-Eu-Bi samples detected at 560 nm. (b) PL decay curves of Z-Eu and Z-Eu-Bi samples detected at 613 nm.

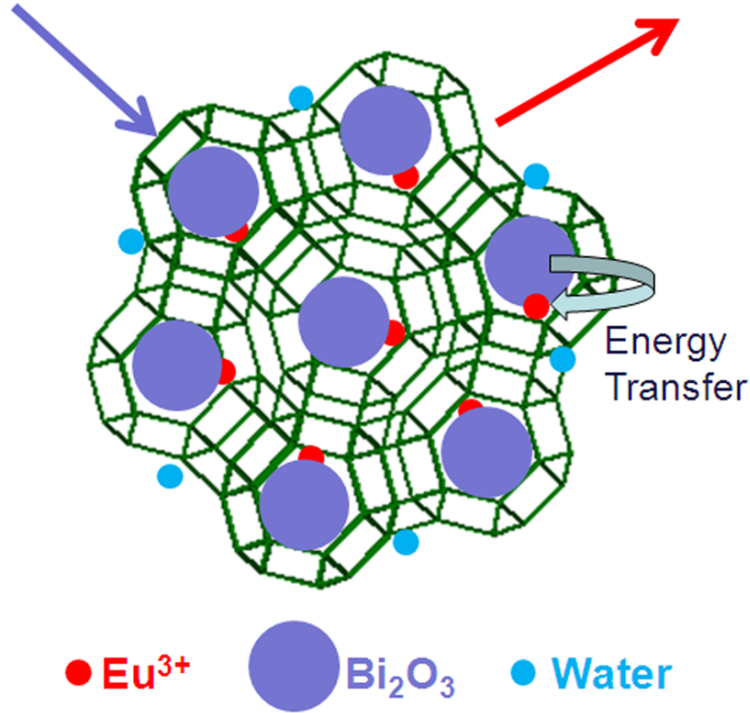


Figure 7.5: Schematic illustrations of the energy transfer process from Bi^{3+} to Eu^{3+} and the blocking property of Bi_2O_3 clusters.

from the broad emission to Eu^{3+} . The energy transfer efficiency (η) can be estimated by

$$\eta = 1 - \frac{\tau_{Eu-Bi}}{\tau_{Bi}}, \quad (7.1)$$

Where τ_{Eu-Bi} and τ_{Bi} are the lifetimes of broad emission in co-doped and singly doped samples, respectively. The calculated η is about 78 %. It is well known that energy transfer efficiency is proportional to the spectral overlap between sensitizer and acceptor. In this case, the broad emission and the Eu^{3+} absorption are overlapped well, thus high energy transfer efficiency (78 %) can be expected in this system.

Figure 7.4 (b) shows the decay curves detected at 613 nm originating from the ${}^5\text{D}_0 \rightarrow {}^7\text{F}_2$ transition of Eu^{3+} in the Z-Eu and Z-Eu-Bi samples. In the Eu singly doped sample, the lifetime is 25.8 μs , which is much shorter than the transition intrinsic lifetime of Eu^{3+} . This is due to nonradiative relaxation of Eu^{3+} : ${}^5\text{D}_0$ state by strong coupling of the excitation to high-frequency vibrations of coordinated water [10]. In contrast, the lifetime is significantly increased to about 2.46 ms in the co-doped zeolites, which is the longest value reported in zeolites. The long lifetime of Eu^{3+} in co-doped samples suggests that Eu^{3+} is well separated from the coordinated water by co-doping Bi in zeolites.

In Bi and rare-earth co-doped zeolites, Sun et al. [18,19] proposed a model that rare-earth ions and Bi^{3+} ions migrate into the pores of zeolites by the ion-exchange process,

and after subsequent high temperature annealing in air, Bi^{3+} ions form Bi_2O_3 clusters, due to the low melting point of bismuth compounds. In this work, the advantages of co-doping Bi in Eu doped zeolites can be summarized into two aspects, as shown in figure 7.5. On one hand, addition of Bi^{3+} ions into the pores can provide an indirect excitation for Eu^{3+} ions through an energy transfer process. It is an effective method to overcome the small absorption cross section of Eu^{3+} ions due to the forbidden nature of intra-4f transitions. On the other hand, the formation of Bi_2O_3 clusters can act as an excellent blockage material to seal the pores of zeolites, which avoids the admission of coordinated water into the pores of zeolites. Therefore, Eu^{3+} ions have chance to show strong and long-lived red emission, even the zeolites contain large amount of water.

7.4 Conclusion

In summary, Eu-Bi co-doped zeolites are prepared by an ion-exchange process, and the optical properties are investigated. Addition of Bi^{3+} strongly enhances the red emission of Eu^{3+} (${}^5\text{D}_0 \rightarrow {}^7\text{F}_2$) in zeolites about 50 times, and the lifetime is significantly increased to 2.46 ms. It is revealed that the $\text{O}^{2-} \rightarrow \text{Eu}^{3+}$ charge transfer band and sensitization of Bi^{3+} ions distinctly enhances the excitation band of Eu^{3+} ions in the UV region. The energy transfer efficiency is estimated to be 78 %. The excellent optical properties make these microporous materials promising in application as white-LEDs.

References

- [1] J. Kido, H. Shionoya, K. Nagai, *Appl. Phys. Lett.* **67**, 2281 (1995).
- [2] P. Waltereit, O. Brandt, A. Trampert, H. T. Grahn, J. Menniger, M. Ramsteiner, M. Reiche, K. H. Ploog, *Nature* **406**, 865 (2000).
- [3] J. DiMaio, B. Kokuoz, J. Ballato, *Opt. Express* **14**, 11412 (2006).
- [4] H. Guo, H. Zhang, R. Wei, M. Zheng, L. Zhang, *Opt. Express* **19**, A201 (2011).
- [5] S. Yan, J. Zhang, X. Zhang, S. Lu, X. Ren, Z. Nie, X. Wang, *J. Phys. Chem. C* **111**, 13256 (2007).
- [6] K. Binnemans, *Chem. Rev.* **109**, 4283 (2009).
- [7] M. Flores-Acosta, R. Perez-Salas, R. Aceves, M. Sotelo-Lerma, R. Ramirez-Bon, *Solid State Commun.* **136**, 567 (2005).
- [8] H. Sun, A. Hosokawa, Y. Miwa, F. Shimaoka, M. Fujii, M. Mizuhata, S. Hayashi, S. Deki, *Adv. Mater.* **21**, 3694 (2009).
- [9] C. Borgmann, J. Sauer, T. Justel, U. Kynast, F. Schuth, *Adv. Mater.* **11**, 45 (1999).
- [10] W. Chen, R. Sammynaiken, Y. Huang, *J. Appl. Phys.* **88**, 1424 (2000).
- [11] D. Sendor, U. Kynast, *Adv. Mater.* **14**, 1570 (2002).
- [12] Y. Wada, M. Sato, Y. Tsukahara, *Angew. Chem. Int. Ed.* **45**, 1925 (2006).
- [13] S. Suzuki, M. Ryo, T. Yamamoto, T. Sakata, S. Yanagida, Y. Wada, *J. Mater. Sci.* **42**, 5991 (2007).
- [14] Y. Wang, H. Li, L. Gu, Q. Gan, Y. Li, G. Calzaferri, *Micropor. Mesopor. Mater.* **121**, 1 (2009).
- [15] X. Huang, Q. Zhang, *J. Appl. Phys.* **107**, 063505 (2010).
- [16] A. Mech, A. Monguzzi, F. Cucinotta, F. Meinardi, J. Mezyk, L. Cola, R. Tubino, *Phys. Chem. Chem. Phys.* **13**, 5605 (2011).

- [17] B. Wu, S. Zhou, J. Ruan, Y. Qiao, D. Chen, C. Zhu, J. Qiu, *Opt. Express* **16**, 2508 (2008).
- [18] H. Sun, T. Hasegawa, M. Fujii, F. Shimaoka, Z. Bai, M. Mizuhata, S. Hayashi, S. Deki, *Appl. Phys. Lett.* **94**, 141106 (2009).
- [19] H. Sun, Y. Sakka, Y. Miwa, N. Shirahata, M. Fujii, H. Gao, *Appl. Phys. Lett.* **97**, 131908 (2010).

Part III

Simultaneously doping of different kinds of lanthanide ions in Bi doped zeolites

Chapter 8

Efficient ultraviolet-blue to near-infrared downconversion in Bi-Dy-Yb doped zeolites

In this chapter, ultraviolet-blue to near-infrared (NIR) downconversion is investigated for the Dy^{3+} - Yb^{3+} couple in zeolites by steady-state and time-resolved photoluminescence (PL) spectra, and PL excitation spectra. Upon excitation of the $^4F_{9/2}$ level of Dy^{3+} , NIR quantum cutting could occur through a two-step energy transfer from one Dy^{3+} ion to two neighboring Yb^{3+} ions via an intermediate level. The energy transfer efficiency from the $^4F_{9/2}$ level is estimated to be 42 %, and the intrinsic PL quantum efficiency of Yb^{3+} emission reaches 54 %. The findings may have potential application in enhancing the energy efficiency of the silicon-based solar cell.

8.1 Introduction

Nowadays, considerable research has been focused on improving solar cell efficiency by better exploitation of the solar spectrum by a photon conversion process [1,2]. It is well known that quantum cutting is an effective method to minimize the energy loss by thermalization of electron-hole pairs, which can convert one photon of high energy into two photons of lower energy [3,4]. The most widely used solar cells are based on crystalline Si, in which the band gap is about 1100 nm [5]. Therefore, the conversion of one ultraviolet (UV)-visible photon into two near-infrared (NIR) photons can greatly enhance the solar cell efficiency [5-13]. Rare-earth ions with abundant energy levels, such as Pr^{3+} [9], Er^{3+} [10], Nd^{3+} [11], and Ho^{3+} [12], have been investigated as donor materials to absorb high

energy photons and transfer the energy to accepters. On the other hand, Yb^{3+} ion is an ideal candidate of the accepter, because of its simple energy state and strong emission at around $1 \mu\text{m}$, where the silicon-based solar cells show an excellent spectral response.

Recently, Meijerink et al [9] reported that a stepwise energy transfer process occurs when the donor has a suitable intermediate state to assist the two-step sequential energy transfer to the accepters. They realized efficient quantum cutting of a single visible photon into two NIR photons using the $\text{Pr}^{3+} - \text{Yb}^{3+}$ couple [9]. As is known, solar spectrum also covers the UV region, especially in the range of 300 - 400 nm. Therefore, to sufficiently utilize solar energy in this region, it is favorable to use a donor with abundant energy levels both in the UV and visible regions. $\text{Dy}^{3+} - \text{Yb}^{3+}$ couple may meet the requirements. Figure 8.1 illustrates the energy level diagram with transitions which may be involved in

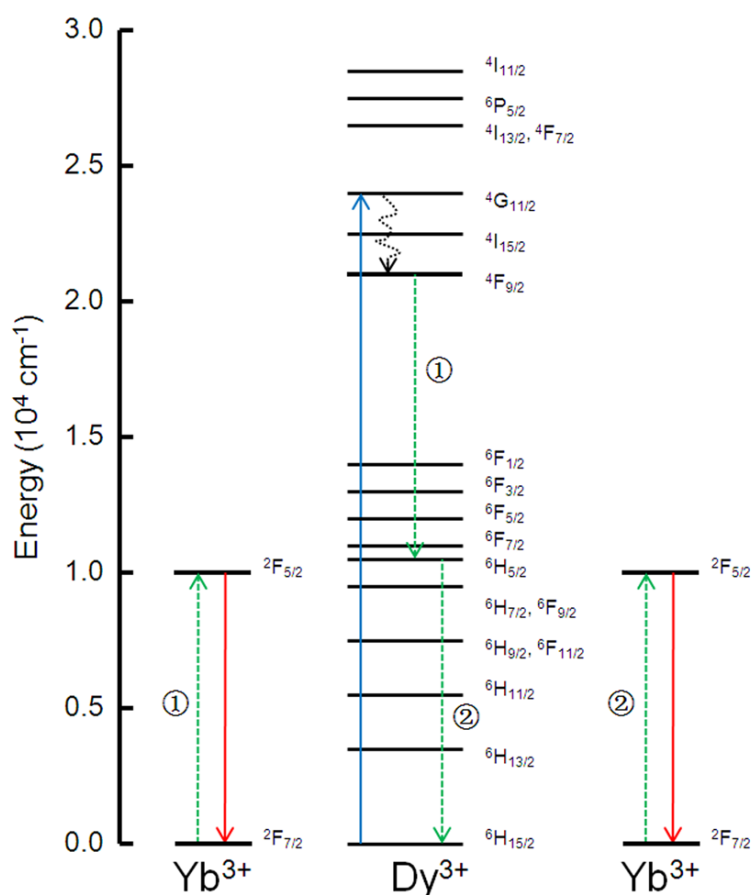


Figure 8.1: Energy level scheme of the $\text{Dy}^{3+} - \text{Yb}^{3+}$ couple showing possible mechanisms for a NIR quantum cutting. One blue photon absorbed by Dy^{3+} is converted into two NIR photons from Yb^{3+} ions through a two-step sequential energy transfer. Solid, dotted, and curved arrows represent optical transition, energy transfer, and nonradiative relaxation, respectively.

the energy transfer process from Dy^{3+} to Yb^{3+} . It is interesting to see that the energy of the $\text{Dy}^{3+}: {}^4\text{F}_{9/2} \rightarrow {}^6\text{H}_{15/2}$ transition is double of the $\text{Yb}^{3+}: {}^2\text{F}_{7/2} \rightarrow {}^2\text{F}_{5/2}$ transition, and moreover, the ${}^6\text{H}_{15/2}$ level is located at around the intermediate level between ${}^4\text{F}_{9/2}$ and ${}^6\text{H}_{15/2}$. Therefore, a two-step energy transfer process can be expected for the Dy^{3+} - Yb^{3+} couple, which is expressed as: $\text{Dy}^{3+}: {}^4\text{F}_{9/2} + \text{Yb}^{3+}: {}^2\text{F}_{7/2} \rightarrow \text{Dy}^{3+}: {}^6\text{H}_{15/2} + \text{Yb}^{3+}: {}^2\text{F}_{5/2}$ followed by $\text{Dy}^{3+}: {}^6\text{H}_{15/2} + \text{Yb}^{3+}: {}^2\text{F}_{7/2} \rightarrow \text{Dy}^{3+}: {}^6\text{H}_{15/2} + \text{Yb}^{3+}: {}^2\text{F}_{5/2}$.

To achieve high-efficiency quantum cutting, precise control of donor and acceptor distributions is crucial because the energy transfer efficiency depends strongly on the ion-to-ion distances. Zeolites are considered to be an attractive host material to realize it, because the regularly organized pores can serve as an ideal environment to organize the optically active guests well dispersed in their framework [14]. In addition, zeolites are thermally stable at relatively high temperatures and optically transparent in the region from UV to NIR [15]. These particular structural and optical properties make it very promising as host materials of optically active centers for constructing novel materials designed at nanosized levels [16-18]. Recently, efficient NIR photoluminescence (PL) from rare-earth ions has been achieved in zeolites by co-doping Bi, due to the formation of Bi related agglomerates, which act as a blockage to seal the optical active centers in the pores [19,20].

In this work, Bi-Dy and Bi-Dy-Yb doped zeolites are prepared and the downconversion for the Dy^{3+} - Yb^{3+} couple is investigated by steady-state and time-resolved PL spectra, and PL excitation spectra. We demonstrate that NIR quantum cutting could occur through a two-step energy transfer from the long-lived ${}^4\text{F}_{9/2}$ level of Dy^{3+} ion to two neighboring Yb^{3+} ions in zeolites. The energy transfer mechanism is discussed, and the intrinsic PL quantum efficiency of Yb^{3+} emission is estimated.

8.2 Experimental details

In this work, faujasite (FAU) type zeolites were used due to the sufficient ion-exchange capacity and high temperature stability. Zeolites were stirred in the aqueous solutions of Bi^{3+} (60 mM) and Dy^{3+} (5 mM) for two days. The half amount of Bi-Dy embedded zeolites were further stirred in a 20 mM aqueous solution of Yb^{3+} prepared from $\text{YbCl}_3 \cdot 6\text{H}_2\text{O}$ at 80 °C for 24 h to dope Yb. The products were removed by centrifugation, then washed with deionized water, and dried in air at 120 °C. The obtained powders were calcined at 900 °C for 1 h in air. Hereafter, the Bi-Dy and Bi-Dy-Yb doped zeolites are denoted as Z-Bi-Dy and Z-Bi-Dy-Yb, respectively. All samples were exposed to the laboratory atmosphere prior to measurements.

The crystallinity of prepared products was studied by an X-ray diffractometer (Rigaku-TTR/S2) with a $\text{CuK}\alpha$ radiation source. The atomic compositions were analyzed by an energy-dispersive X-ray spectrometer (EDS). Visible and NIR PL spectra were mea-

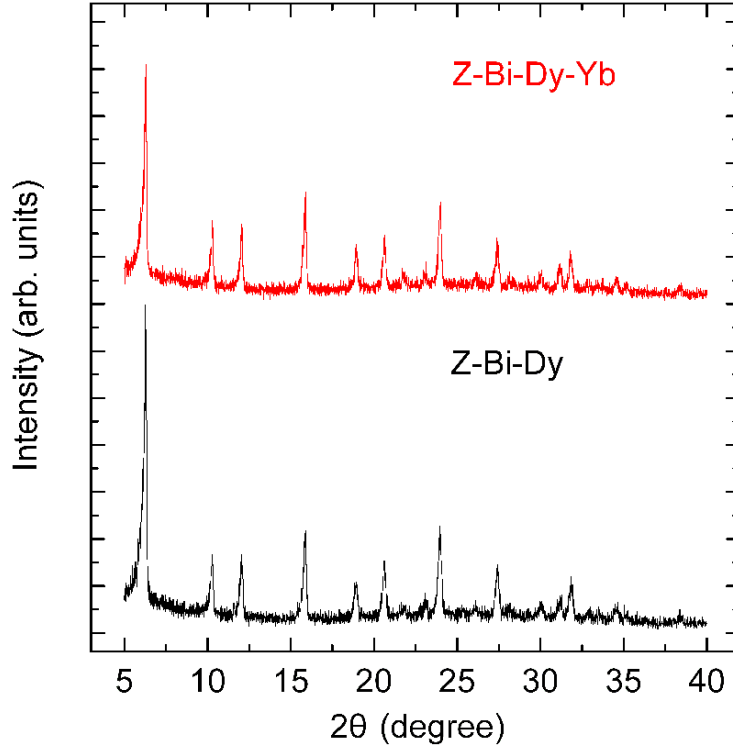


Figure 8.2: X-ray diffraction patterns of the Z-Bi-Dy and Z-Bi-Dy-Yb samples.

sured by using a monochromator equipped with liquid-nitrogen-cooled CCD and InGaAs detectors, respectively. The excitation sources for PL measurements were 430 nm light from an optical parametric oscillator (OPO) pumped by the third harmonic of a Nd:YAG laser, and 805 nm light from a Ti: sapphire laser. Excitation spectra were obtained by a NIR PL spectrophotometer equipped with an InGaAs detector. Time-resolved luminescence measurements were performed by detecting the modulated luminescence signal with a photomultiplier tube (Hamamatsu, R5509-72), and then analyzing the signal with a photon-counting multichannel scaler. The excitation source for decay time measurements was 430 nm light from the OPO (pulse width 5 ns, repetition frequency 20Hz). All measurements were performed at room temperature.

Table 8.1: Atomic concentrations of Bi, Dy and Yb in the final products

Sample	Bi at. %	Dy at. %	Yb at. %
Z-Bi-Dy	1.45	0.19	-
Z-Bi-Dy-Yb	1.38	0.17	0.58

8.3 Results and discussion

Figure 8.2 shows the XRD patterns of the Z-Bi-Dy and Z-Bi-Dy-Yb samples. The data of the diffraction peaks agree well with the standard values for the Zeolite Y (JCPDS No. 45-0112), indicating that the obtained samples are single phase and the doping and annealing do not cause any significant change of the crystal structure. Table 8.1 presents the atomic concentrations of Bi, Dy and Yb in the final products. It can be seen that the Bi and Dy concentrations are kept almost the same within two samples, and the atomic ratio of Yb/Dy in the Z-Bi-Dy-Yb sample is estimated to be about 3.4.

Figure 8.3 (a) and (b) show the PL spectra of the Z-Bi-Dy and Z-Bi-Dy-Yb samples excited at 430 and 805 nm, respectively. Upon the excitation at 430 nm, in the Z-Bi-Dy sample, characteristic emission peaks from Dy^{3+} ion are observed at 486, 575, 664, 754, 848, 940, 1018, and 1180 nm, which can be assigned to the electronic transitions of the ${}^4\text{F}_{9/2}$ to the ${}^6\text{H}_{15/2}$, ${}^6\text{H}_{13/2}$, ${}^6\text{H}_{11/2}$, ${}^6\text{H}_{9/2}$ (${}^6\text{F}_{11/2}$), ${}^6\text{H}_{7/2}$ (${}^6\text{F}_{9/2}$), ${}^6\text{H}_{5/2}$, ${}^6\text{F}_{7/2}$, and ${}^6\text{F}_{5/2}$, respectively. Interestingly, the emission from Dy^{3+} ion is significantly decreased for the Z-Bi-Dy-Yb sample, and in addition, strong Yb^{3+} emissions at 978 and 1018 nm are detected, corresponding to the transitions from the lowest Stark level of the Yb^{3+} : ${}^2\text{F}_{7/2}$ multiplet to the different Stark levels of the ${}^2\text{F}_{5/2}$ multiplet [21]. It is well known that there is no energy level enabling the direct excitation of Yb^{3+} emission with 430 nm light. Therefore, it is reasonable to consider that the observation of strong Yb^{3+} emission and the decrease of Dy^{3+} emission are due to the energy transfer from Dy^{3+} to Yb^{3+} .

To get more information about the energy transfer between Dy^{3+} and Yb^{3+} , PL excitation spectra are measured. The excitation spectra of the Z-Bi-Dy sample detected at 1018 nm, and the Z-Bi-Dy-Yb sample detected at 978 nm are shown in figure 8.4. The excitation spectrum of the Z-Bi-Dy sample is characterized by the presences of six peaks centered at 348, 362, 384, 424, 448, and 468 nm, which are ascribed to the transitions of Dy^{3+} ion from the ${}^6\text{H}_{15/2}$ ground state to the ${}^4\text{I}_{11/2}$, ${}^6\text{P}_{5/2}$, ${}^4\text{I}_{13/2}$ (${}^4\text{F}_{7/2}$), ${}^4\text{G}_{11/2}$, ${}^4\text{I}_{15/2}$, and ${}^4\text{F}_{9/2}$, respectively. In the Z-Bi-Dy-Yb sample, the excitation spectrum of the Yb^{3+} emission at 978 nm is in good agreement with the Dy^{3+} absorption, which convincingly proves the existence of the energy transfer. The results reveal that the UV-blue light can be converted into NIR light by using the Dy^{3+} - Yb^{3+} couple.

In the following, we will discuss the energy transfer mechanism and demonstrate the existence of the two-step energy transfer process. Figure 8.5 (a) shows the decay curves of the Dy^{3+} emission at 575 nm (${}^4\text{F}_{9/2}$ \rightarrow ${}^6\text{H}_{13/2}$) in the Z-Bi-Dy and Z-Bi-Dy-Yb samples, respectively. The decay curve of the Z-Bi-Dy sample can be fitted by a single-exponential function, and by the addition of Yb^{3+} ion, the lifetime becomes shorter and the shape becomes non-exponential. The mean lifetimes (τ_m) are also shown in figure 5a, which are

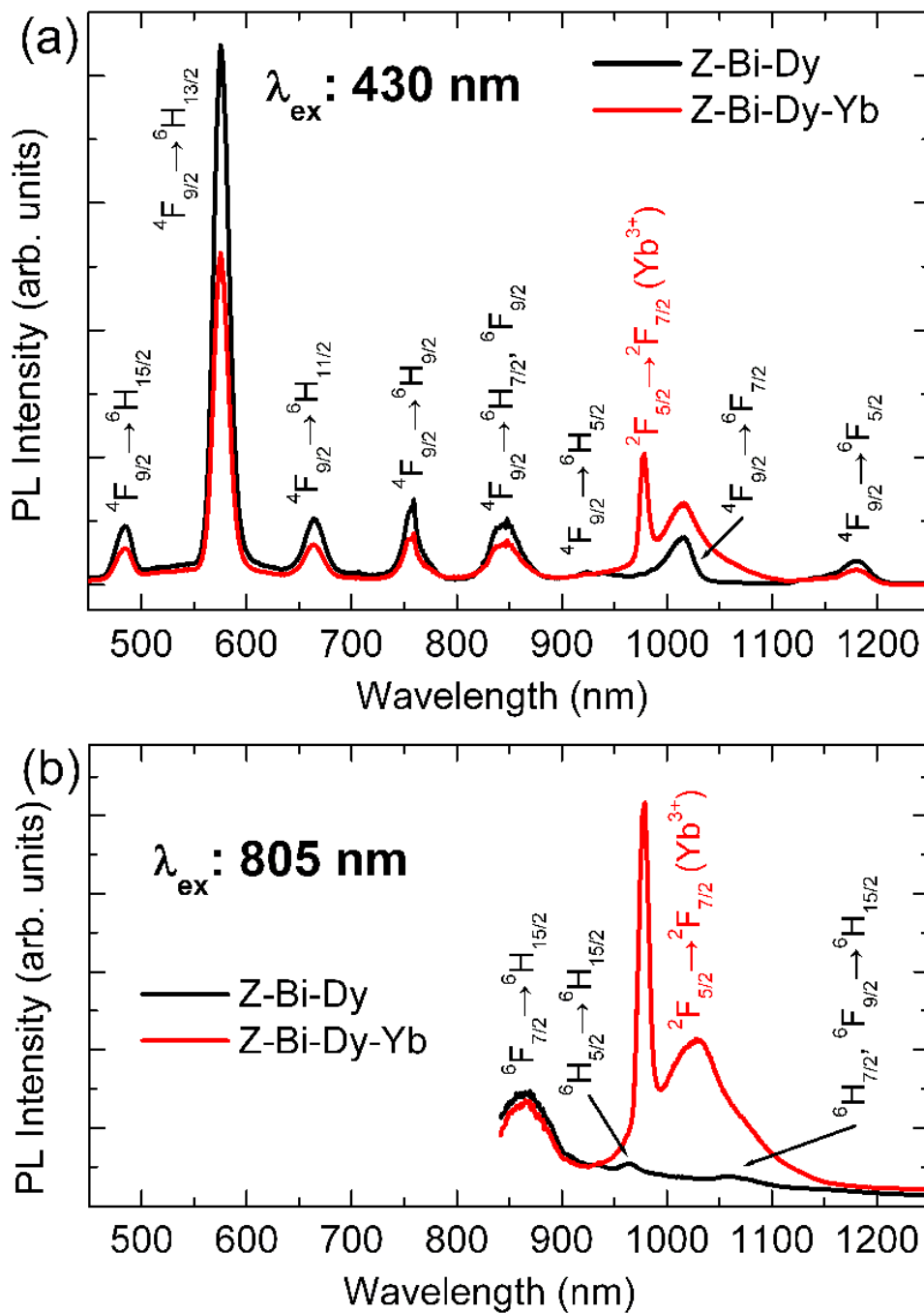


Figure 8.3: Emission spectra of the Z-Bi-Dy and Z-Bi-Dy-Yb samples excited by (a) 430 nm and (b) 805 nm.

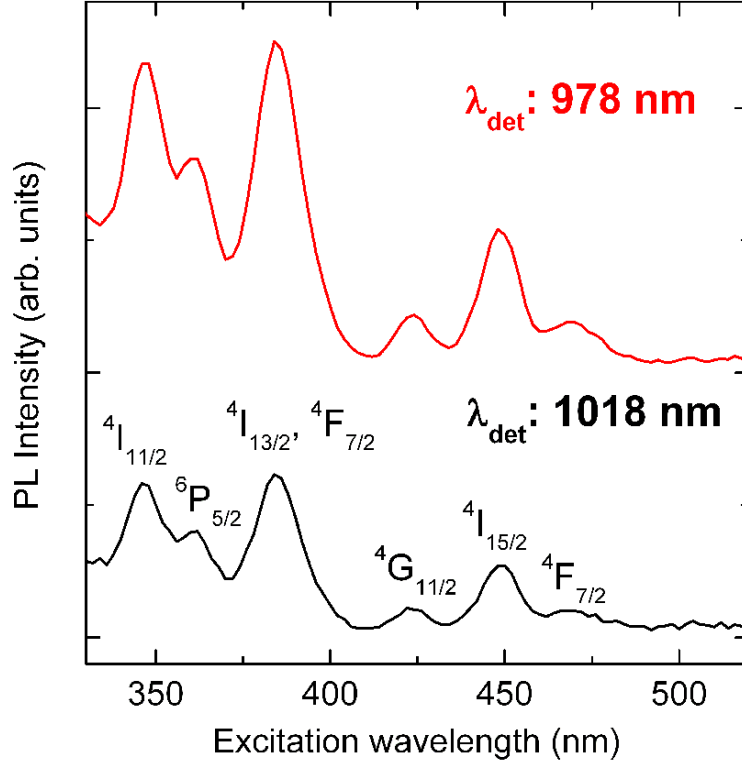


Figure 8.4: Excitation spectra of the Z-Bi-Dy sample detected at 1018 nm, and the Z-Bi-Dy-Yb sample detected at 978 nm.

obtained by

$$\tau_m = \int_{t_0}^{\infty} [I(t)/I_0] dt, \quad (8.1)$$

Where $I(t)$ is the luminescence intensity as a function of time t and I_0 is the maximum of $I(t)$ that occurs at the initial time t_0 . The shortening of the lifetime indicates that the addition of Yb^{3+} introduces a new non-radiative relaxation process in the ${}^4\text{F}_{9/2}$ level of Dy^{3+} . The lifetime results combined with the decrease of Dy^{3+} emission intensity by Yb^{3+} doping in figure 3a prove the occurrence of the first step energy transfer process in the Z-Bi-Dy-Yb sample, which can be expressed as: $\text{Dy}^{3+}: {}^4\text{F}_{9/2} + \text{Yb}^{3+}: {}^2\text{F}_{7/2}$
 $\text{Dy}^{3+}: {}^6\text{H}_{5/2} + \text{Yb}^{3+}: {}^2\text{F}_{5/2}$. From the degree of the shortening of the lifetime, the energy transfer efficiency (η) from the ${}^4\text{F}_{9/2}$ level can be estimated:

$$\eta = 1 - \frac{\tau_{\text{Bi-Dy-Yb}}}{\tau_{\text{Bi-Dy}}}, \quad (8.2)$$

Where $\tau_{\text{Bi-Dy-Yb}}$ and $\tau_{\text{Bi-Dy}}$ are the lifetimes of Dy^{3+} emission with and without Yb^{3+} ions, respectively. The η is calculated to be 42 % in the Z-Bi-Dy-Yb sample. Note that the value is mean energy transfer efficiency in the present sample. The non-exponential decay curve for the Z-Bi-Dy-Yb sample in figure 5a indicates that the energy transfer

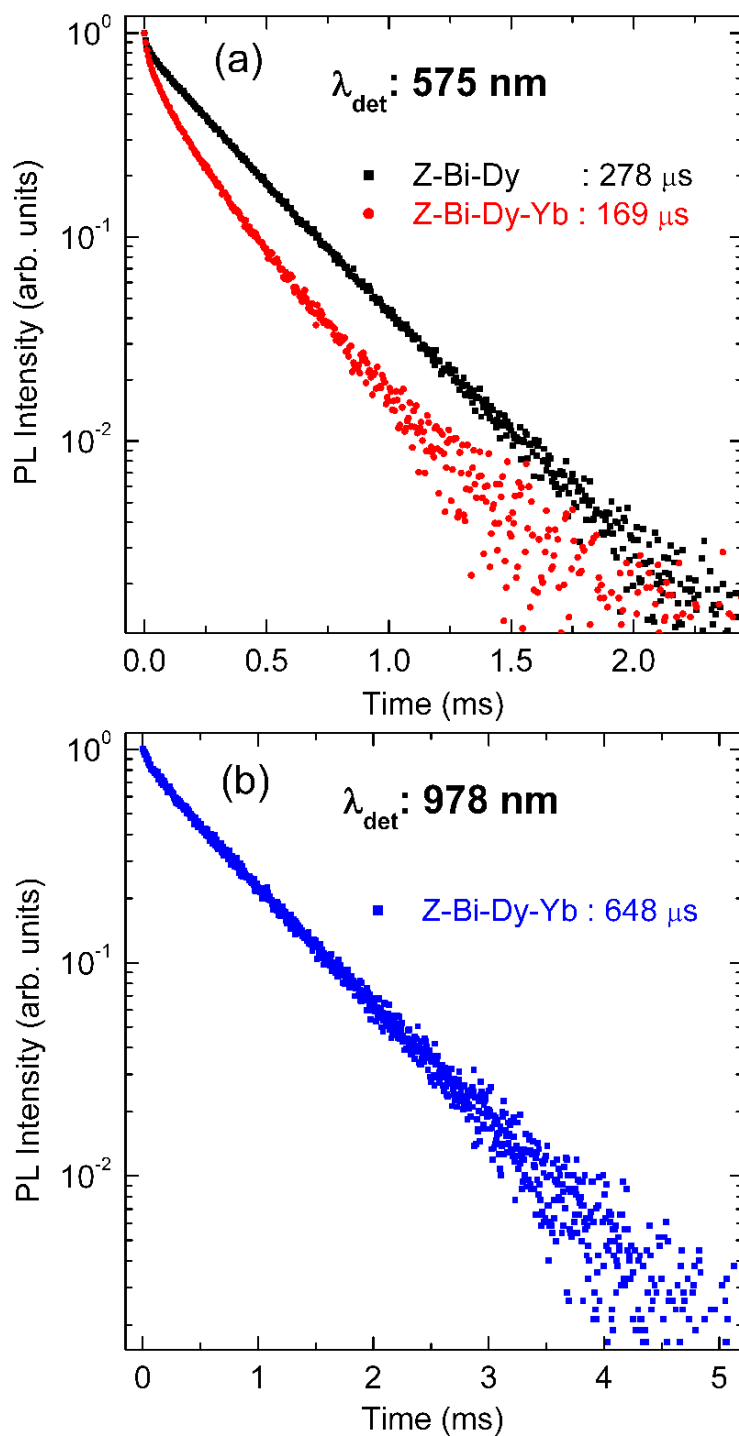


Figure 8.5: (a) Decay curves of the Dy^{3+} emission at 575 nm (${}^4F_{9/2} \rightarrow {}^6H_{13/2}$) in the Z-Bi-Dy and Z-Bi-Dy-Yb samples, respectively. (b) Decay curve of the Yb^{3+} emission at 978 nm in the Z-Bi-Dy-Yb sample. The excitation wavelength for decay time measurements is 430 nm.

efficiency is distributed due probably to the existence of the Dy^{3+} - Yb^{3+} couples with different geometries.

As can be seen in figure 8.1, the Dy^{3+} ion relaxed to the ${}^6\text{H}_{5/2}$ level by the first step energy transfer process still possesses enough energy to excite another Yb^{3+} ion because of the resonance between the $\text{Dy}^{3+}({}^6\text{H}_{5/2} \rightarrow {}^6\text{H}_{15/2})$ and $\text{Yb}^{3+}({}^2\text{F}_{7/2} \rightarrow {}^2\text{F}_{5/2})$ transitions. To clarify whether the second step energy transfer from Dy^{3+} to Yb^{3+} occurs, the PL spectra are taken under the excitation at 805 nm. Note that Bi doped zeolites have no absorption at this wavelength, so they could not be energy donors for Yb^{3+} [18]. As shown in figure 3 (b), the Z-Bi-Dy sample shows NIR emission bands at 865, 962, and 1060 nm originating from the transitions from the ${}^6\text{F}_{7/2}$, ${}^6\text{H}_{5/2}$, and ${}^6\text{H}_{7/2}$ (${}^6\text{F}_{9/2}$) to the ${}^6\text{H}_{15/2}$ ground state, respectively. In the Z-Bi-Dy-Yb sample, the emission from Dy^{3+} at 865 nm and the strong emission from Yb^{3+} at 978 and 1018 nm are detected. The indirect excitation of Yb^{3+} ions is a clear evidence that Yb^{3+} ions can be excited by the energy transfer from Dy^{3+} ions when they are in the levels around ${}^6\text{F}_{7/2}$, ${}^6\text{H}_{5/2}$, and ${}^6\text{H}_{7/2}$ (${}^6\text{F}_{9/2}$). Considering the degree of the spectral overlap with the ${}^2\text{F}_{7/2} \rightarrow {}^2\text{F}_{5/2}$ transition of Yb^{3+} ion, $\text{Dy}^{3+}: {}^6\text{H}_{5/2} + \text{Yb}^{3+}: {}^2\text{F}_{7/2} \rightarrow \text{Dy}^{3+}: {}^6\text{H}_{15/2} + \text{Yb}^{3+}: {}^2\text{F}_{5/2}$ is the most plausible energy transfer process. Therefore, the remaining energy of the $\text{Dy}^{3+}: {}^6\text{H}_{5/2}$ level can be further transferred to another Yb^{3+} ion by the second step energy transfer. Although the present results demonstrate the existence of the two-step energy transfer process to convert one UV-blue photon to two NIR photons, the efficiency of the second step energy transfer process could not be estimated. For the practical application of the present system, quantitative discussion of the efficiency and the optimization of the sample parameters are necessary, and these researches are underway in our laboratory.

The decay curve of the Yb^{3+} emission at 978 nm in the Z-Bi-Dy-Yb sample is given in figure 8.5 (b). The Yb^{3+} emission shows a single-exponential decay, and the lifetime reaches 648 μs . The intrinsic PL quantum efficiency (Φ) of Yb^{3+} is estimated to be 54 % by using the equation:

$$\Phi = \frac{\tau_e}{\tau_r}, \quad (8.3)$$

where τ_e and τ_r are the experimental and radiative (1.2 ms) lifetimes of Yb^{3+} emission, respectively [22]. The highly efficient NIR emission from Yb^{3+} benefits from the effective isolation of the optical active centers from the coordinated water by Bi related agglomerates in zeolites [19,20].

8.4 Conclusion

In conclusion, Bi-Dy and Bi-Dy-Yb doped zeolites are prepared by an ion-exchange process and subsequent high temperature annealing. Emission, excitation, and decay measurements were performed to investigate the downconversion process from Dy^{3+} to

Yb^{3+} . We demonstrate the existence of a two-step energy transfer process from the long-lived $^4\text{F}_{9/2}$ level of Dy^{3+} to two neighboring Yb^{3+} ions in zeolites. The energy transfer efficiency from the $^4\text{F}_{9/2}$ level is determined to be 42 %, and the intrinsic PL quantum efficiency of Yb^{3+} emission reaches 54 %. The high energy transfer efficiency and the efficient Yb^{3+} emission suggest that the materials may have potential application in enhancing the energy efficiency of the silicon-based solar cell.

References

- [1] T. Trupke, M. Green, P. Würfel, *J. Appl. Phys.* **92**, 1668 (2002).
- [2] C. Strumpel, M. McCann, G. Beaucarne, V. Arkhipov, A. Slaoui, V. Svrcek, C. del Canizo, I. Tobias, *Sol. Energy Mater. Sol. Cells.* **91**, 238 (2007).
- [3] B. S. Richards, *Sol. Energy Mater. Sol. Cells.* **90**, 1189 (2006).
- [4] D. Timmerman, I. Izeddin, P. Stallinga, I. N. Yassievich, T. Gregorkiewicz, *Nat. Photonics.* **2**, 105 (2008).
- [5] P. Vergeer, T. J. H. Vlugt, M. H. F. Kox, M. I. den Hertog, J. P. J. M. van der Eerden, A. Meijerink, *Phys. Rev. B.* **71**, 014119 (2005).
- [6] Q. Zhang, G. Yang, Z. Jiang, *Appl. Phys. Lett.* **91**, 051903 (2007).
- [7] S. Ye, B. Zhu, J. Chen, J. Luo, J. Qiu, *Appl. Phys. Lett.* **92**, 141112 (2008).
- [8] J. Ueda, S. Tanabe, *J. Appl. Phys.* **106**, 043101 (2009).
- [9] B. M. van der Ende, L. Aarts, A. Meijerink, *Adv. Mater.* **21**, 3073 (2009).
- [10] J. J. Eilers, D. Biner, J. T. van Wijngaarden, K. Kramer, H. U. Gudel, A. Meijerink, *Appl. Phys. Lett.* **96**, 151106 (2010).
- [11] D. Chen, Y. Yu, H. Lin, P. Huang, Z. Shan, Y. Wang, *Opt. Lett.* **35**, 220 (2010).
- [12] K. Deng, T. Gong, L. Hu, X. Wei, Y. Chen, M. Yin, *Opt. Express* **19**, 1749 (2011).
- [13] D. Yu, S. Ye, M. Peng, Q. Zhang, J. Qiu, J. Wang, L. Wondraczek, *Sol. Energy Mater. Sol. Cells.* **95**, 1590 (2011).
- [14] Y. Wada, T. Okubo, M. Ryo, T. Nakazawa, Y. Hasegawa, S. Yanagida, *J. Am. Chem. Soc.* **122**, 8583 (2000).
- [15] J. Rocha, L. D. Carlos, *Curr. Opin. Solid State Mater. Sci.* **7**, 199 (2003).
- [16] M. Lezhnina, F. Laeri, L. Benmouhadi, U. Kynast, *Adv. Mater.* **18**, 280 (2006).

- [17] A. Monguzzi, G. Macchi, F. Meinardi, R. Tubino, M. Burger, G. Calzaferri, *Appl. Phys. Lett.* **92**, 123301 (2008).
- [18] H. Sun, A. Hosokawa, Y. Miwa, F. Shimaoka, M. Fujii, M. Mizuhata, S. Hayashi, S. Deki, *Adv. Mater.* **21**, 3694 (2009).
- [19] H. Sun, T. Hasegawa, M. Fujii, F. Shimaoka, Z. Bai, M. Mizuhata, S. Hayashi, S. Deki, *Appl. Phys. Lett.* **94**, 141106 (2009).
- [20] Z. Bai, H. Sun, M. Fujii, Y. Miwa, T. Hasegawa, M. Mizuhata, S. Hayashi, *J. Phys. D: Appl. Phys.* **44**, 155101 (2011).
- [21] Z. Burshtein, Y. Kalisky, S. Z. Levy, P. L. Goullanger, S. Rotman, *IEEE J. Quantum Electron.* **36**, 1000 (2000).
- [22] N. M. Shavaleev, R. Scopelliti, F. Gumy, J. G. Buzli, *Inorg. Chem.* **48**, 7937 (2009).

Chapter 9

Conclusion

In this thesis, we studied the effect of the doping concentration and annealing atmosphere on the optical properties of Bi doped zeolites. Moreover, we investigated the structural and optical properties of rare-earth ions and bismuth co-doped zeolites, such as Er-Bi, Nd-Bi, Yb-Bi, Eu-Bi, and Dy-Yb-Bi. The particular optical properties of these nanoparticles have potential applications in optical telecommunication, optical coherence tomography, biological imaging, and solar cell.

In chapter 2, the mechanism of efficient near-infrared (NIR) emission from Bi doped zeolites was studied by analyzing photoluminescence (PL) and Raman scattering data for the samples with different Bi concentrations. The NIR PL intensity increases significantly with increases Bi concentration; it increases 178 times when the concentration is changed from 0.3 to 1.5 at.%. The significant increase of the intensity is accompanied by the lengthening of the lifetime. The observed Bi concentration dependence of the PL data clearly indicates that doped Bi acts not only as optically active centers, but also as pore-sealing substances to isolate the centers. Therefore, in this system, Bi concentration is a very important parameter to have the maximum luminescence efficiency. The comparison of PL and Raman data suggests that in addition to previously proposed Bi_2O_3 , other Bi-related materials, probably Bi metal, play an important role to isolate the active centers.

In chapter 3, the effect of annealing atmosphere on the optical properties of Bi doped zeolites is studied by diffuse reflectance, steady state and time-resolved PL, and PLE spectra. The results reveal that zeolites can be used as an excellent host material to stabilize multiple Bi centers (Bi^{3+} , Bi^{2+} , and Bi-related NIR active centers) in the framework, which shows ultra-broadband emission from visible to NIR range. Annealing in N_2 leads to the partial conversion of Bi^{3+} ions into Bi^{3+} and Bi-related NIR active centers. Most of Bi-related NIR active centers are well isolated from the coordinated water in zeolites due to sealing the pores of zeolites by Bi_2O_3 and BiO clusters. Our results demonstrate that the broadband infrared emission may be attributed to the electronic transition of Bi low valence state, rather than a higher valence state.

In chapter 4, we have shown that tunable and highly efficient broadband NIR luminescence can be realized in Er-Bi co-doped zeolites. The emission covers the ranges of 930 - 1450 nm and 1450 - 1630 nm. The intensity ratio of the two bands can be tuned by adjusting the concentration of Er and excitation wavelength. Steady state and time-resolved PL, and PL excitation measurements indicate that two kinds of emitters coexist in the pores of zeolites, and that near infrared active bismuth simultaneously acts as a sensitizer of Er. The present results demonstrate an important rational strategy for the design of a tunable near-infrared emitting zeolite-based nanosystem.

In chapter 5, a series of Nd-Bi co-doped zeolites were prepared, and the optical properties were investigated by PL and PL excitation spectra, and decay time measurements. The results show that the NIR emission of Nd³⁺ ions is significantly enhanced by the introduction of bismuth in co-doped samples, and the lifetime reaches 246 μ s. Furthermore, it is revealed that NIR active Bi acts as a sensitizer of Nd³⁺ ions. The energy transfer efficiency is also estimated. The peculiar optical properties make them promising for potential application in biological probes.

In chapter 6, we studied the structural and optical properties of Yb-Bi co-doped zeolites. We observe two strong NIR emission bands overlapping in the range of 930 - 1480 nm, corresponding to the electronic transitions of bismuth-related NIR active centres and Yb³⁺ ions, respectively. In the obtained products, the excitation wavelength of Yb³⁺ is extended to the range of 420 - 850 nm, and the lifetime reaches 665 μ s. In the zeolite matrix, Bi ions exist as bismuth-related NIR active centres and Bi compounds agglomerates. The former one act as a sensitizer of Yb³⁺ ions, and the latter one act as a blockage to seal the pores of zeolites, which enable Yb³⁺ ions to show efficient NIR emission even the zeolites contain large amount of coordinated water. The excellent optical and structural properties make these NIR emitting nanoparticles promising in application as biological probes.

In chapter 7, the optical properties of Eu doped zeolites is investigated by co-doping Bi. The addition of Bi³⁺ strongly enhances the red luminescence of Eu³⁺ (⁵D₀ \rightarrow ⁷F₂) in zeolites about 50 times, and the lifetime is significantly increased from 25.8 μ s to 2.46 ms. The results reveal that the O²⁻ \rightarrow Eu³⁺ charge transfer band and sensitization of Bi³⁺ ions distinctly enhances the excitation band of Eu³⁺ ions in the ultraviolet region. The energy transfer efficiency is estimated to be 78 %. It is expected that the present Eu-Bi co-doped zeolites have potential application in white-LEDs.

In chapter 8, we investigate the ultraviolet-blue to NIR downconversion for the Dy³⁺ - Yb³⁺ couple in zeolites by steady-state and time-resolved PL spectra, and PL excitation spectra. We demonstrate the existence of a two-step energy transfer process from the long-lived ⁴F_{9/2} level of Dy³⁺ to two neighboring Yb³⁺ ions in zeolites. The energy transfer efficiency from the ⁴F_{9/2} level is estimated to be 42 %, and the intrinsic PL

quantum efficiency of Yb^{3+} emission reaches 54 %. The high energy transfer efficiency and the efficient Yb^{3+} emission suggest that the materials may have potential application in enhancing the energy efficiency of the silicon-based solar cell.

Acknowledgment

First of all, I would like to thank my supervisor Prof. Minoru Fujii. Thank you for giving me the opportunity to conduct my doctoral course in your group and for all the advice and guidance that you gave me in the last three years. The discussions at our weekly meetings were always very inspiring and they were the breeding ground to develop many new ideas. I want to express my deep acknowledgment to Dr. Hong-Tao Sun for his fruitful discussions and valuable comments on this thesis.

I would like to express my sincere gratitude to Professor Shinji Hayashi for his enormous support and insightful comments throughout the course of this study. I want to make my acknowledgment to Associate Professor Kazuyuki Moriwaki for his encouragement and helpful comments in this work. I also wish to extend special acknowledgment to Assistant Professor Kenji Imakita for his continuous supports throughout this work, and for valuable discussions leading to the experimental and theoretical ideas implemented in this thesis.

I would like to thank Professor Minoru Mizuhata, Mr. Takashi Hasegawa and Mr. Yuki Mori for the successful collaboration that we started two years ago. It was a pleasure to take XRD, EDS, and SEM measurements in your laboratory but also to discuss together our experiments. I wish to express my thanks to Professor Takashi Kita for his careful reading and useful comments on this thesis.

This work has been done at Mesoscopic Material Laboratory, Department of Electrical and Electronics Engineering, Faculty of Engineering, Kobe University under the direction of Professor Minoru Fujii. I wish to give my highest appreciation to my co-workers in the laboratory who have contributed to this work, particularly, to Mr. Fumiaki Shimaoka and Mr. Yuji Miwa, for their excellent technical assistance on the study of the optical measurements. I thank all colleges in the Mesoscopic Material Laboratory.

Finally, I would like to thank my family for their support and their encouragement throughout the years. I had a good time in Kobe also because of the friends I met here and with whom I had a lot of fun.

List of Publications

Journal Papers

- [1] Zhenhua Bai, Hong-Tao Sun, Takashi Hasegawa, Minoru Fujii, Fumiaki Shimaoka, Yuji Miwa, Minoru Mizuhata, Shinji Hayashi,
"Efficient near-infrared luminescence and energy transfer in erbium/bismuth codoped zeolites"
Optics Letters, Vol. 35, No 11, pp. 1926-1928, June, 2010.
(Chapter 4)
- [2] Zhenhua Bai, Minoru Fujii, Yuki Mori, Yuji Miwa, Minoru Mizuhata, Hong-Tao Sun, Shinji Hayashi,
"Efficient near-infrared emission from neodymium by broadband sensitization of bismuth in zeolites"
Optics Letters, Vol. 36, No 6, pp. 1017-1019, March, 2011. (Highlighted in " Virtual Journal for Biomedical Optics, May 4, 2011 ")
(Chapter 5)
- [3] Zhenhua Bai, Hong-Tao Sun, Minoru Fujii, Yuji Miwa, Takashi Hasegawa, Minoru Mizuhata, Shinji Hayashi,
"Bismuth sensitized efficient near-infrared luminescence from ytterbium in zeolites"
Journal of Physics D: Applied Physics, Vol. 44, No 15, pp. 155101-1-5, March, 2011.
(Chapter 6)
- [4] Zhenhua Bai, Minoru Fujii, Takashi Hasegawa, Kenji Imakita, Yuji Miwa, Minoru Mizuhata, Shinji Hayashi,
"Effect of doping concentration on optical properties of Bi doped zeolites"

Microporous and Mesoporous Materials, Vol. 145, pp. 21-25, April, 2011.

(Chapter 2)

- [5] Zhenhua Bai, Minoru Fujii, Takashi Hasegawa, Kenji Imakita, Minoru Mizuhata, Shinji Hayashi,

"Efficient ultraviolet-blue to near-infrared downconversion in Bi-Dy-Yb doped zeolites"

Journal of Physics D: Applied Physics, Vol. 44, No 45, pp. 455301-1-5, October, 2011.

(Chapter 8)

- [6] Zhenhua Bai, Minoru Fujii, Takashi Hasegawa, Shohei Kitano, Kenji Imakita, Minoru Mizuhata, Shinji Hayashi,

"Co-existence of Bi with multiple valence states in zeolites - Controlling the optical properties by annealing atmosphere"

Optical Materials, Vol. 34, pp. 821-825, January, 2012.

(Chapter 3)

- [7] Zhenhua Bai, Minoru Fujii, Takashi Hasegawa, Kenji Imakita, Minoru Mizuhata, Shinji Hayashi,

"Enhanced red luminescence and energy transfer in Eu-Bi codoped zeolites for white LEDs"

Journal of Luminescence, 2012. (under review)

(Chapter 7)

Conference Papers

- [1] Zhenhua Bai, Minoru Fujii, Yuki Mori, Yuji Miwa, Minoru Mizuhata, Hong-Tao Sun, Shinji Hayashi,

"Efficient near-infrared luminescence and energy transfer in Nd-Bi codoped zeolites"

MRS Proceeding, Vol. 1342, mrss11-1342-v04-03, October, 2011.

(Chapter 5)

Articles to which the auther also contributed

- [1] Hong-Tao Sun, Takashi Hasegawa, Minoru Fujii, Fumiaki Shimaoka, Zhenhua Bai, Minoru Mizuhata, Shinji Hayashi, Shigehiko Deki,
"Highly-efficient and air-stable near infrared emission in Erbium/Bismuth codoped zeorites"
Applied Physics Letters, Vol. 94, No 14, pp. 141106-1-3, April, 2009.

- [2] Hong-Tao Sun, Takashi Hasegawa, Minoru Fujii, Fumiaki Shimaoka, Zhenhua Bai, Minoru Mizuhata, Shinji Hayashi, Shigehito Deki,
"Significantly enhanced superbroadband near infrared emission in Bismuth/Aluminum doped high-silica zeolite derived nanoparticles"
Optics Express, Vol. 17, No 8, pp. 6239-6244, April, 2009.

- [3] Hong-Tao Sun, Minoru Fujii, Yoshio Sakka, Zhenhua Bai, Naoto Shirahata, Liyan Zhang, Yuji Miwa, Hong Gao,
"Near infrared photoluminescence and raman characterization of bismuth embedded sodalite nanocrystals"
Optics Letters, Vol. 35, No 11, pp. 1743-1745, June, 2010.

- [4] Hong-Tao Sun, Junjie Yang, Minoru Fujii, Yoshio Sakka, Yufang Zhu, Takayuki Asahara, Naoto Shirahata, Masaaki Ii, Zhenhua Bai, Ji-Guang Li,
"Highly fluorescent silica-coated bismuth-doped aluminosilicate nanoparticles for near-infrared bioimaging"
Small, Vol. 7, No 2, pp. 199-203, January, 2011.

- [5] Hong-Tao Sun, Yoshio Sakka, Hong Gao, Yuji Miwa, Minoru Fujii, Naoto Shirahata, Zhenhua Bai, Ji-Guang Li,
"Ultrabroad near-infrared photoluminescence from $\text{Bi}_5(\text{AlCl}_4)_3$ crystal"
Journal of Materials Chemistry, Vol. 21, No 12, pp. 4060-4063, February, 2011.